7-1-2016

Sedimentation, pedogenesis, and paleoclimate conditions in the Paleocene San Juan Basin, New Mexico, U.S.A.

Kevin Hobbs

Kevin Michael Hobbs

Candidate

Earth and Planetary Sciences

Department

This dissertation is approved, and it is acceptable in quality and form for publication:

Approved by the Dissertation Committee:

Dr. Peter Fawcett, Chairperson

Dr. Leslie McFadden

Dr. Gary Weissmann

Dr. Thomas Williamson

SEDIMENTATION, PEDOGENESIS, AND PALEOCLIMATE CONDITIONS IN THE PALEOCENE SAN JUAN BASIN, NEW MEXICO, U.S.A.

by

KEVIN MICHAEL HOBBS

B.S., Geology, The University of the South, 2006
M.S., Geological Sciences, The University of Idaho, 2010

DISSERTATION

Submitted in Partial Fulfillment of the
Requirements for the Degree of

Doctor of Philosophy
Earth and Planetary Sciences

The University of New Mexico
Albuquerque, New Mexico

July 2016

ACKNOWLEDMENTS

I thank the following persons for professional help in the form of discussions, critique of ideas, or suggestions during the research and writing of this dissertation:

From the Earth and Planetary Sciences Department:
Viorel Atudorei, Adrian Brearley, Ben Burnett, Jeff Carritt, Laura Crossey, Magdalena Donahue, Maya Elrick, John Geissmann, Nick George, Karl Karlstrom, Bekah Levine, Grant Meyer, Corrinne Myers, Lyman Persico, Jane Selverstone, Zach Sharp, Mike Spilde.

From the University of the South:
Karen Kuers, Nicole Nunley, Bran Potter, Steve Shaver, Sarah Sherwood, Ken Smith, Scott Torreano.

From farther afield:
Tim Gallagher, Judy Parrish, Leighton Reid, Tom Williams.

I thank committee member Tom Williamson of the New Mexico Museum of Natural History and Science for introducing me to many of the San Juan Basin field sites described herein and for his patience in my slow acquisition of the basin's complexities.

I thank my UNM EPS committee members Peter Fawcett, Les McFadden, and Gary Weissmann for suggestions, discussion, and critique of ideas that helped to improve this work.

I thank my family: Rachel Hobbs for her support, love, and encouragement during a program of study that seemed to have no end and for reminding me that it did; Labrador retriever Cocoa for her companionship and devotion during field work; and Rio Grande rathound Scruffy for providing constant good cheer, excitement, and humor.

Funding for these studies came from the University of New Mexico Graduate and Professional Student Association, the Colorado Scientific Society, and the Earth and Planetary Sciences Department.

SEDIMENTATION, PEDOGENESIS, AND PALEOCLIMATE CONDITIONS IN THE PALEOCENE SAN JUAN BASIN, NEW MEXICO, U.S.A.

by

Kevin Michael Hobbs

B.S., Geology, The University of the South, 2006
M.S., Geological Sciences, The University of Idaho, 2010
Ph.D., Earth and Planetary Sciences, The University of New Mexico, 2016

ABSTRACT

This dissertation follows the hybrid format as defined by the Office of Graduate Studies at the University of New Mexico. The three chapters herein were prepared as manuscripts to be submitted for publication to peer-reviewed journals in the field of Earth sciences. Chapter 1 will be submitted to *New Mexico Geology*. Chapter 2 will be submitted to *Geology*. Chapter 3 will be submitted to the *Geological Society of America Bulletin*. The main theme of these works is an exploration of paleoenvironmental conditions recorded in the Paleocene siliciclastic sediments of the San Juan Basin, northwestern New Mexico. Chapter 1 is an investigation of the lithologic and stratigraphic properties of Cretaceous and Paleogene terrestrial siliciclastic rock units in the San Juan Basin. I used petrography, stratigraphy, and geochemistry to show that marked changes occurred in sedimentation styles, sedimentary sources, and regional landscape evolution in the study area during the Laramide Orogeny and that these changes caused observable trends in San Juan Basin rocks. Chapter 2 explores the enigmatic silcretes of the Nacimiento Formation. My work shows that these silcretes represent a product of silica diagenesis that cannot be explained using currently accepted

models of silcrete genesis and that significant accumulation of volcanic ash occurred in the Paleocene San Juan Basin. Chapter 3 is an exploration of the paleosols preserved in the Nacimiento Formation. This work shows that widely used methods of estimating paleoclimate conditions based upon the geochemical composition of paleosols will produce inaccurate estimates in many realistic sedimentary basin environments. The major properties of Nacimiento Formation paleosols appear to be controlled by non-climate factors. I show that the evolution of a fluvial system can explain the observed trends.

Table of Contents

EPIGRAPH

"We must not only consider how things are, but how they came to be so. 'Tis pleasant to look upon a tree in the summer, covered with its green leaves, decked with blossoms, or laden with fruit, and casting a pleasing shade under its spreading boughs; but to consider how this tree with all its furniture sprang from a little seed; how nature shaped it and fed it in its infancy and growth; added new parts, and still advanced it by little and little, till it came to this greatness and perfection, this, methinks, is another sort of pleasure, more rational, less common…So to view this earth as it is now complete, distinguished into the several orders of bodies of which it consists, every one perfect and admirable in its kind; this is truly delightful and a very good entertainment of the mind; but to see all these in their first seeds; to take in pieces this frame of nature, and melt it down into its first principles; …this, methinks, is another kind of joy, which pierceth the mind more deep, and is more satisfactory."

-Thomas Burnet, *Sacred Theory of the Earth,* 1691

"When we are unable to explain the monuments of past changes, it is always more probable that the difficulty arises from our ignorance of all the existing agents, or all their possible effects in an indefinite lapse of time, than that some cause was formerly in operation which has ceased to act…"

-Charles Lyell, *Principles of Geology, Vol. I,* 1830

Chapter 1

Ojo Alamo Sandstone: New interpretations of its sedimentologic and tectonic significance

Kevin M. Hobbs[1], *Gary S. Weissmann*[1], *Peter J. Fawcett*[1]

[1]Department of Earth and Planetary Sciences, Northrop Hall, University of New Mexico, Albuquerque, New Mexico 87131, USA

ABSTRACT

Fluvial siliciclastic rocks bracketing the Cretaceous-Paleogene boundary in the San Juan Basin (SJB), New Mexico, provide records of regional fluvial and tectonic evolution during the Laramide Orogeny. Petrographic analyses of sandstones from the Upper Cretaceous Fruitland Formation and Kirtland Shale and the Paleocene Ojo Alamo Sandstone and Nacimiento Formation show that the rivers depositing these sediments were sourced in areas where unroofing of crystalline basement rocks took place, introducing an increasing proportion of immature detrital grains into the fluvial system through time. After the Cretaceous-Paleogene boundary, rivers deposited an increasing amount of potassium feldspar relative to plagioclase feldspar, suggesting a growing source in crystalline basement rocks. Geochemical analyses show significant differences between Al- and K-poor Upper Cretaceous sandstones and Al- and K-rich lower Paleocene sandstones in the San Juan Basin.

The high proportion of sand-size material in the Ojo Alamo Sandstone suggests that it was deposited in a basin with a low sediment supply/accommodation ratio. However, magnetostratigraphic age constraints suggest it had a relatively high sedimentation/subsidence rate of up to 0.39 m/kyr. The sediment supply must have been

significantly high in order to deposit a basin-wide coarse sand-dominated package, suggesting rapid creation of topographic relief in the San Juan Uplift, the proposed source area of the Ojo Alamo fluvial system.

The observed sedimentary architecture and age constraints of the Ojo Alamo Sandstone, including kilometers-wide sand bodies and limited overbank mudstones throughout most of the outcrop area, are difficult to reconcile with accepted models of aggradation and avulsion in fluvial systems, but available age and lithologic data do not allow for complete understanding of Paleocene SJB fluvial systems and basin evolution. Here, we present lithologic, petrographic, and thickness information from SJB K/Pg fluvial siliciclastic units and interpretations of their origins.

INTRODUCTION

Since the 1970s, Ojo Alamo Sandstone research has focused primarily on the interpretation of the formation's position at or near the Cretaceous-Paleogene (K-Pg) boundary, its potential economic role as a hydrocarbon reservoir or uranium source, and its importance as a marker of regionally-extensive Laramide tectonic activity. Few studies have offered basin-scale sedimentation, tectonic, and paleoenvironmental interpretations for the Ojo Alamo Sandstone. Recent advances in understanding of fluvial sedimentary processes and preservation potential (Owen et al., 2015, and references therein), Laramide tectonic deformation history of the southern Rocky Mountains (Heller et al., 2012, and references therein), and radiometric and magnetostratigraphic age controls for Cretaceous and Paleogene rocks of the San Juan Basin (SJB) (Donahue, 2016) allow for updated interpretations of the depositional history, lithostratigraphic

relationships, and tectonic significance of the Ojo Alamo Sandstone which we present here.

The K-Pg boundary in the SJB of northwestern New Mexico is located within or between the Late Cretaceous Kirtland Formation and the Paleocene Ojo Alamo Sandstone. The exact position of the boundary has been subject to conflicting interpretations throughout the 20th Century (*e.g.*, Bauer 1916, Reeside 1924, Dane 1936, Baltz et al. 1966, Lindsay et al. 1981, Fassett 1985). Though still debated (*e.g.* Fassett et al. 2011; Lucas et al. 2009), the K-Pg boundary is generally accepted to lie at the base of the Ojo Alamo Sandstone *sensu* Baltz (1967), *i.e.*, at the base of the "Kimbeto Member" of the Ojo Alamo Sandstone *sensu* Powell (1973). We use that position throughout this paper and note that the exact position of the boundary does not affect our interpretations of basin sedimentary architecture and tectonics. We use Baltz's (1967) definition of the Ojo Alamo Sandstone in this study; *i.e.*, we do not include the Naashoibito Member in the Ojo Alamo Sandstone.

The intricacies of spatial and temporal relationships between aggradation/progradation, degradation, system quiescence, accommodation, and extrabasinal controls lead to complex sedimentary records in fluvially-dominated terrestrial basins. Recent work shows that many fluvial siliciclastic packages preserved in modern continental sedimentary basins and in the rock record are the deposits of prograding distributive fluvial systems (DFSs) or megafans (Hartley et al. 2010; Weissmann et al. , 2010, 2013, 2015; Kukulski et al. 2013). Other workers highlight the abundance of both modern and ancient fluvial deposits that do not meet the criteria for DFS, suggesting that tributary fluvial systems are at least as likely as DFSs to be

preserved in the rock record (Fielding et al., 2012, Latrubesse, 2015). In either setting, tributary or distributive, incision and downcutting occur when the rate of sediment volume supply is greater than the rate at which sediment can be accommodated by subsidence in the basin (Shanley & McCabe, 1994; Holbrook et al., 2006). Conversely, when the creation of accommodation is greater than the rate of sediment volume supply, the fluvial system experiences aggradation. Aggrading/prograding fluvial systems cannot uniformly deposit sediment throughout a basin at any one point in time. Rather, deposition occurs in and around individual active channels occupying a small portion of the total basin area (Shukla et al., 2001; Nichols and Fisher, 2007). Over time as the active channels change position, most or all of the basin area will accumulate sediment. Basin-wide lithologically similar beds or deposits, therefore, must be interpreted as diachronous.

Sedimentation in Laramide basins in the North American Cordillera from the Late Cretaceous to the Eocene was simultaneous with uplift in the regions surrounding the basins (Dickinson et al. 1988). Sediments preserved in Laramide basins often provide the highest-resolution records of local to regional deformation and associated syntectonic responses. Laramide basin sediments have been investigated for insights into paleogeography, paleotectonics, and mantle processes (Dickinson et al., 1988; Heller et al., 2003; Yonkee & Weil, 2015). These investigations share the premise that uplift led to erosion of materials in the uplifted areas surrounding basins, transport downgradient towards basins, and subsequent deposition and storage within basins as the basins subsided. As such, the fluvial deposits preserved in Laramide basins are directly related

to the fluvial, magmatic, climatic, and tectonic conditions present during their erosion, transport, and deposition.

Geologic Setting

The San Juan Basin is located in the Four Corners region of New Mexico and Colorado (Fig. 1) in the Navajo section of the Colorado Plateau physiographic province (Fenneman and Johnson 1946). The SJB is an asymmetrical broken-foreland structural basin formed during the Laramide Orogeny and containing Paleozoic through early Cenozoic sediments (Dickinson et al., 1988; Cather, 2004). The axial trace of the SJB is arcuate, located near the northern and eastern basin margins with steeply dipping northern and eastern limbs and shallowly dipping southern and western limbs. Like most of the sedimentary cover of the Colorado Plateau, the central, southern, and western SJB is relatively undeformed, with regional dips of <5°. The eastern basin margin is highly deformed along the Nacimiento uplift, with Mesozoic and Cenozoic units steeply dipping to overturned (Woodward et al., 1972). The northern basin margin is moderately deformed along the San Juan uplift, Archuleta Anticlinorium, and Hogback monocline, with Paleozoic through Cenozoic units moderately to steeply dipping (Steven et al., 1974). The western and southern basin margins are slightly deformed along the Defiance upwarp and Zuni Mountains uplift, respectively, with Mesozoic and Cenozoic units gently dipping (Baltz, 1967). The structure of the SJB leads to a bullseye pattern in map view, with Eocene bedrock in the central basin surrounded by rings of Paleocene, Upper Cretaceous, and middle Cretaceous units.

The SJB was located on the western margin of the Cretaceous Interior Seaway (CIS) during its maximum inundation from approximately 95 Ma (Cenomanian) until

approximately 74 Ma (Campanian) and accumulated as much as 1900 m of marine sands and muds during three major transgressive-regressive episodes (Leipzig, 1982; Klute, 1986; Roberts & Kirschbaum, 1995). Following the retreat of the CIS at approximately 74 Ma, the SJB accumulated as much as 625 m of fluvioclastic sediment during the Campanian and Maastrichtian (Klute, 1986; Sikkink, 1987; Cather, 2004; Donahue 2016). These deposits include the Fruitland Formation and the Kirtland Formation. During the onset of the major Laramide regional deformation in the Paleocene, the SJB accumulated as much as 700 m of fluvioclastic sediment (Sikkink, 1987; Williamson & Lucas, 1992; Williamson; 1996; Russell, 2009). These deposits include the McDermott Formation, Animas Formation, Ojo Alamo Sandstone and Nacimiento Formation. Fluvioclastic deposition continued into the Eocene after major Laramide uplifts occurred adjacent to the SJB, resulting in the accumulation of up to 650 m of fluvioclastic sediment of the San Jose Formation (Smith, 1988; 1992; Milner et al. 2005). Episodic deposition likely continued through the Oligocene (Cather et al., 2008), but SJB bedrock units younger than Eocene are not preserved within the basin. A generalized stratigraphic column showing units relevant to this paper is presented in Figure 2.

Previous Work

Throughout the 20th Century, the issues of age and nomenclature surrounding the K/Pg units in the SJB were addressed by Sinclair & Grainger (1914), Reeside (1924), Dane (1936), Baltz (1953, 1967), Anderson (1960), Baltz et al. (1966), O'Sullivan et al. (1972), Clemens (1973), Fassett (1973, 1974), Lindsay et al. (1978, 1981), Klute (1986), and Sikkink (1987). Baltz et al. (1966) designated the lower conglomerate and dinosauriferous middle shale of Bauer (1916) to the Kirtland Formation and restricted the name Ojo Alamo Sandstone to the upper conglomerate and pebbly sandstone. Fassett

(1966) extended this designation to include the medium- to thickly-interbedded shales and channel sandstones overlying the shales of the Kirtland Formation at Mesa Portales in the southeasternmost outcrop area near Cuba, New Mexico (these facies are absent in other portions of the SJB). The debate over these designations has continued for half a century and is fueled by contradictory absolute age estimates, geographically-limited field studies, varying interpretations of conformable vs. disconformable contacts, and confusion surrounding nomenclature.

Powell (1973) provided the first basin-scale sedimentation model for the Ojo Alamo Sandstone. His investigation of the pebbly sandstone and conglomerate that make up the Ojo Alamo Sandstone of Baltz et al. (1966) and Fassett (1966) included measurement of >7,000 paleocurrent direction indicators throughout the outcrop area in New Mexico. His interpretation of these data suggests a mean fluvial transport azimuth of 138° for the Ojo Alamo Sandstone of Baltz (1967). Given the direction and consistency of paleocurrent indicators, Powell suggested a single sedimentary source area to the northwest of the SJB in the vicinity of the present western San Juan Mountains or La Plata Mountains. Powell's interpreted depositional environment for the Ojo Alamo Sandstone is an alluvial plain that resulted from the downgradient transport of sands and gravels from alluvial fans located proximal to the source area.

An investigation of outcrops of Ojo Alamo Sandstone by Klute (1986) included sedimentologic, petrographic, and paleocurrent analyses and interpretations. Klute interpreted the depositional environment of the Ojo Alamo Sandstone as South Saskatchewan- or Platte-type sandy braided rivers. The sandy braided river models of Miall (1981, 1986) best fit most of the Ojo Alamo Sandstone sedimentary features

described by Klute (1986), but neither Miall nor Klute suggested a perfect modern analog for the Ojo Alamo depositional system. Klute attributed the relative homogeneity of the Ojo Alamo Sandstone throughout most of the study area to the avulsion of active channels through the basin and the subsequent reworking of sediment during channel shifting and flood events. In addition, Klute's petrographic analyses show that the Ojo Alamo Sandstone is enriched in potassium feldspar and sedimentary lithic grains relative to the underlying Kirtland Shale fluvial sandstone.

Sikkink (1987) analyzed lithofacies in the Ojo Alamo Sandstone and adjacent units in order to provide interpretations of depositional history near the K-Pg boundary in the SJB. Sikkink interpreted the Ojo Alamo Sandstone to be synchronous with both the Animas Formation and the Nacimiento Formation; interfingering of the Ojo Alamo Sandstone and Animas Formation (McDermott Member) is noted in the northwestern SJB near Farmington. Her interpretations include a source area in an early Laramide volcanic/intrusive center near the present-day La Plata Mountains that shifted shortly thereafter to a source in a basement-cored uplift near the present-day central to eastern San Juan Mountains. Sikkink suggested that K-Pg McDermott Formation and Animas Formation conglomeratic fluvial and debris flow deposits in the northernmost SJB were shed from these emerging highlands while the finer-grained fluvial deposits, including the Ojo Alamo Sandstone, were their distal meandering stream counterparts.

In the early 21st Century, several studies focused on the Ojo Alamo Sandstone because of isolated dinosaur fossils found within it (*e.g.* Fassett et al. 2011; 2009; 2002; Lucas et al. 2009; Sullivan et al. 2005). These studies were focused in the geographic and stratigraphic vicinity of the dinosaur fossils in question and lead to little new

understanding of Ojo Alamo sedimentation; however, they focused new attention on the age of what was variously interpreted as the Ojo Alamo Sandstone (*sensu* Baltz et al. (1966)) or the Kimbeto Member of the Ojo Alamo Sandstone (*sensu* Powell (1973)). Of interest to this study, the magnetostratigraphy utilized by the above studies suggest that the unconformity below the Ojo Alamo Sandstone represents a deposition hiatus of 2-4 million years (Lindsay et al., 1981; Butler & Lindsay, 1985; Lucas et al. 2006). However, radiogenic isotope age estimates derived from detrital zircons and sanidines in the Kirtland Formation, Ojo Alamo Sandstone, and Nacimiento Formation suggest that the hiatus between these formations was as short as 1.5 Myr (zircon) and 0.4 Myr (sanidine) (Mason et al., 2013, Donahue, 2016), further decreasing the K-Pg hiatus in the SJB.

Here, we document lithologic and petrographic changes in SJB K-Pg fluvial sedimentary rocks. When combined with geographic and age constraints, these changes document the evolution of the fluvial systems that deposited sediment in the SJB during part of the Laramide Orogeny and allow for increased understanding of regional paleogeography. In addition, we report on the fluvial sedimentology of the Ojo Alamo Sandstone, which comprises the first record of SJB sedimentation during and after the major Laramide reorganization of paleogeographic and paleofluvial features. This formation shows that basin-wide fluvial sedimentation can occur rapidly and does not always produce the sedimentary architecture expected in an avulsive fluvial system.

METHODS

Stratigraphic sections were measured in the San Juan Basin. Section sites were selected on the basis of correlation with other units, amount of exposure, completeness of section, and accessibility. In addition to our own measurements, we utilize petrographic

data and lithologic descriptions from measured sections previously published by Baltz (1967), Baltz et al. (1966), Powell (1973), Leipzig (1982), Klute (1986), Sikkink (1987), and Wegert and Parker (2011). Electric well logs were analyzed in order to obtain subsurface thickness measurements. Petrographic data were collected with thin section point counts using the Folk method (Folk 1957). Whole-rock bulk geochemical analyses of sandstones and mudstones were performed on a Rigaku ZSX Primus II X-ray fluorescence spectrometer by the Analytical Chemistry Laboratory in the Department of Earth and Planetary Sciences at the University of New Mexico in order to investigate geochemical trends among K-Pg formations preserved in the SJB.

RESULTS

The Ojo Alamo Sandstone

The 5 to 120 m-thick Ojo Alamo Sandstone contains pebbly arenite and wacke, mud-clast conglomerate, claystone, and siltstone. Generalized stratigraphic columns with major lithologic designations and their locations are presented in Figures 3 and 4. In most areas, the formation is characterized by pebbly medium- to coarse-grained arenite with local lenses and horizons of claystone. Beds range in thickness from 0.5-15 m. Sandstones are typically light brown to yellow brown and sometimes develop reddish brown weathering surfaces or desert varnish. Claystones and siltstones are typically light brown, brown, or dark brown and are often covered in colluvium. Sandstone beds often overlie scour surfaces in claystones while claystones conformably overlie gradational boundaries. Sand grains are angular to subrounded and consist of quartz, feldspar, sedimentary and volcanic lithic fragments, chert, and mafic minerals. Medium- and coarse-grained sandstones are predominately clay-cemented with minor silica cements. Less common fine-grained sandstones are cemented with roughly equal parts clay and

silica. Bedforms include both trough and tabular crossbeds, convolute bedding, horizontal plane bedding, lenticular bedding, wavy bedding, and fluid escape structures. Silicified stumps, wood fragments, and logs up to 34 m long are common in the sandstones of the Ojo Alamo Sandstone. Leaf fossils are present but uncommon in the formation's claystones (Flynn et al. 2014).

Conglomerates and conglomeratic sandstones of the Ojo Alamo Sandstone are either pebble conglomerates/conglomeratic sandstone or mud-clast conglomerate. Pebble conglomerates/conglomeratic sandstones contain clasts from 2 to 100 mm (-1 to -7 ϕ) diameter and include subrounded to well-rounded pebbles of chert, alkali feldspar granite, quartzite, silicified wood, trachyandesite, sandstone, limestone, and metapelite. Mud-clast conglomerates contain clasts from 30 to 500 mm (-5 to -9 ϕ) diameter of subangular to very angular claystone. The mud-clast conglomerate lithofacies is restricted to cut-and-fill structures that represent scouring in both intraformational claystones as well as the underlying Cretaceous claystones at the base of Ojo Alamo Sandstone.

Descriptions of Ojo Alamo Sandstone Facies

We categorize the Ojo Alamo Sandstone into three broad facies associations: (1) amalgamated channel belt deposits; (2) overbank floodplain deposits; and (3) isolated channel-fill deposits; described below:

Amalgamated Channel Belt Deposits.---The amalgamated channel belt facies contains poorly- to well-sorted medium- to coarse-grained pebbly crossbedded and plane bedded sandstones. These lithological compositions and sedimentary structures, along with abundant petrified wood and lack of marine or estuarine fossils, suggest deposition in fluvial channel environments (Gibling 2006; Bridge 2003; Robinson and McCabe

1998; Miall 1978). Tabular and trough crossbeds represent downstream and oblique bar-face deposits (Best et al. 2003) and range from 0.3 to 1.5 m thickness. The abundance of tangential crossbeds suggests high sediment transport rates (Bridge 2003; Sallenger 1979; Bagnold 1954). Planar horizontal beds represent vertically-accreted bar-top deposits and range from 0.2 to 1.5 m thickness. These beds suggest high bed shear stress and sediment transport rates (Bridge 2003; Bridge and Best 1997, 1988). These facies commonly exhibit highly contorted bedding, especially near the tops of stories. Cut-and-fill structures are found both at the base of and within these deposits (Fig. 5). Where these facies overlie mudstones, clay clasts from the underlying deposits are found within the sandstones and conglomerates.

The deposits of this facies association form simple and multi-story bodies up to 11 km wide and up to 19 m thick. Wider and thicker units may exist. Individual channel belts are impossible to recognize in the field. In the southern and western SJB, these facies contain multiple stories that represent erosion within former channel deposits, suggesting reworking of material and a low accommodation/sediment supply ratio (Owen et al. 2015b; Kjemperud et al. 2008). Multiple stories, lateral continuity, and the lack of identifiable channel-belt margins collectively suggest that vertical and lateral amalgamation of channel deposits was a widespread process occurring throughout both the temporal and spatial range of deposition of fluvial units (Wang et al. 2011; Friend et al. 1979). While there is no significant downcurrent thinning of these facies, they do exhibit a downgradient reduction in mean and maximum grain size from coarse sand and cobbles in the La Plata area in the northwest to medium sand and pebbles at Mesa Portales in the southeast.

Overbank Floodplain Deposits.---The overbank floodplain facies contains sandy mudstones with interbedded fine-grained sandstones. This facies' laterally discontinuous sand lenses, organic-rich fossil hash layers, and leaf fossils (Flynn et al. 2014) suggest deposition in fluvial floodplain environments (Alexander and Fielding 2006; Kraus and Gwinn 1997). Paleosols are uncommon; when present, they exhibit entisol-like properties. Bedding is difficult to observe in most outcrops, but is thin and tabular to laminar where observed. Mudstones in these facies contain considerable sand and silt, suggesting deposition in close proximity to channels, high sediment supply, or high flood magnitude (Owen et al. 2015; Pizzuto 1997; Guccione 1993). The poor sorting and overall sandiness of these deposits is similar to the proximal overbank deposits of Hajek and Edmonds (2014) and Slingerland and Smith (2004), which they show to be associated with vertically-accreting systems in aggradational settings. These facies conformably overlie sandy channel deposits and are overlain by amalgamated channel belt deposits and cut-and-fill structures.

Deposits of this facies association form laterally-extensive complexes with widths of greater than 1 km and thicknesses of up to 7 m. These deposits are often truncated by channel sandstones (Fig. 6). In the southern SJB at Mesa Portales and the western SJB at Head Canyon, these facies separate up to four thick, laterally-extensive amalgamated channel belt complexes, leading to the bluff-and-slope topography common in the Ojo Alamo outcrop area at those locations (Fig. 7).

Isolated Channel-fill Deposits.---The isolated channel-fill facies contains poorly- to moderately-sorted medium- to coarse-grained sandstones and pebbly sandstones that fill simple channels with well-defined channel geometry in cross-section. Their geometry

(Fig. 6B) suggests incision of a simple channel into overbank or channel deposits followed by deposition from a non-migrating channel. These deposits often contain clay rip-ups when overlying mudstones. Both symmetric and asymmetric channel forms are present. Wings associated with levee and/or crevasse-splay deposits are absent. Some isolated channel-fill deposits are found in close proximity to one another in the same stratigraphic interval (Fig. 6B), suggesting possible anastomosing fluvial form. Given the lithologic similarity to the sandstones of the amalgamated channel belt facies through which they incised, these isolated channel-fill deposits might represent possible periods of low stage during which the depositional rivers assumed an anastomosing form that was not present during periods of higher stage. Alternatively, these deposits could represent cross-bar channels. This interpretation does not require a stage-dependent variation in fluvial form and is in accord with inferred reworking of sediment arising from the observed lithologic homogeneity between isolated channel-fill deposits and amalgamated channel belt deposits.

Deposits of this facies form lens-shaped bodies of 5 to 90 m width and 1 to 9 m thickness that cut into underlying sandstones and mudstones. These deposits are overlain by sandstones along distinct boundaries. Isolated channel-fill deposits in the Ojo Alamo Sandstone exhibit no appreciable upwards fining trends, suggesting that they are not abandoned main channels (Bridge 2003; Miall 1996). These deposits are difficult to observe unless exposed in vertical cliff faces, leading to a probable underestimation of their abundance. Given their relative thinness and narrowness when compared to geometries of amalgamated channel belt deposits, we do not interpret the channel

dimensions recorded in the isolated channel-fill facies as representative of the main channels of the Ojo Alamo Sandstone fluvial depositional system.

Sedimentary Architecture

The sedimentary architecture of the Ojo Alamo Sandstone varies across the outcrop area. In some sections, such as the Shannon Bluffs south of Farmington and in the La Plata River valley, the Ojo Alamo Sandstone forms a single 12-70 m thick amalgamated complex channel belt sandstone cliff with no observed mudstones. These multi-story sand bodies are laterally continuous for up to 3 km. In other locations, such as Head Canyon and Mesa Portales, the Ojo Alamo Sandstone consists of laterally continuous sand bodies separated by mudstone interbeds. In either setting, wide sandstone bodies show a high degree of lateral and vertical amalgamation, suggesting a low accommodation/sediment supply ratio (Weissmann et al. 2013; Huerta et al. 2011). Where mudstones are present, they are often laterally truncated by overlying channel deposits, making mudstones less laterally extensive than sandstones. In the Bisti/De-na-zin Wilderness Area and Escavada Wash, the Ojo Alamo Sandstone has a 6-10 m-thick single-story form. These thinner single-story forms contain abundant very coarse sand and pebbles, perhaps representing high-energy barhead or confluence scouring and minimal deposition of relatively coarse material.

Sandstone Petrography

Petrographic data from sandstones immediately above and below the base of the Ojo Alamo Sandstone are presented in Figure 8. Sandstones form the Fruitland Formation are well-sorted fine- to medium-grained subrounded to rounded quartz arenites. Kirtland Formation sandstones show significant variation in mineralogic composition; they are moderately- to well-sorted fine- to medium-grained subrounded to

subangular arkosic arenites and lithic arenites. Sandstones from the Ojo Alamo Sandstone are poorly- to moderately-sorted medium- to coarse-grained subrounded to very angular arkosic arenites; two of the 39 samples are lithic arenites. Sandstones from the lower Nacimiento Formation (Arroyo Chijuillita Member of Williamson and Lucas (1992)) are moderately- to well-sorted fine- to medium-grained angular to well-rounded feldspathic arenites and arkosic arenites. Sandstones are cemented with clays and amorphous silica.

Detrital grains in SJB K/Pg sandstones include quartz, plagioclase feldspar, potassium feldspar, chert, lithic fragments, hornblende, micas, amphibole, and heavy minerals. Both monocrystalline and polycrystalline quartz grains are present. The wide range of roundness in quartz and chert grains suggests reworking of sand grains from older sedimentary rocks among all three formations. Detrital feldspars in the Ojo Alamo Sandstone display a wide range of physical weathering and chemical alteration by sericitization and vacuolization (Fig. 9), with chemically-altered feldspars becoming less common upsection.

Relative proportions of plagioclase feldspar and potassium feldspar for sandstones from the Kirtland Formation and Ojo Alamo Sandstone are presented in Figure 10. Mean values for 25 Kirtland Formation sandstones are 62% plagioclase feldspar and 38% potassium feldspar. Mean values for 39 Ojo Alamo Sandstone sandstones are 37% plagioclase feldspar and 63% potassium feldspar. These data show that while the total feldspar content in both formations is not significantly different, there is significant variation in the plagioclase feldspar/potassium feldspar ratios in the San Juan Basin across the K-Pg boundary, with the Ojo Alamo Sandstone being richer in potassium feldspar.

Geochemical Analyses

The bulk geochemical compositions of 57 sandstones from the Ojo Alamo Sandstone and immediately adjacent formations are presented in Table 1. The results are typical for the arkosic arenites, feldspathic arenites, and lithic arenites analyzed. SiO_2 and Al_2O_3 comprise 60-89% of the sandstones by mass. The Ojo Alamo Sandstone is richer in K and Al than the sandstones of the Kirtland Formation (Figs. 11 and 12). The geochemical composition of the Nacimiento Formation sandstones is more variable and overlaps with those of the Kirtland Formation and Ojo Alamo Sandstone.

INTERPRETATIONS

Changing Sediment Sources Across K-Pg Boundary

As shown in Figure 8, significant petrographic variation exists among the sandstones of the Fruitland Formation, Kirtland Formation, Ojo Alamo Sandstone, and Nacimiento Formation. The quartz arenites of the Fruitland Formation (Leipzig 1982) suggest that the rivers that deposited the Fruitland Formation during middle to late Campanian time were sourcing mature sediments, likely reworked from underlying Cretaceous marine sands. The scarcity of feldspars and lithic grains is indicative of either very distal deposits of a mature fluvial system or a quartz-rich source area, such as a broad coastal plain underlain by beach deposits of the ultimate CIS regression, now preserved as the Pictured Cliffs Sandstone. The increase in feldspar and lithic grains in sandstones of the Kirtland Formation could be indicative of unroofing of basement rocks in the sediment source area, an increase in volcanic activity in the drainage basin, a significant reorganization of regional drainage patterns leading to a different sediment source area, or some combination of these. Given the conformable character of the Fruitland Formation/Kirtland Formation contact (Klute 1986; Baltz 1967), significant

reorganization of regional drainage patterns between the deposition of these two formations is unlikely. Instead, we interpret the increase in feldspar and lithic grains in Kirtland Formation Sandstone as the result of evolving upland source areas related to the early phase of Laramide localized uplift. The sandy Vermejo Formation in the Raton Basin ~250 km east of the SJB is synchronous to the Kirtland Formation and contains detrital grains indicative of up to 1 km of localized uplift in the headwaters of its depositional fluvial system (Cather 2004). Similar-scale uplift and fluvial response likely occurred in source areas of rivers in the SJB, leading to the increase in feldspathic and lithic detrital grains in the Kirtland Formation. In light of the paleocurrent and paleogeography information presented by Heller et al. (2012), Cather (2004), and Baltz (1967), we suggest that this relief might have been created in the first stages of the Laramide Zuni or Defiance Uplifts or the regional uplift and unroofing of the Mogollon Rim.

Sandstones in the Ojo Alamo Sandstone show an increase in both the total proportion of lithic grains and in the potassium feldspar/plagioclase feldspar ratio relative to the underlying Cretaceous sandstones. The increase in the potassium feldspar/plagioclase feldspar ratio in the Ojo Alamo Sandstone suggests development of a sediment source in crystalline igneous or metamorphic terrains; potentially the Needle Mountains in the western San Juan Mountains ~125 km north of the SJB or the Mogollon Rim ~300 km southwest of the SJB. The paleocurrent analyses of Sikkink (1987) and Powell (1972) both support a northerly source area for the Paleocene Ojo Alamo fluvial system. The Needle Mountains in the western San Juan Mountains contain the nearest and largest exposures of crystalline basement rocks and, in light of the above

paleocurrent analyses, were upstream of the Ojo Alamo Sandstone depocenter, making them the likely source for basement-derived detritus in the Ojo Alamo Sandstone. The increase in proportions of hornblende, mica, and heavy mineral grains in the Ojo Alamo Sandstone suggests that it had a sediment source in an igneous terrain. Donahue (2016) and Bush et al. (2015) present data showing a significant population of detrital zircons from the Ojo Alamo Sandstone with ages as young as 68.0 ±1.4 Ma, suggesting a young igneous source within the Ojo Alamo drainage area, most likely the Colorado Mineral Belt-associated La Plata magmatic center ~100 km north of the SJB. This interpretation is in accord with the paleocurrent analyses as well as the presence of minerals present in both the La Plata magmatic center and the more proximal McDermott Formation (Wegert & Parker 2011; Gonzales 2010; O'Shea 2009).

Sandstones in the lower Nacimiento Formation have similar petrographic compositions to the Ojo Alamo Sandstone. Unaltered detrital grains of plagioclase feldspar, potassium feldspar, and hornblende suggest a crystalline igneous and/or metamorphic source area, likely shared with the Ojo Alamo Sandstone. Sericitized feldspars and well-rounded quartz and chert grains suggest reworking of sediment from older sedimentary units. The >5 km-thick exposed section of Paleozoic and Mesozoic sedimentary rocks between the San Juan Uplift and the SJB depocenter provides abundant potential sources for the variety of grain composition and texture in Nacimiento Formation sandstones. The petrographic composition, interfingering contact with the underlying Ojo Alamo Sandstone, and earliest Paleocene age of the Nacimiento Formation all suggest that it is the deposit of the same fluvial system(s) that deposited the Ojo Alamo Sandstone.

Regional Landscape Evolution Recorded in SJB K-Pg Deposits

The relative homogeneity, lateral surface and subsurface stratigraphic continuity, and improved age constraints from the Ojo Alamo Sandstone and adjacent units provide a unique opportunity for interpretation of the sedimentary, tectonic, and fluvial factors at work during deposition across the K-Pg boundary, shown in paleogeographic maps in Figs. 13-15. Campanian and lower Maastrichtian fluvial deposits in this study area record rivers flowing from highlands in the southwest towards the coastal plain of the retreating Cretaceous Interior Seaway (Potochnik et al., 1989; Cather et al., 2012; Dickinson, 2013) (Fig. 13). Detrital zircons in these sediments are predominately Phanerozoic in age, suggesting a limited source of Proterozoic crystalline basement rocks during this depositional period (Dickinson et al., 2012; Bush et al., 2015; Donahue, 2016). The orientation of these rivers was similar to the north/northeast-flowing Turonian rivers proposed by Blum & Pecha (2014), indicating that the lower Kirtland Formation provides the final record of sedimentation in the study area prior to significant regional drainage reorganization caused by the Laramide orogeny. The relatively large areal expanse of these deposits suggests limited localized basin subsidence.

After deposition of the Fruitland Formation and the majority of the Kirtland Formation by north/northeast-flowing rivers, there was a period of non-deposition and erosion in the San Juan Basin (Fig. 14). This erosion removed more sediment from the southeast SJB than from the northwest SJB (Fassett 1974; 1985; Newman 1987), resulting in preservation of younger pre-erosion rocks in the northwest than in the southeast. This differential erosion is perhaps due to uplift in the southeast related to the incipient Nacimiento Uplift. We propose that this period of non-deposition and erosion represents the interval of SJB drainage reorganization resulting from regional landscape

changes associated with the onset of Laramide uplift and subsidence. The late Maastrichtian age of this depositional hiatus (Williamson & Weil 2008) is in accord with proposed regional- (Mackey et al., 2012; Bush et al. 2015) to continental-scale (Galloway et al. 2011; Cather et al. 2012; Blum & Pecha 2014) drainage reorganization events. Given the lack of sedimentary rocks in the SJB from this interval, it is unclear whether or not the La Plata magmatic center or the San Juan Uplift contributed sediment to the SJB via south/southeast-flowing streams during this interval. As shown in Figure 14, we interpret the erosive Maastrichtian fluvial systems to have the same general orientation as those that deposited the Kirtland Formation, supported by the variation in the thickness of the Ojo Alamo Sandstone across the SJB (Figs. 16 and 17) that is potentially explained by accommodation of earliest Paleocene (*i.e.*, Ojo Alamo Sandstone) sediment in incised valleys left by north/northeast-flowing Maastrichtian erosive streams. The variation in Ojo Alamo Sandstone thickness in the central SJB could have resulted from merging tributaries of north/northeast-draining latest Cretaceous erosive streams. A potential interpretation of the age and thickness patterns of the Ojo Alamo Sandstone in the central SJB is that they are the result of infilling paleovalleys by earliest Paleocene fluvial systems. The lack of abnormally thick sandstone units in the bottoms of these features, as evidenced from well e-log interpretation and illustrated in Figure 17, calls this interpretation into question.

The Maastrichtian hiatus ended with the deposition of the first basin-filling sediments by south/southeast-flowing fluvial systems in the latest Maastrichtian and earliest Paleocene beginning with the Naashoibitio Member of the Kirtland Formation and the Ojo Alamo Sandstone. Detrital zircon (Donahue, 2016), volcaniclastic grain

petrography (O'Shea, 2009; Gonzales, 2010; Wegert & Parker 2011), and paleocurrent (Powell, 1973; Sikkink 1987) evidence suggest a source area in the La Plata magmatic center and San Juan Uplift, requiring a south/southeast paleoflow direction for the Ojo Alamo depositional system (Fig. 15). The accommodation of Laramide uplift-derived sediment in the SJB represents two significant changes in regional landscape evolution: first, a greater than 90° shift in regional drainage directions resulting from reorganization of regional-scale topography; and second, a preferential storage of sediment in isolated subsiding basins rather than on wide coastal plains. The first shift is recorded nearly simultaneously in other basins (Heller et al. 2012). The second shift is in accord with K-Pg sedimentary records on the western Gulf Coastal Plain that show a lack of earliest Paleocene sediments there (Galloway et al., 2011; Mackey et al., 2012). The south/southeast-flowing Paleocene depositional system persisted through the deposition of the Nacimiento Formation.

Avulsion and Preservation During Ojo Alamo Sandstone Deposition

Fluvial depositional systems are affected by external (allogenic) boundary conditions and processes such as climate, base level, subsidence, and uplift, as well as internal (autogenic) processes and variability such as avulsion, channel morphometry, roughness, and bank strength. It is not always apparent whether a signal observed in the rock record is the result of autogenic or allogenic variability. Wang et al. (2011) suggested that over shorter time scales, fluvial depositional systems will aggrade sediment somewhat randomly whereas over longer timescales, systems will preferentially aggrade via compensation, the tendency for depositional systems to fill topographic lows. The time period above which allogenic variability seems to overpower autogenic variability is different for each system and difficult to constrain (Paola et al., 1992; Sheets

et al., 2002; Covault et al., 2010), but is affected by roughness and aggradation rate (Wang et al. 2011). The uppermost Naashoibito Member of the Kirtland Formation, the entire Ojo Alamo Sandstone, and the lowermost Nacimiento Formation are all contained within chron C29r (Peppe et al., 2013; Williamson et al., 2014), which had a maximum duration of as little as 345±18 kyr (Sprain et al., 2015), thus the Ojo Alamo Sandstone represents less than ~345 kyr of deposition, assuming constant deposition. The erosional unconformity between the Ojo Alamo Sandstone and the underlying Naashoibito Member of the Kirtland Formation precludes constant deposition through chron C29r, therefore shortening the assumed duration Ojo Alamo Sandstone deposition. In order better to understand relationships between allogenic processes, autogenic variability, and deposition of the Ojo Alamo Sandstone, we used age constraints of chron C29r from Sprain et al. (2015), observed outcrop and well log formation thickness data (presented in Table 2), and the methods of Wang et al. (2011) to produce a range of compensation time scales (T_C). T_C estimates represent the sedimentation time durations above which alluvial sediments present forms influenced purely by allogenic processes and is defined as

$$T_C = \frac{l}{r}$$

where l is a roughness length scale in m and r is the basin-wide sedimentation rate in m/kyr (Wang et al. 2011). Sedimentation time durations below T_C will produce sediments that record both autogenic and allogenic variations. For roughness length scales, we use the depth of the thickest channel deposits we observe in the Ojo Alamo Sandstone, 10 m. Sedimentation rates are calculated from available age constraints and formation thickness data (Table 2). Our T_C estimates range from 26 kyr (using the highest sedimentation rate) to 79 kyr (using the lowest sedimentation rate). These T_C values essentially represent the

time duration required for the fluvial system to have filled its deepest channels with sediment. These estimates are an order of magnitude less than the duration of sedimentation for the entire Ojo Alamo Sandstone estimated above. Therefore, it is likely that the Ojo Alamo Sandstone's sedimentary architecture is the result of predominately allogenic processes. This conclusion is supported by the formation's wide geographic distribution, which would have been unlikely to occur in a system controlled by autogenic processes.

Estimated Ojo Alamo Sandstone sedimentation rates are 1.1-6.2 times greater than estimated sedimentation rates of the overlying Nacimiento Formation of Williamson (1996), suggesting a rapidly growing sediment source, rapidly subsiding basin, or combination of the two. The Nacimiento Formation estimated sedimentation rates of Williamson (1996) are minimum estimates as they do not take into account the numerous sedimentary hiatuses evidenced by well-developed paleosols throughout the formation (Hobbs and Fawcett 2014). In fluvial-dominated continental basins, high sedimentation rates are usually associated with mudstones, since a subsiding basin will create accommodation for storage of even fine-grained easily transportable sediment. Therefore, the deposition of up to 120 m of coarse sands by the Ojo Alamo fluvial system in as little as ~345 kyr is paradoxical. With the exception of minor muds preserved at Mesa Portales, a large proportion of the fine sands and muds must have bypassed through the San Juan Basin and their subsequent downgradient depocenter removed by post-deposition uplift and erosion. By the late Paleocene, fluvial systems were routing sediment from the Southern Rockies Laramide highlands to the western Gulf of Mexico coastal plain (Galloway et al., 2011; Mackey et al., 2012;), but Paleocene sediments

along the presumed paleoriver paths between the San Juan Basin and the Gulf coastal plain are not preserved. In light of these considerations, the Ojo Alamo Sandstone in the San Juan Basin highlights the problems associated with assuming that the present structural basin in which fluvial sedimentary rocks are preserved can be directly equated to the fluvial basin in which those sediments were deposited. The lithologic composition (*e.g.*, predominant coarse sandstones and scarcity of mudstones) and the proximity to major Laramide tectonic features (*e.g.*,<1 km from the Nacimiento Fault, a major Laramide uplift-bounding reverse fault with ~2 km of vertical offset) suggest that the present outcrop and subsurface area of the Ojo Alamo Sandstone represent a small portion of the area of the entire fluvial system in which the sediments were deposited. Recent studies of well-preserved intact paleofluvial basins have shown that the deposits of a single fluvial system show significant lithologic and stratigraphic variation over spatial scales of 10^2 km (Klausen et al. 2014; 2015; Owen et al. 2015b). Deposits of such systems are subject to post-deposition deformation (Klausen et al. 2014), and partial exhumation and removal (Owen et al. 2015b), making interpretation of the remnants of the system subject to inherent problems associated with incomplete stratigraphic records. While there is no evidence for major vertical downcutting or erosion after deposition of the Ojo Alamo Sandstone, some portion of it has been removed around the basin margins.

Several workers have addressed the topic of recognizing avulsion deposits in fluvial sedimentary packages (*e.g.*, Jones & Hajek 2007; Slingerland & Smith 2004; Kraus & Wells 1999; Smith et al. 1989). Though the specific type of avulsion affects the exact sedimentary signature of the event, avulsion deposits are generally recognized as having a lower coal or paleosol overlain by a general coarsening-upwards sequence of

heterolithic fine sandy deposits and channel sandstones/channel belts, and an upper paleosol representing abandonment of the developed channel system (Fig. 18) (Kraus & Wells 1999). The lack of paleosols and scarcity of overbank mudstones and heterolithic fine sandy deposits, both indicative of relatively stable non-channel environments, in the Ojo Alamo Sandstone makes interpreting the avulsion history of its depositional system difficult. The formation is spatially widespread, exhibits subparallel paleocurrent indicators throughout its outcrop area, and appears to have a common source area in the La Plata magmatic center/San Juan Dome area, which all suggest that it was deposited by a fluvial system characterized by migrating channels. Avulsion is considered a requisite process for such systems to form. However, the sedimentary architecture of the Ojo Alamo Sandstone does not provide the expected record of avulsive processes outlined above (Fig. 18). Reconciling the seeming necessity of avulsion in the system with the observed lack of well-defined avulsion deposits requires interpretation of the processes and products of the Ojo Alamo fluvial system. One possible cause, illustrated in Figure 19, is that the Ojo Alamo fluvial system did not undergo random avulsion in the typical sense. Fassett (1985) suggested that the Ojo Alamo Sandstone depositional system shifted eastward through time due to development of accommodation in that direction during the development of the Laramide foreland basin and uplifts (Fig. 19). This could explain the fining-eastward lithologic changes noted by Sikkink (1987). If overbank muds were stored preferentially at any one time on the east side of the fluvial system due to increased accommodation there, then perhaps they were subsequently removed when the channel belt shifted eastward. In this scenario, the only remnants of the overbank muds are the thin discontinuous mudstones observed among the channel belt deposits. The

abundant channel scours into and through muds (Fig. 6A) are evidence of mud removal during Ojo Alamo Sandstone deposition; perhaps this process was more important has been previously considered. Better constraints on west-east age relationships of the Ojo Alamo Sandstone are needed in order to develop this hypothesis more fully, but the Ojo Alamo Sandstone presents a case in which the prevailing accepted explanations for processes and products of avulsion in continental fluvial systems cannot be applied.

An alternative interpretation of the Ojo Alamo Sandstone is that it represents the deposits of roughly parallel coalescing alluvial systems draining the La Plata Magmatic Center, San Juan Dome, and/or Colorado Mineral Belt uplifts during an episode of rapid uplift. This interpretation is supported by the subparallel paleocurrent indicators of Powell (1973) and Sikkink (1987), perpendicular-to-paleoflow lithologic changes of Sikkink (1987), and thickness variation (Figs. 16 and 17) of the formation. The rapid uplift of a northerly source area would have provided an abundance of coarse material for south-flowing streams that rapidly filled accommodation space and bypassed most fines through the SJB. By the time of deposition of the overlying Nacimiento Formation, the sediment supply/accommodation ratio was lower, leading to accumulation of more fines.

CONCLUSIONS

The fluvial siliciclastic rocks bracketing the K-Pg boundary in the SJB record evidence of changing fluvial conditions during the development of a foreland basin. Petrographic and paleocurrent evidence records evolution of paleorivers' source area through the Late Cretaceous and Paleocene. The first rivers depositing sediment in the SJB after the retreat of the Cretaceous Interior Seaway flowed north-northeast and deposited the quartz sands of the Fruitland Formation. The high quartz content suggests

reworking of older sediments and little igneous or metamorphic material in the source area. By the Maastrichtian Age, the same north-northeast-flowing rivers deposited the arkosic sands of the Kirtland Formation, suggesting unroofing of igneous or crystalline metamorphic rock in their source areas southwest of the SJB. Reorganization of regional fluvial systems after deposition of most of the Kirtland Formation in the Maastrichtian resulted in removal of some early Maastrichtian and possibly upper Campanian fluvial sediments and a basin-wide erosional unconformity. This reorganization is likely related to the onset of a phase of Laramide deformation at ~67 Ma. By the beginning of the Paleocene, area paleorivers flowed south-southeast from the La Plata Magmatic Center/San Juan Uplift and through the SJB, depositing the arkosic sandstones and conglomerates of the Ojo Alamo Sandstone. The Ojo Alamo Sandstone's relative enrichment in potassium feldspar relative to plagioclase feldspar suggests a source area rich in potassium feldspar; the nearest known and most likely such area being the Needle Mountains of the western San Juan Uplift. Early- to middle-Paleocene sandstones of the Nacimiento Formation show similar paleocurrent indicators and mineralogic composition to the Ojo Alamo Sandstone. This petrographic information, combined with the interfingering depositional contact between the Ojo Alamo Sandstone and the Nacimiento Formation, suggest that the latter records the continuation of the same fluvial system(s) that deposited the former in an incipient and evolving broken foreland basin.

The Ojo Alamo Sandstone's occurs entirely within chron C29r, which gives it a maximum deposition duration of as little as 345 kyr and a sedimentation/subsidence rate of as high as 0.39 m/kyr. This sedimentation/subsidence rate is indicative of significant subsidence during the early Paleocene. Since the wide sandstone bodies that comprise the

majority of the Ojo Alamo Sandstone are associated with low accommodation/sediment supply ratios, the Ojo Alamo Sandstone must represent a period of high sediment supply during which predominately coarse sand and pebbles were deposited in the incipient SJB. Given the inclusion of detrital zircons from the La Plata Magmatic Center and the abundance of potassium feldspar presumably from crystalline basement rocks in the San Juan Uplift, this high sediment supply is likely related to the rapid development of topographic relief in the source area of the Ojo Alamo fluvial system. Finer sands and muds were bypassed through the system, possibly deposited in a more distal reach of the paleoriver system that since has been lost to uplift and erosion.

Standard sedimentary models of avulsion stratigraphy are not compatible with the sedimentary architecture observed in the Ojo Alamo Sandstone. The formation's high estimated sedimentation rates, predominance of coarse sands, and lack of paleosols provide little evidence of long-term landscape stability (*i.e.*, neither erosion nor deposition) in the fluvial system during the early Paleocene depositional interval. Because of this, evidence of avulsions (establishment of new fluvial channels in and/or on former floodplains) in the Ojo Alamo fluvial system are difficult to recognize. However, the formation's conformable relationship with the overlying formation, lateral continuity, and broad geographic distribution all suggest that it must have been deposited by a long-lived and spatially migrating fluvial system. A potential explanation that reconciles the absence of expected avulsion stratigraphy with the necessity of a spatially migrating fluvial system is that the system did not avulse with the typical compensation-driven processes associated with rivers in unconfined basins. Rather, the Ojo Alamo fluvial system potentially was driven unidirectionally eastward across the incipient SJB

by relatively increased uplift in the west, relatively increased subsidence in the east, or some combination of the two during the onset of a new phase of Laramide deformation in the earliest Paleocene. The observed lack of avulsion stratigraphy throughout most of the Ojo Alamo Sandstone alternatively could be explained by the interpretation that the formations represents not the deposits of one fluvial system but rather the coalesced deposits of multiple alluvial systems draining a rapidly uplifted northerly source area. Further work is needed regarding the timing of uplifts adjacent to the San Juan Basin in order better to constrain SJB depositional history and to inform understanding of relationships between tectonics and sedimentation.

REFERENCES CITED

Alexander, J., and Fielding, C.R., 2006, Coarse-grained floodplain deposits in the seasonal tropics: towards a better facies model: Journal of Sedimentary Research, v. 76, p. 539-556.

Anderson, R.Y., 1960, Cretaceous-Tertiary palynology, eastern side of the San Juan Basin, New Mexico: New Mexico Bureau of Mines and Mineral Resources Memoir 6, 59 p.

Bagnold, R.A., 1954, Experiments on the gravity-free dispersion of large solid spheres in a Newtonian fluid under shear: Proceedings of the Royal Society of London, v. 187A, p. 49-63.

Baltz, E.H., 1953, Stratigraphic relationships of Cretaceous and early Tertiary rocks of a part of northwestern San Juan Basin: M.S. thesis, University of New Mexico, 101 p.

---------, 1967, Stratigraphy and regional tectonic implications of part of Upper Cretaceous and Tertiary rocks, East-Central San Juan Basin, New Mexico: USGS Prof. Paper 552, 101 p.

Baltz, E.H., Ash, S.R., and Anderson, R.Y., 1966, History of nomenclature and stratigraphy of rocks adjacent to the Cretaceous-Tertiary boundary, western San Juan Basin, New Mexico: USGS Prof. Paper 524-D, 23 p.

Bauer, C.M., 1916, Contributions to the geology and paleontology of San Juan County, New Mexico, part I: Stratigraphy of a part of the Chaco River Valley: USGS Prof. Paper 98-P, p. 271-278.

Best, J.L., Ashworth, P.J., Bristow, C.S., and Roden, J., 2003, Three-dimensional sedimentary architecture of a large, mid-channel sand braid bar, Jamuna River, Bangladesh: Jou. Of Sedimentary Research, v. 73, p. 516-530.

Blum, M., and Pecha, M., 2014, Mid-Cretaceous to Paleocene North American drainage reorganization from detrital zircons: Geology, v. 42, n. 7, p. 607-610.

Bridge, J.S., 2003, Rivers and Floodplains: Forms, Processes, and Sedimentary Record: Blackwell Publishing, 491 p.

Bridge, J.S., and Best, J.L., 1988, Flow, sediment transport and bedform dynamics over the transition from upper-stage plane beds: implications for the formation of planar laminae: Sedimentology, v. 35, p. 753-763.

Bridge, J.S., and Best, J.L., 1997, Preservation of planar laminae arising from low-relief bed waves migrating over aggrading plane beds: comparison of experimental data with theory: Sedimentology, v. 44, p. 253-262.

Brown, B., 1910, The Cretaceous Ojo Alamo beds of New Mexico, with description of the new dinosaur genus *Kritosaurus*: American Museum of Natural History Bulletin, v. 28, p. 267-274.

Bush, M., Horton, B., Murphy, M., and Stockli, D., 2015, Provenance record of Paleogene exhumation and Laramide basin evolution along the southern Rocky Mountain front: American Geophysical Union Abstracts with Program,AGU Fall Meeting.

Butler, R.F., and Lindsay, E.H., 1985, Mineralogy of magnetic minerals and revised magnetic polarity stratigraphy of continental deposits, San Juan Basin, New Mexico: Journal of Geology, v. 93, p. 535-554.

Cain, S.A., & Mountney, N.P., 2011, Downstream changes and associated fluvial-aeolian interactions in an ancient terminal fluvial system: the Permian Organ Rock Formation, SE Utah, USA, *in* Davidson, S.K., Leleu, S., and North, C., eds., From River to Rock Record: The Preservation of Fluvial Sediments and Their Subsequent Interpretation: SEPM, Special Publication 97, p. 1-19.

---------, 2009, Spatial and temporal evolution of a terminalfluvial fan system: the Permian Organ Rock Formation, southeast Utah, USA: Sedimentology, v. 56, p. 1774-1800.

Cather, S.M., 2004, Laramide orogeny in central and northern New Mexico and southern Colorado, *in* Mack, G.H., and Giles, K.A., eds., The Geology of New Mexico: A Geologic History: New Mexico Geological Society Special Publication 11, p. 203-248.

Cather, S.M., Chapin, C.E., and Kelley, S.A., 2012, Diachronous episodes of Cenozoic erosion in southwestern North America and their relationship to surface uplift, paleoclimate, paleodrainage, and paleoaltimetry: Geosphere, v. 8, p. 1177-1206.

Cather, S.M., Connell, S.D., Chamberlin, R.M., McIntosh, W.C., Jones, G.E., Potochnik, A.R., Lucas, S.G., and Johnson, P.S., 2008, The Chuska erg: Paleogeomorphic and paleoclimatic implications of an Oligocene sand sea on the Colorado Plateau: GSA Bulletin, v. 120, p. 13-33.

Clemens, W.A., 1973, The roles of fossil vertebrates in interpretation of Late Cretaceous stratigraphy of the San Juan Basin, New Mexico, *in* Fassett, J.E., ed., Cretaceous and Tertiary rocks of the southern Colorado Plateau: Four Corners Geological Society Memoir, p. 154-167.

Condon, S. M., 1990, Geologic and structure contour map of the Southern Ute Indian Reservation and adjacent areas, southwestern Colorado and northwest New Mexico: United States Geological Survey Miscellaneous Investigations Series Map I-1958, 1:100,000 scale.

Covault, J.A., Romans, B.W., Fildani, A., McGann, M., and Graham, S.A., 2010, Rapic climatic signal propagation from source to sink in a southern California sediment-routing system: Journal of Geology, v. 118, p. 247-259.

Dane, C.H., 1936, The La Ventana-Chacra Mesa coal field, part 3 of Geology and fuel resources of the southern part of the San Juan Basin, New Mexico: USGS Bulletin 860-C, p. 81-161.

Dickinson, W.R., 2013, Rejection of the lake spillover model for initial incision of the Grand Canyon, and discussion of alternatives: Geosphere, v. 9, no. 1, p. 1-20.

Dickinson, W.R., Lawton, T.F., Pecha, M., Davis, S.J., Gehrels, G.E. and Young, R.A., 2012, Provenance of the Paleogene Colton Formation (Uinta Basin) and the Cretaceous-Paleogene provenance evolution in the Utah foreland: Evidence from U-Pb ages of detrital zircons, paleocurrent trends, and sandstone petrofacies: Geosphere, v. 8, no. 4, p.1-27.

Dickinson, W.R., Klute, M.A., Hayes, M.J., Janecke, S.U., Lundin, E.R., McKittrick, M.A., and Olivares, M.D., 1988, Paleogeographic and paleotectonic setting of Laramide sedimentary basins in the central Rocky Mountain region: GSA Bulletin, v. 100, p. 1023-1039.

Donahue, M.S., 2016, Episodic uplift of the Rocky Mountains: Evidence from U-Pb detrital zircon geochronolgy and low-temperature thermochronology with a

chapter on using mobile technology for geoscience education: Ph.D. Dissertation, University of New Mexico, Albuquerque, 1177 p.

Fassett, J.E., 1966, Geologic Map of the Mesa Portales Quadrangle, Sandoval County, New Mexico: USGS GQ-590, 1:24,000 scale.

---------, 1973, The saga of the Ojo Alamo Sandstone or the rock-stratigrapher and the paleontologist should be friends, *in* Fassett, J.E., ed., Cretaceous and Tertiary rocks of the southern Colorado Plateau: Four Corners Geological Society Memoir, p. 123-130.

---------, 1974, Cretaceous and Tertiary rocks of the eastern San Juan Basin, New Mexico and Colorado, *in* Siemers, C.T., ed., Ghost Ranch (Central-Northern New Mexico): New Mexico Geological Society Guidebook, 25th Field Conference, p. 225-230.

---------, 1985, Early Tertiary paleogeography and paleotectonics of the San Juan Basin area, New Mexico and Colorado, *in* Kaplan, S.S., and Flores, R.M., eds., Cenozoic paleogeography of the west-central United States: Society of Economic Paleontologists and Mineralogists, Rocky Mountain Section, Rocky Mountain Paleogeography Symposium III, P. 317-334.

--------, 1988, Geometry and depositional environment of Fruitland Formation coal beds, San Juan basin, New Mexico and Colorado---Anatomy of a giant coal-bed methane deposit, *in* Fassett, J.E., ed., Geology and coal-bed methane resources in the northern San Juan basin, Colorado and New Mexico: Rocky Mountain Association of Geologists, p. 23-38.

---------, 2000, Geology and coal resources of the Upper Cretaceous Fruitland Formation, San Juan Basin, New Mexico and Colorado, *in* Kirschbaum, M.A., Roberts, L.N.R., and Biewick, L.H.R., eds., Geologic Assessment of Coal in the Colorado Plateau: Arizona, Colorado, New Mexico, and Utah, Chapter Q: USGS Prof. Paper 1625-B, CD-ROM.

--------, 2009, New geochronologic and stratigraphic evidence confirms the Paleocene age of the dinosaur-bearing Ojo Alamo Sandstone and Animas Formation in the San Juan Basin, New Mexico and Colorado: Palaeontologia Electronica, v. 12, no. 1, 146 p. (online pub. at http://palaeo-electronica.org/splash/index12_1.html).

Fassett, J.E., Heaman, L.M., and Simonetti, A., 2011, Direct U-Pb dating of Cretaceous and Paleocene dinosaur bones, San Juan Basin, New Mexico: Geology, v. 39, n. 2, p. 159-162.

Fassett, J.E., Zielinski, R.A., and Budahn, J.R., 2002, Dinosaurs that did not die: Evidence for Paleocene dinosaurs in the Ojo Alamo Sandstone, San Juan Basin, New Mexico, *in* Koeberl, C., and MacLeod, K.G., eds., Catastrophic Events and Mass Extinctions: Impacts and Beyond: Boulder, Colorado, Geological Society of America Special Paper 356, p. 307-336.

Fenneman, N.M., and Johnson, D.W., 1946, Physiographic divisions of the United States: U.S.G.S. Map, 1:7,000,000 scale.

Fielding, C.R., Ashworth, P.J., Best, J.L., Prokocki, E.W., Sambrook Smith, G.H., 2012, Tributary, distributary and other fluvial patters: What *really* represents the norm in the continental rock record?: Sedimentary Geology, v. 261-262, p. 15-32.

Flynn, A., Peppe, D., Abbuhl, B., and Williamson, T., 2014, Early Paleocene floras from the San Juan Basin, New Mexico, USA: Implications for local and regional responses to the Cretaceous-Paleogene extinction event: Geological Society of America Abstracts with Programs, V. 46, n. 6, p. 757.

Folk, R.L., 1957, Petrology of Sedimentary Rocks: Hemphill Publishing, Austin, Texas, 111 p.

Friend, P.F., Slater, M.J., and Williams, R.C., 1979, Vertical and lateral building of river sandstone bodies, Ebro Basin, Spain: Geological Society of London Journal, V. 136, p. 39-46.

Galloway, W.E., Whiteaker, T.L., and Ganey-Curry, P., 2011, History of Cenozoic North American drainage basin evolution, sediment yield, and accumulation in the Gulf of Mexico basin: Geosphere, v. 7, n. 4, p. 938-973.

Gibling, M.R., 2006, Width and thickness of fluvial channel bodies and valley fills in the geological record: a literature compilation and classification: Jou. Of Sedimentary Research, v. 76, p. 731-770.

Gonzales, D.A., 2010, The enigmatic Late Cretaceous McDermott Formation: New Mexico Geological Society Guidebook, 61st Field Conference, Four Corners Country, p. 157-162.

Gough, L.P., and Severson, R.C., 1981, Biogeochemical variability of plants at native and altered sites, San Juan Basin, New Mexico: U.S. Geological Survey Professional Paper 1134-D, 34 p.

Guccione, M.J., 1993, Grain size distribution of overbank sediment and its use to locate channel position, *in* Marzo, M., and Puigdefabregas, C., eds., Alluvial Sedimentation: International Association of Sedimentologists, Special Publication 17, p. 185-194.

Gulliford, A.R., Flint, S.S., and Hodgson, D.M., 2014, Testing applicability of models of distributive fluvial systems or trunk rivers in ephemeral systems: reconstructing 3-D fluvial architecture in the Beaufort Group, South Africa: Journal of Sedimentary Research, v. 84, p. 1147-1169.

Hajek, E.A., Heller, P.L., and Sheets, B.A., 2010, Significance of channel-belt clustering in alluvial basins: Geology, v. 38, p. 535-538.

Hajek, E.A., and Edmonds, D.A., 2014, Is river avulsion style controlled by floodplain morphodynamics?; Geology, v. 42, p. 199-202.

Hartley A.J., Weissmann G.S., Nichols G.J., Warwick G.L., 2010, Large distributive fluvial systems: characteristics, distribution and controls on development: Journal of Sedimentary Research, v. 80, p. 167–183.

Heller, P.L., Mathers, G., Dueker, K., and Foreman, B., 2012, Far-traveled latest Cretaceous-Paleocene conglomerates of the Southern Rocky Mountains, USA: Record of transient Laramide tectonism: GSA Bulletin, v. 125, n. 3-4, p. 490-498.

Heller, P.L., Dueker, K.G., and McMillan, M.E., 2003, Post-Paleozoic alluvial gravel transport as evidence of continental tilting in the U.S. Cordillera: GSA Bulletin, v. 115, p. 1122-1132.

Heller, P.L., and Paola, C., 1996, Downstream changes in alluvial architecture: An exploration of controls on channel-stacking patterns, Journal of Sedimentary Research, v. 66, p. 297-306.

Hobbs, K.M., and Fawcett, P.J., 2014, Relationships between paleosols and paleoenvironments in Paleocene (Danian-Selandian) fluvial sedimentary rocks of the San Juan Basin, New Mexico: Geological Society of America Abstracts with Programs, v. 46, n. 6, p. 354.

Holbrook, J.M., Scott, R.W., and Oboh-Ikuenobe, F.E., 2006, Base-level buffers and buttresses: a model for upstream vs. downstream control on preservation of fluvial geometry and architecture within sequences: Journal of Sedimentary Research, v. 76, p. 162-174.

Huerta, P., Armenteros, I., and Silva, P.G., 2011, Large-scale architecture in non-marine basins: the response to the interplay between accommodation space and sediment supply: Sedimentology, v. 58, p. 1716-1736.

Jones, H.L., and Hajek, E.A., 2007, Characterizing avulsion stratigraphy in ancient alluvial deposits: Sedimentary Geology, v. 202, p. 124-137.

Kjemperud, A.V., Schomacker, E.R., and Cross, T.A., 2008, Architecture and stratigraphy of alluvial deposits, Morrison Formation (Upper Jurassic), Utah: AAPG Bulletin v. 92, p. 1055-1076.

Klausen, T.G., Ryseth, A.E., Helland-Hansen, W., Gawthorpe, R., and Laursen, I., 2015, Regional development and sequence stratigraphy of the Middle to Late Triassic Snadd Formation, Norwegian Barents Sea: Marine and Petroleum Geology, v. 62, p. 102-122.

---------, 2014, Spatial and temporal changes in geometries of fluvial channel bodies from the Triassic Snadd Formation of offshore Norway: Journal of Sedimentary Research, v. 84, p. 567-585.

Klute, M.A., 1986, Sedimentology and sandstone petrography of the upper Kirtland Formation and Ojo Alamo Sandstone, Cretaceous-Tertiary boundary, western and southern San Juan Basin, New Mexico: American Journal of Science, v. 286, p. 463-488.

Kraus, M.J., and Gwinn, B., 1997, Facies and facies architecture of Paleogene floodplain deposits, Willwood Formation, Bighorn Basin, Wyoming, USA: Sedimentary Geology, v. 114, p. 33-54.

Kraus, M.J., and Wells, T.M., 1999, Recognizing avulsion deposits in the ancient stratigraphic record, *in* Smith, N.D., and Rogers, J., eds., Fluvial Sedimentology VI, Special Publication of the International Association of Sedimentologists, v. 28, p. 251-268.

Kukulski, R.B., Hubbard, S.M., Moslow, T.F., and Raines, M.K., 2013, Basin-scale stratigraphic architecture of upstream fluvial deposits: Jurassic-Cretaceous foredeep, Alberta Basin, Canada: Journal of Sedimentary Research, v. 83, p. 704-722.

Latrubesse, E.M., 2015, Large rivers, megafans and other Quaternary avulsive fluvial systems: a potential "who's who" in the geological record: Earth Sci. Rev., v. 146, p. 1-30.

Leipzig, M.R., 1982, Stratigraphy, sedimentation and depositional environments of the Late Cretaceous Pictured Cliffs Sandstone, Fruitland Formation, Kirtland Shale, and Early Tertiary Ojo Alamo Sandstone, Eastern San Juan Basin, New Mexico: Milwaukee, Wisconsin, University of Wisconsin-Milwaukee Master's Thesis, 141 p.

Lindsay, E.H., Butler, R.F., and Johnson, N.M., 1981, Magnetic polarity of Late Cretaceous and Paleocene continental deposits, San Juan Basin, New Mexico: American Journal of Science, V. 281, P. 390-435.

Lindsay, E.H., Jacobs, L.L., and Butler, R.F., 1978, Biostratigraphy and magnetostratigraphy of Paleocene terrestrial deposits, San Juan Basin, New Mexico: Geology, v. 6, p. 425-429.

Lorraine, M.M., and Gonzales, D.A., 2003, Lahars or not lahars? An evaluation of the volcanic connection for the late Cretaceous McDermott Formation near Durango, Colorado: Geological Society of America Rocky Mountain Section Meeting, abstract no. 13-3.

Lucas, S.G., Hunt, A.P., and Sullivan, R.M. 2006. Stratigraphy and age of the Upper Cretaceous Fruitland Formation, west-central San Juan Basin, New Mexico. New Mexico Museum of Natural History and Science Bulletin v. 35, p. 1-6.

Lucas, S.G., Sullivan, R.M., Cather, S.M., Jasinski, S.E., Fowler, D.W., Heckert, A.B., Speilmann, J.A., and Hunt, A.P., 2009, No definitive evidence of Paleocene dinosaurs in the San Juan Basin: Paleontologia Electronica, v. 12, 10 p.

Mackey, G.N., Horton, B.K., and Milliken, K.L., 2012, Provenance of the Paleocene-Eocene Wilcox Group, western Gulf of Mexico basin: Evidence for integrated drainage of the southern Laramide Rocky Mountains and Cordilleran arc: GSA Bulletin, v. 124, n. 5-6, p. 1007-1024.

Mason, I.P., Heizler, M.T., and Williamson, T.E., 2013, $^{40}Ar/^{39}Ar$ sanidine chronostratigraphy of K-Pg boundary sediments of the San Juan Basin, NM: Geological Society of America, Rocky Mountain Section, Abstracts with Programs, v. 45, n. 5, p. 33.

Miall, A.D., 1978, Lithofacies types and vertical profile models in braided river deposits: a summary, *in* Miall, A.D., ed., Fluvial Sedimentology: Canadian Society of Petroleum Geologists, Memoir 5, p. 597-604.

---------, 1981, Analysis of fluvial depositional systems: AAPG Education Note Series, n. 20, 75 p.

---------, 1996, The Geology of Fluvial Deposits: Sedimentary Facies, Basin Analysis, and Petroleum Geology: Berlin, Springer-Verlag, 582 p.

Milner, M.K., Johnson, C., and Bereskin, S.R., 2005, Interpretation of the Paleocene-Eocene sequence boundary, northwest San Juan Basin, New Mexico: The Mountain Geologist, v. 42, n. 1, p. 11-22.

Newman, K.R., 1987, Biostratigraphic correlation of Cretaceous-Tertiary rocks, Colorado and San Juan Basin, New Mexico, *in* Fassett, J.E., and Rigby, J.K., Jr., eds., The Cretaceous-Tertiary boundary in the San Juan and Raton Basins, New Mexico and Colorado: Geological Society of America Special Paper 209, p. 151-164.

Nichols, G.J., and Fisher, J.A., 2007, Processes, facies and architecture of fluvial distributary system deposits: Sedimentary Geology, v. 195, p. 75-90.

O'Shea, C.O., 2009, Volcanic influence over fluvial sedimentation in the Cretaceous McDermott Member, Animas Formation, southwestern Colorado: Bowling Green, Ohio, Bowling Green State University Master's Thesis, 90 p.

O'Sullivan, R.B., Repenning, C.A., Beaumont, E.C., and Page, H.G., 1972, Stratigraphy of the Cretaceous rocks and Tertiary Ojo Alamo Sandstone, Navajo and Hopi Reservations, Arizona, New Mexico, and Utah: USGS Prof. Paper 521-E, p. 1-65.

Owen, A., Jupp, P.E., Nichols, G.J., Hartley, A.J., Weissmann, G.S., and Sadykova, D., 2015a, Statistical estimation of the position of an apex: application to the geologic record: Journal of Sedimentary Research, v. 85, p. 142-152.

Owen, A., Nichols, G.J., Hartley, A.J., Weissmann, G.S., and Scuderi, L.A., 2015b, Quantification of a distributive fluvial system: the Salt Wast DFS of the Morrison Formation, SW USA: Journal of Sedimentary Research, v. 85, p. 544-561.

Paola, C., Heller, P.L., and Angevine, C.L., 1992, The large-scale dynamics of grain-size viriation in alluvial basins, 1: Theory: Basin Research, v. 4, p. 73-90.

Peppe, D.J., Heizler, M.T., Williamson, T.E., Mason, I.P., Brusatte, S.L., Weil, A., and Secord, R., 2013, New age constraints on Late Cretaceous through early Paleocene age rocks in the San Juan Basin, New Mexico: Geological Society of America, Abstracts with Programs, v. 45, n. 7, p. 290.

Pizzuto, J.E., 1987, Sediment diffusing during overbank flows: Sedimentology, v. 34, p. 301-317.

Potochnik, A.R., 1989, Depositional style and tectonic implications of the Mogollon Rim Formation (Eocene), east-central Arizona, *in* Anderson, O.J., Lucas, S.G., Love, D.W., and Cather, S.M., eds., Southeastern Colorado Plateau: New Mexico Geological Society 40th Annual Field Conference Guidebook, p. 107–118.

Powell, J.S., 1973, Paleontology and sedimentation models of the Kimbeto Member of the Ojo Alamo Sandstone, *in* Fassett, J.E., ed., Cretaceous and Tertiary rocks of the southern Colorado Plateau: Four Corners Geological Society Memoir, p. 111-122.

Reeside, J.B., Jr., 1924, Upper Cretaceous and Tertiary formations of the western part of the San Juan Basin, Colorado and New Mexico: USGS Prof. Paper 134, 117 p.

Ridgley, J.L., Condon, S.M., and Hatch, J.R., 2013, Geology and oil and gas assessment of the Fruitland Total Petroleum System, San Juan Basin, New Mexico and Colorado, chap. 6 of U.S. Geological Survey San Juan Basin Assessment Team, Total petroleum systems and geologic assessment of undiscovered oil and gas resources in the San Juan Basin Province, exclusive of Paleozoic rocks, New Mexico and Colorado: U.S. Geological Survey Digital Data Series 69–F, p. 1–100.

Roberts, L.N.R., and Kirschbaum, M.A., 1995, Paleogeography of the Late Cretaceous of the wesern interior of middle North America: coal distribution and sediment accumulation: U.S. Geological Survey Professional Paper 1561, 115 p.

Robinson, J.W., and McCabe, P.J., 1998, Evolution of a braided river system: the Salt Wash Member of the Morrison Formation (Jurassic) in southern Utah, *in* Shanley, K.W., and McCabe, P.J., eds., Relative Role of Eustasy, Climate, and Tectonism in Continental Rocks: SEPM, Special Publication 59, p. 93-107.

Russell, C.S., 2009, Ojo Alamo Sandstone Geology: Four Corners Geological Society, 16 p.

Sallenger, A., 1979, Inverse grading and hydraulic equivalence in grain-flow deposits: Journal of Sedimentary Petrology, v. 49, p. 553-562.

Schumm, S.A., 1960, The effect of sediment type on the shape and stratification of some modern fluvial deposits: Am. Jour. of Sci., v. 258, p. 177-184.

Shanley, K.W., & McCabe, P.J., 1994, Perspectives on the sequence stratigraphy of continental strata: American Association of Petroleum Geologists Bulletin, v. 78, p. 544-568.

Sheets, B., Hickson, T.A., and Paola, C., 2002, Assembling the stratigraphic record: Depositional patterns and time-scales in an experimental alluvial basin: Basin Research, v. 14, p. 287-301.

Shukla, U.K., Singh, I.B., Sharma, M., and Sharma, S., 2001, A model of alluvial megafan sedimentation: Ganga Megafan: Sedimentary Geology, v. 144, p. 243-262.

Sikkink, P.G.L., 1987, Lithofacies relationships and depositional environment of the Tertiary Ojo Alamo Sandstone and related strata, San Juan Basin, New Mexico and Colorado, *in* Fassett, J.E., and Rigby, J.K., Jr., eds., The Cretaceous-Tertiary Boundary in the San Juan and Raton Basins, New Mexico and Colorado: GSA Special Paper 209, p. 81-104.

Sinclair, W.J., & Grainger, W., 1914, Paleocene deposits of the San Juan Basin, New Mexico: American Museum of Natural History Bulleting, v. 33, p. 297-316.

Slingerland, R., and Smith, N.D., 2004, River avulsions and their deposits: Annu. Rev. Earth Planetary Sci., v. 32, p. 257-285.

Smith, L.N., 1988, Basin analysis of the lower Eocene San Jose Formation, San Juan Basin, New Mexico and Colorado: Albuquerque, New Mexico, University of New Mexico Ph.D. Dissertation, 166 p.

---------, 1992, Upper Cretaceous and Paleogene stratigraphy and sedimentation adjacent to the Nacimiento Uplift, southeastern San Juan Basin, New Mexico: New Mexico Geological Society Guidebook, v. 43, p. 251-256.

Smith, N.D., Cross, T.A., Duffey, J.P., and Clough, S.R., 1989, Anatomy of an avulsion: Sedimentology, v. 36, p. 1-23.

Sprain, C.J., Renne, P.R., Wilson, G.P., and Clemens, W.A., 2015, High-resolution chrnostratigraphy of the terrestrial Cretaceous-Paleogene transition and recovery interval in the Hell Creek region, Montana: GSA Bulletin, v. 127, p. 393-409.

Steven, T.A., Lipman, P.W., Hall, W.J., Barker, F., and Luedke, R.G., 1974, Geologic map of the Durango quadrangle, southwestern Colorado: USGS I-764, 1:250,000 scale.

Sullivan, R.M., Lucas, S.G., and Braman, D.R., 2005, Dinosaurs, pollen, and the Cretaceous-Tertiary boundary in the San Juan Basin, New Mexico: New Mexico Geological Society 56th Field Conference Guidebook, p. 395-407.

Wang, Y., Straub, K.M., and Hajek, E.A., 2011, Scale-dependent compensational stacking: An estimate of autogenic time scales in channelized sedimentary deposits: Geology, v. 38, p. 811-814.

Wegert, D., and Parker, D.F., 2011, Petrogenesis of the McDermott Formation trachyandesite, San Juan basin, Colorado and New Mexico: Rocky Mountain Geology, v. 46, n. 2, p. 183-196.

Weissmann, G.S., Hartley, A.J., Nichols, G.J., Scuderi, L.A., Olsen, M., Buehler, H., and Banteah, R., 2010, Fluvial form in modern continental sedimentary basins: distributive fluvial systems: Geology, v. 38, p. 39-42.

Weissmann, G.S., Hartley, A.J., Scuderi, L.A., Nichols, G.J., Davidson, S.K., Owen, A., Atchley, S.C., Bhattacharyya, P., Chakraborty, T., Ghosh, P, Nordt, L.C., Michel, L., and Tabor, N.J., 2013, Prograding distributive fluvial systems: geomorphic models and ancient examples, *in* Dreise, S.G., Nordt, L.C., and McCarthy, P.L, eds., New Frontiers in Paleopedology and Terrestrial Paleoclimatology, SEPM, Special Publication 104, p. 131-147.

Weissmann, G.S., Hartley, A.J., Scuderi, L.A., Nichols, G.J., Owen, A., Wright, S., Felicia, A.L., Holland, F., and Anaya, F.M.L., 2015, Fluvial geomorphic elements in modern sedimentary basins and their potential preservation in the rock record: A review: Geomorphology, v. 250, p. 187-219.

Williamson, T.E., 1996, The beginning of the age of mammals in the San Juan Basin, New Mexico: Biostratigraphy and evolution of Paleocene mammals of the Nacimiento Formation: New Mexico Museum of Natural History and Science, Bulletin 8, 141 p.

Williamson, T.E., and Lucas, S.G., 1992, Stratigraphy and mammalian biostratigraphy of the Paleocene Nacimiento Formation, southern San Juan Basin, New Mexico: New Mexico Geological Society Guidebook, v. 43, p. 265-296.

Williamson, T.E., and Weil, A., 2008, Metatherian mammals from the Naashoibito Member, Kirtland Formation, San Juan Basin, New Mexico and their biochronologic and paleobiogeographic significance: Journal of Vertebrate Paleontology, v. 28, no. 3, p. 803-815.

Williamson, T.E., Peppe, D.J., Heizler, M.T., Brusatte, S.L., and Secord, R., 2014, Chronostratigraphy of the Cretaceous-Paleogene transition in the San Juan Basin,

northwestern New Mexico: Journal of Vertebrate Paleontology, Program and Abstracts, v. 2014, p. 215-216.

Woodward, L.A., McLelland, D., Anderson, J.B., and Kaufman, W.H., 1972, Geologic map of the Cuba Quadrangle, Sandoval County, New Mexico: New Mexico Bureau of Mines and Mineral Resources, GM-25, 1:24,000 scale.

FIGURES

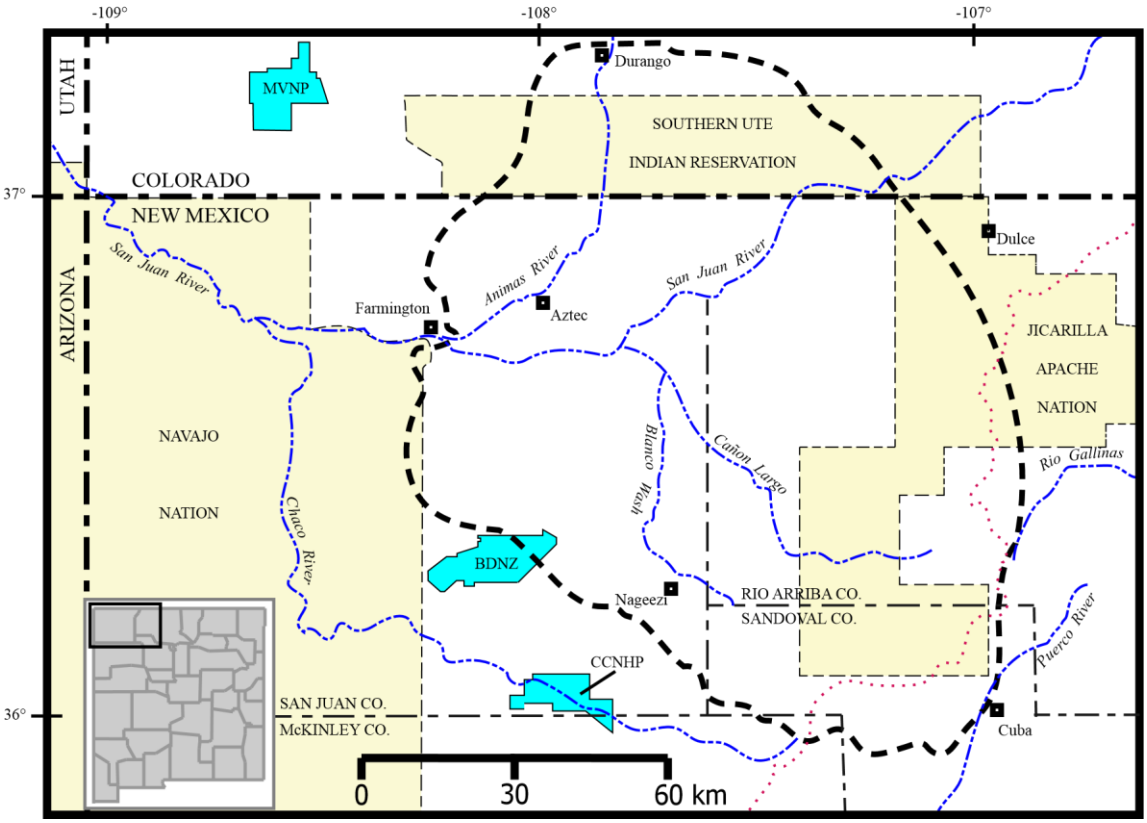

Figure 1. Location map of study area. Thick dashed line marks the approximate lower contact of Paleogene sedimentary rocks in the San Juan Basin. Red dotted line marks the present-day continental divide. Inset map shows location within New Mexico. BDNZ = Bisti De-Na-Zin Wilderness Area; CCNHP = Chaco Culture National Historical Park; MVNP = Mesa Verde National Park.

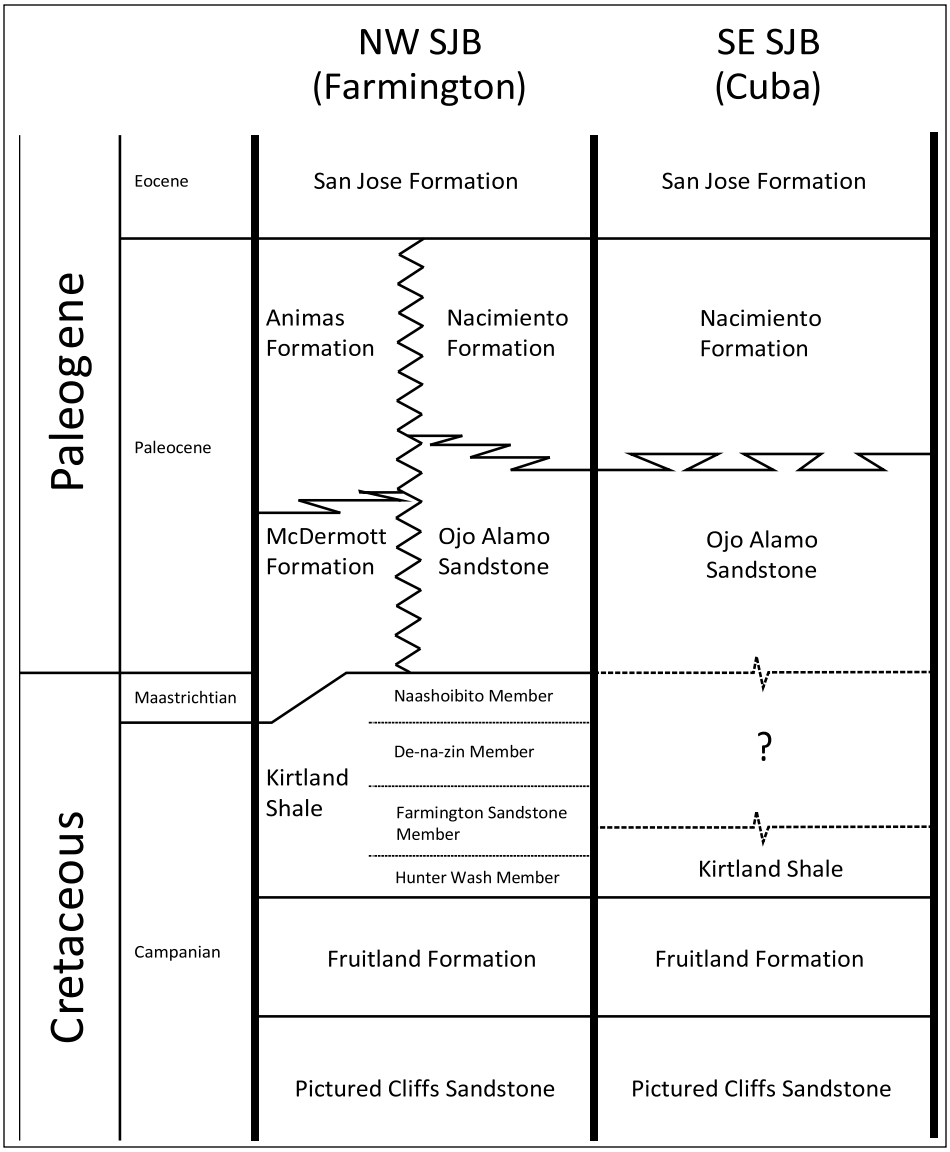

Figure 2. Generalized stratigraphic column of upper Cretaceous and Paleogene units in the San Juan Basin.

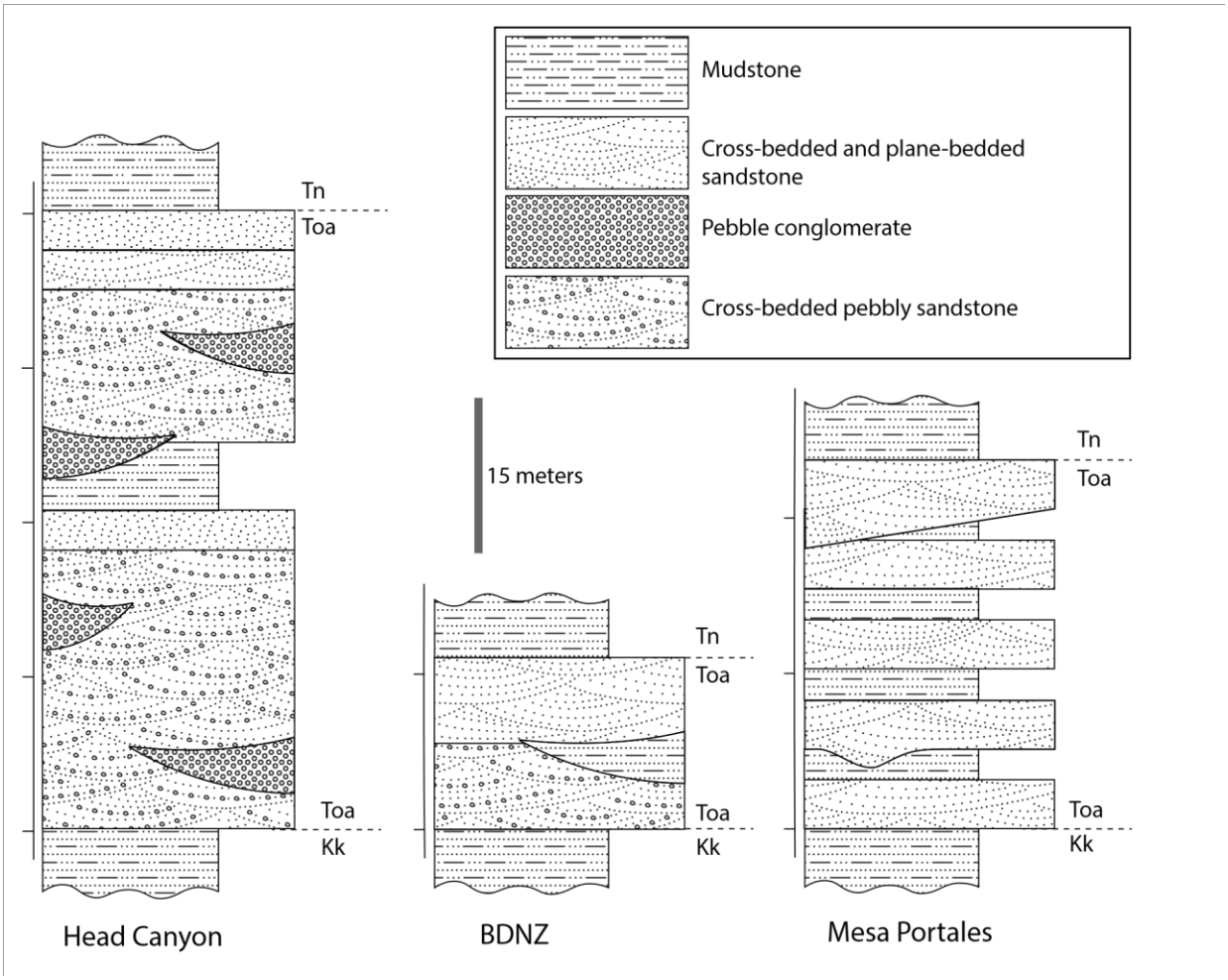

Figure 3. Generalized stratigraphic sections and major lithofacies at three representative Ojo Alamo Sandstone outcrop areas.

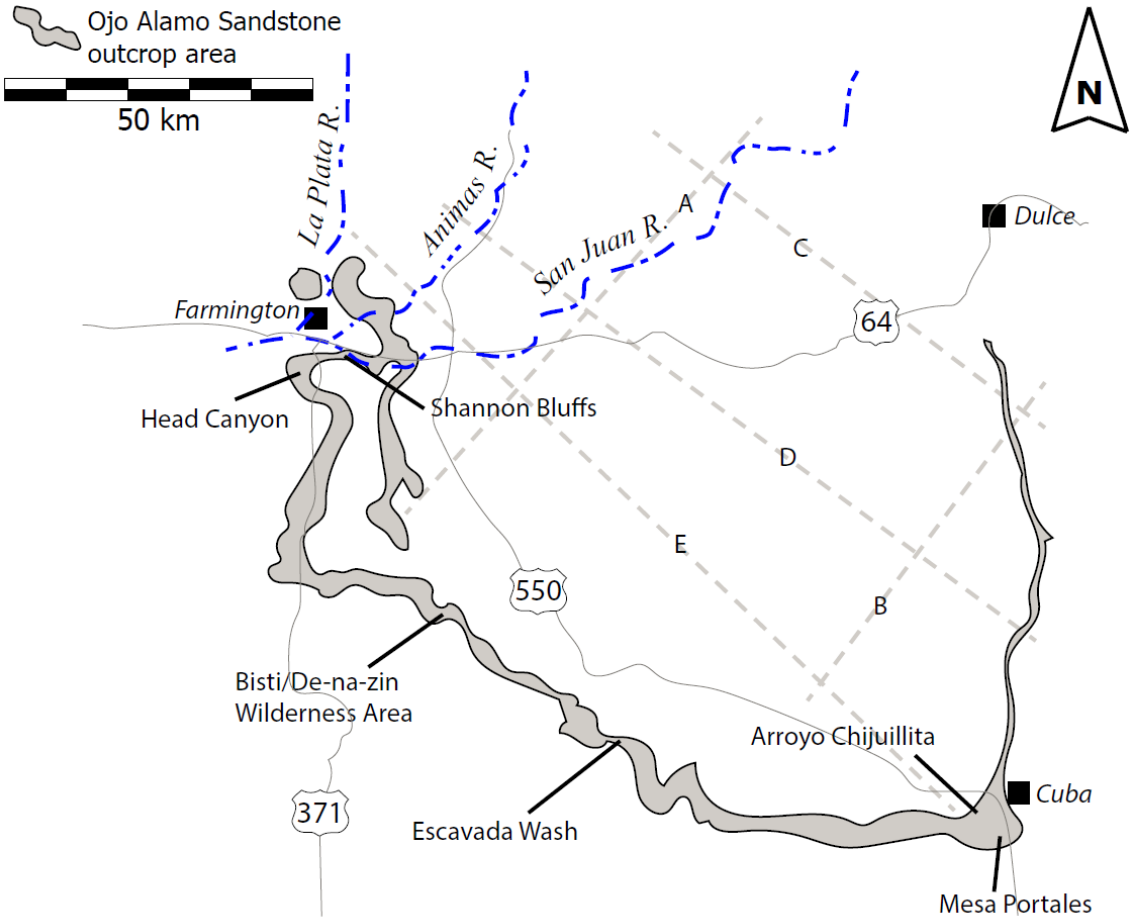

Figure 4. Location map of selected study sites and cross-section lines within the Ojo Alamo Sandstone outcrop area, San Juan Basin, New Mexico.

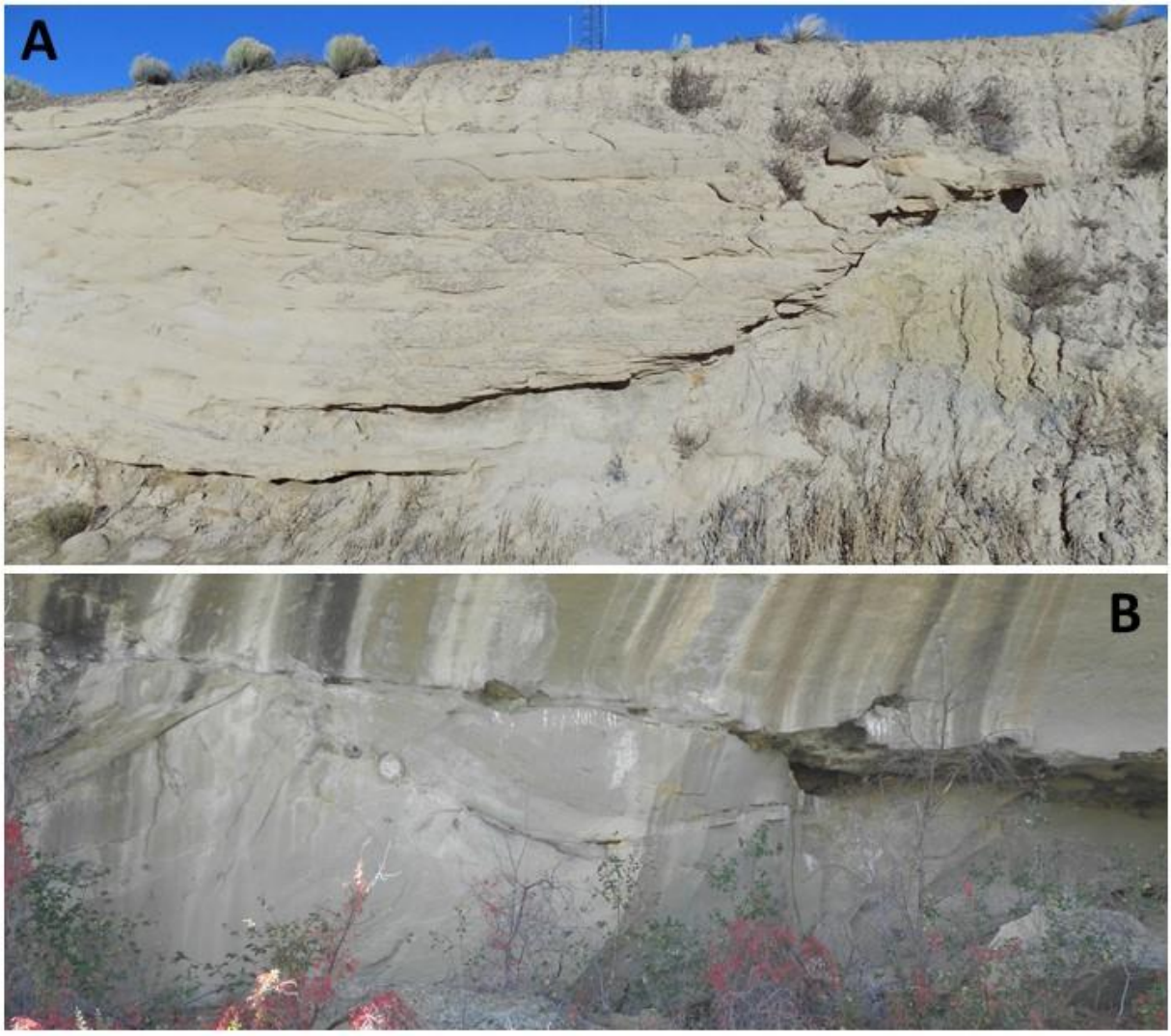

Figure 5. Cut-and-fill structures in the Ojo Alamo sandstone. A: Complex 1.2 m thick structure cut into intraformational mudstone 2 km southwest of Farmington, New Mexico. B: Simple 1.1 m thick structure cut into, filled with, and overlain by medium-grained sandstone, Arroyo Chijuilla, New Mexico.

Figure 6. Overbank floodplain deposits of the Ojo Alamo Sandstone (outlined in yellow; partially obscured by boulder talus) truncated by medium-grained channel sandstone. Note the wide shelf at left formed by retreat of sandstone overlying mudstone; shelf is absent at right and the vertically-stacked sandstone bodies form a continuous subvertical exposure. Kinaird Arroyo, New Mexico. Scale varies; sandstone bodies are 5-9 m thick.

Figure 7. Succession of vertical faces of channel sandstone and vegetated slopes of overbank mudstones within the Ojo Alamo Sandstone. Mesa Portales, New Mexico. Scale varies; sandstone bodies are 4-12 m thick.

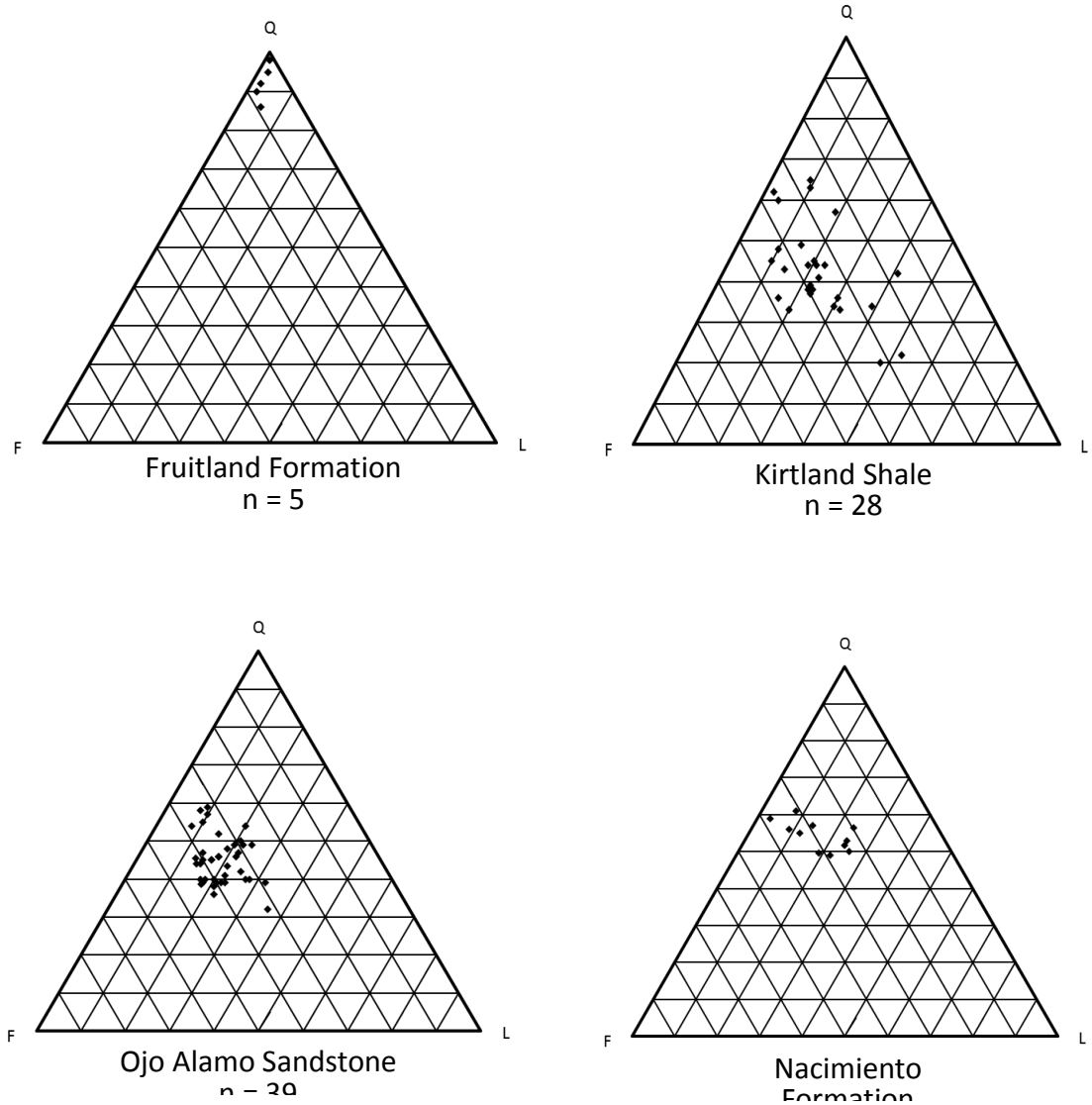

Figure 8. Ternary diagrams showing composition of detrital grains of San Juan Basin K/Pg sandstones.

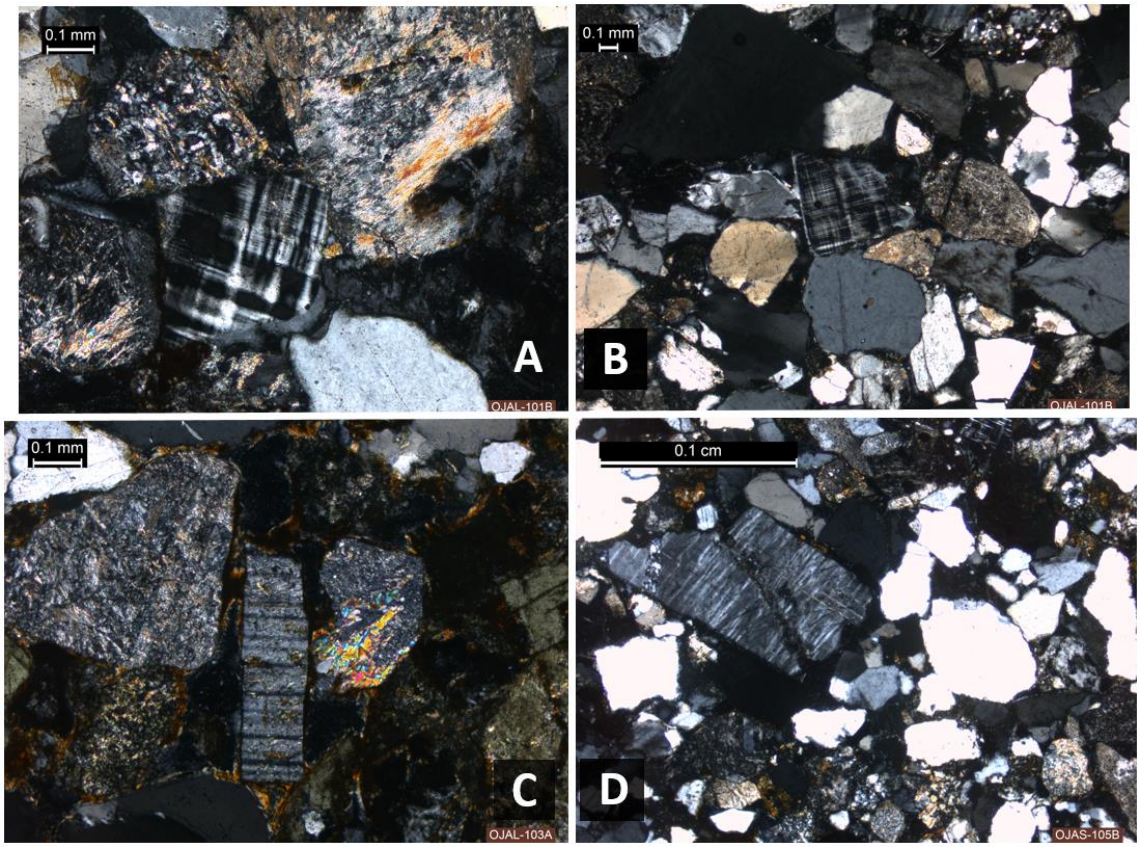

Figure 9. Feldspars from the Ojo Alamo Sandstone. A: Unaltered microcline surrounded by sericitized feldspars and quartz. B: Unaltered microcline, polycrystalline quartz, monocrystalline quartz, lithic grains, and untwinned feldspars. C: Angular plagioclase feldspar showing albite twinning and minor sericitization (center), subangular plagioclase feldspar showing relict albite twinning and sericitization (upper left), and subangular sericitized feldspar (right of center), all with iron oxide staining on grain boundaries. D: Angular unaltered untwinned feldspar with exsolution lamellae (NE-SW), polycrystalline quartz, monocrystalline quartz, lithic grains, and untwinned feldspars.

Figure 10. Relative proportions of plagioclase feldspar and potassium feldspar from sandstones of the Kirtland Shale and Ojo Alamo Sandstone.

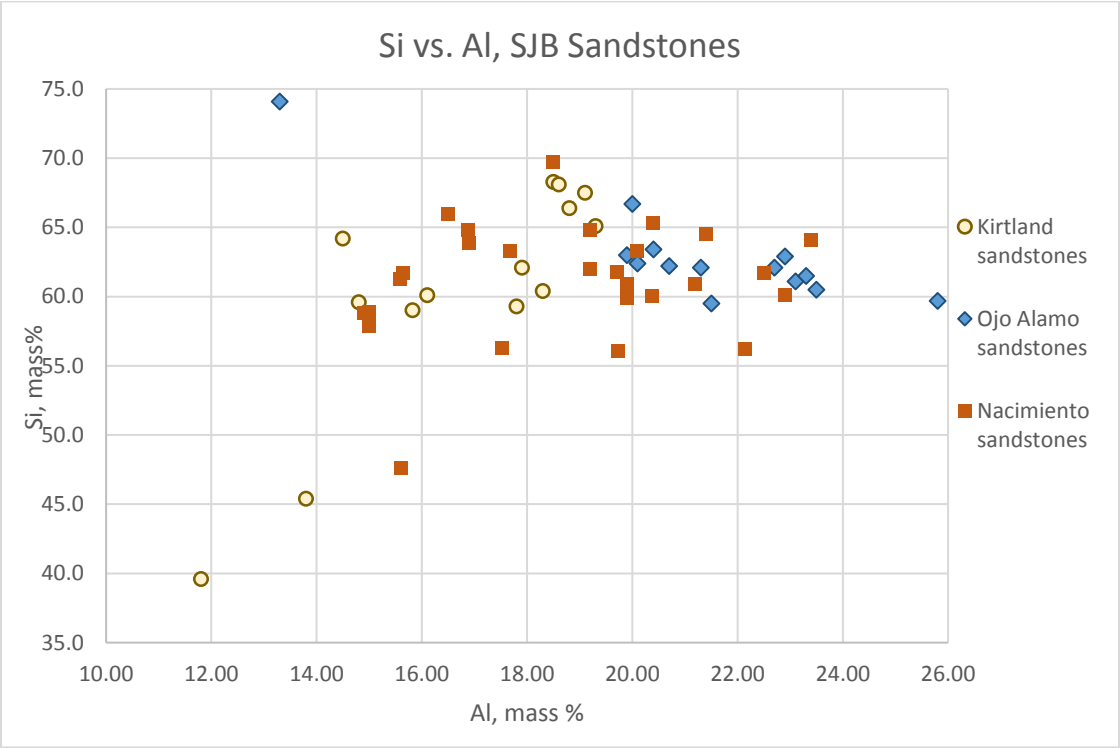

Figure 11. Si/Al ratios for sandstones from Kirtland Shale, Ojo Alamo Sandstone, and Nacimiento Formation.

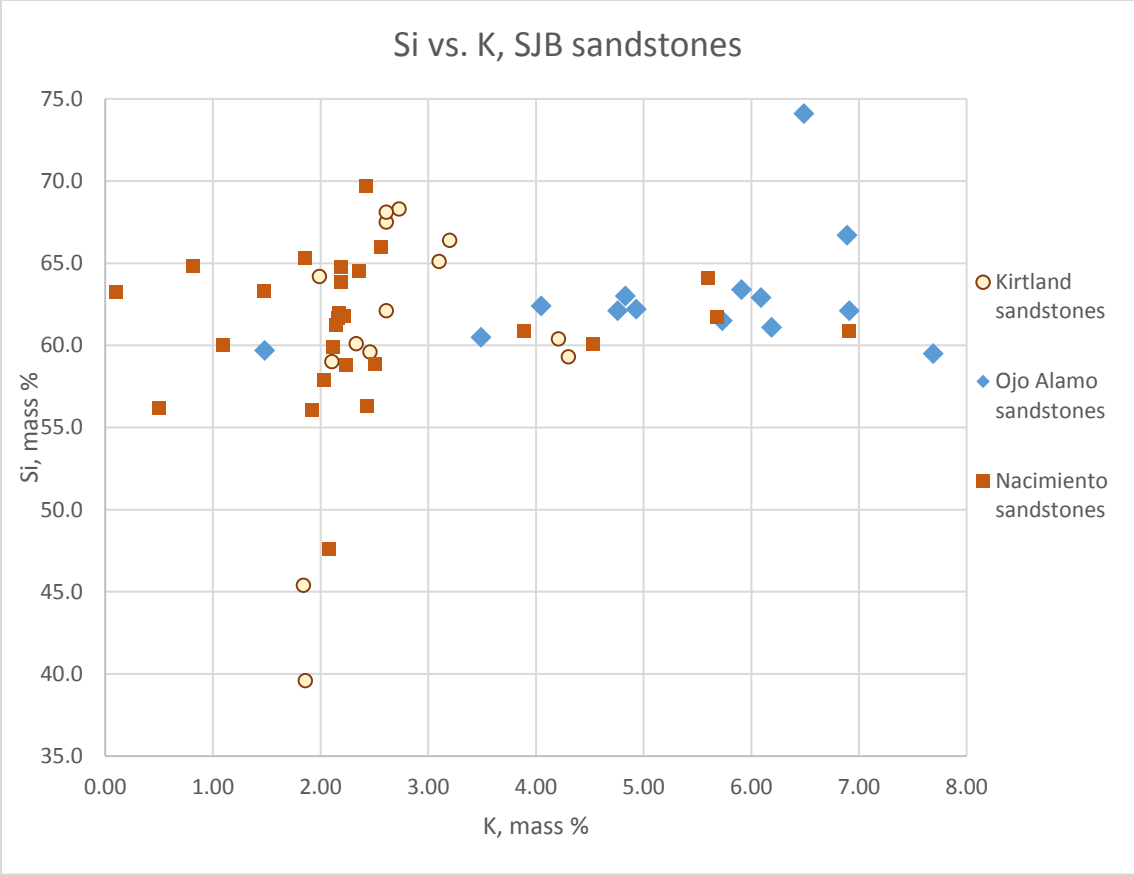

Figure 12. Si/K ratios for sandstones from Kirtland Shale, Ojo Alamo Sandstone, and Nacimiento Formation.

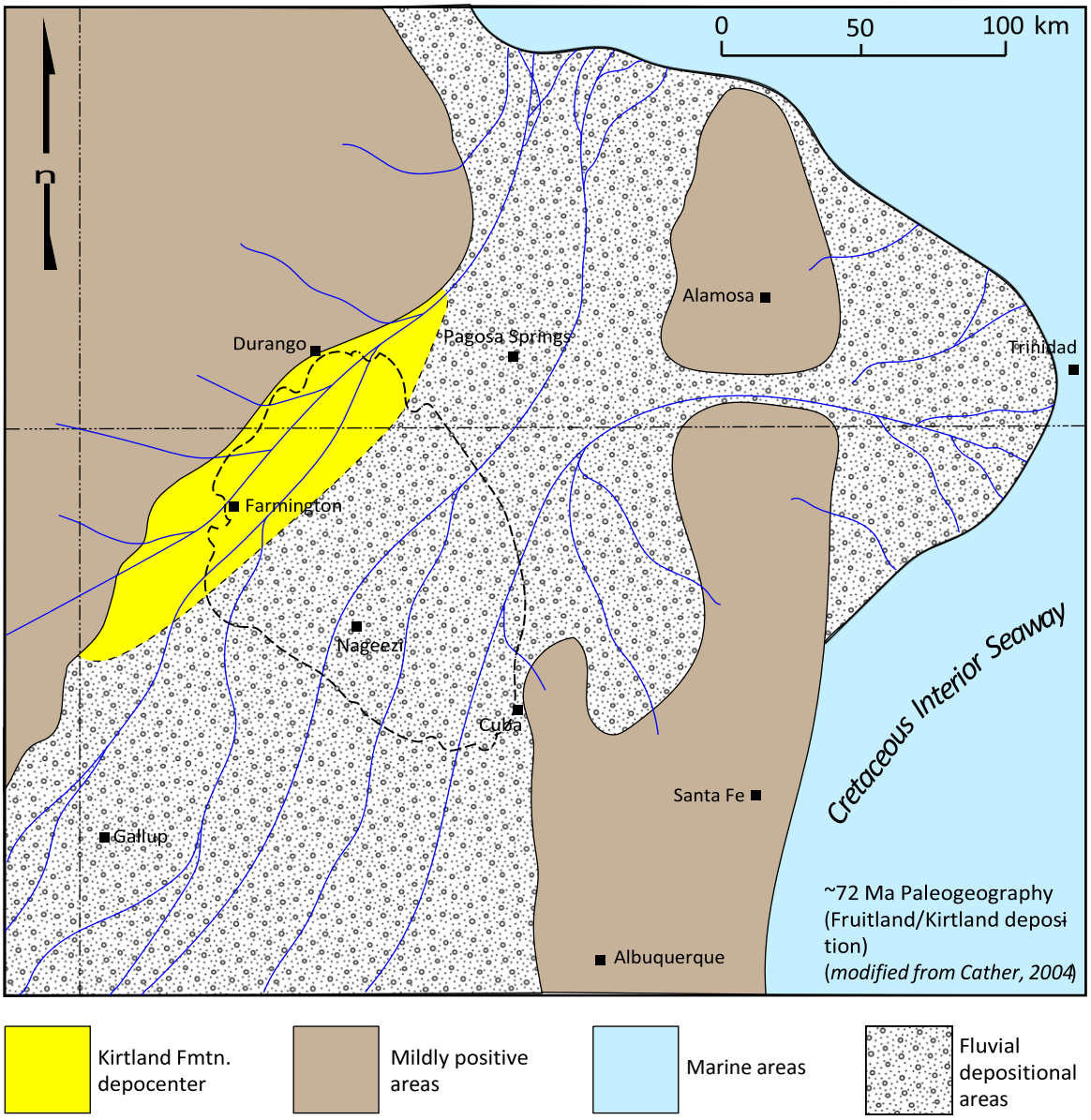

Figure 13. Paleogeographic interpretation of San Juan Basin and surrounding areas during the Campanian. Low-gradient streams flowing from the Mogollon Highlands in the southwest towards the retreating Cretaceous Interior Seaway deposit well-sorted sands and muds across much of the region. The thickest accumulations are preserved in the northwestern SJB. Modified from Cather (2004).

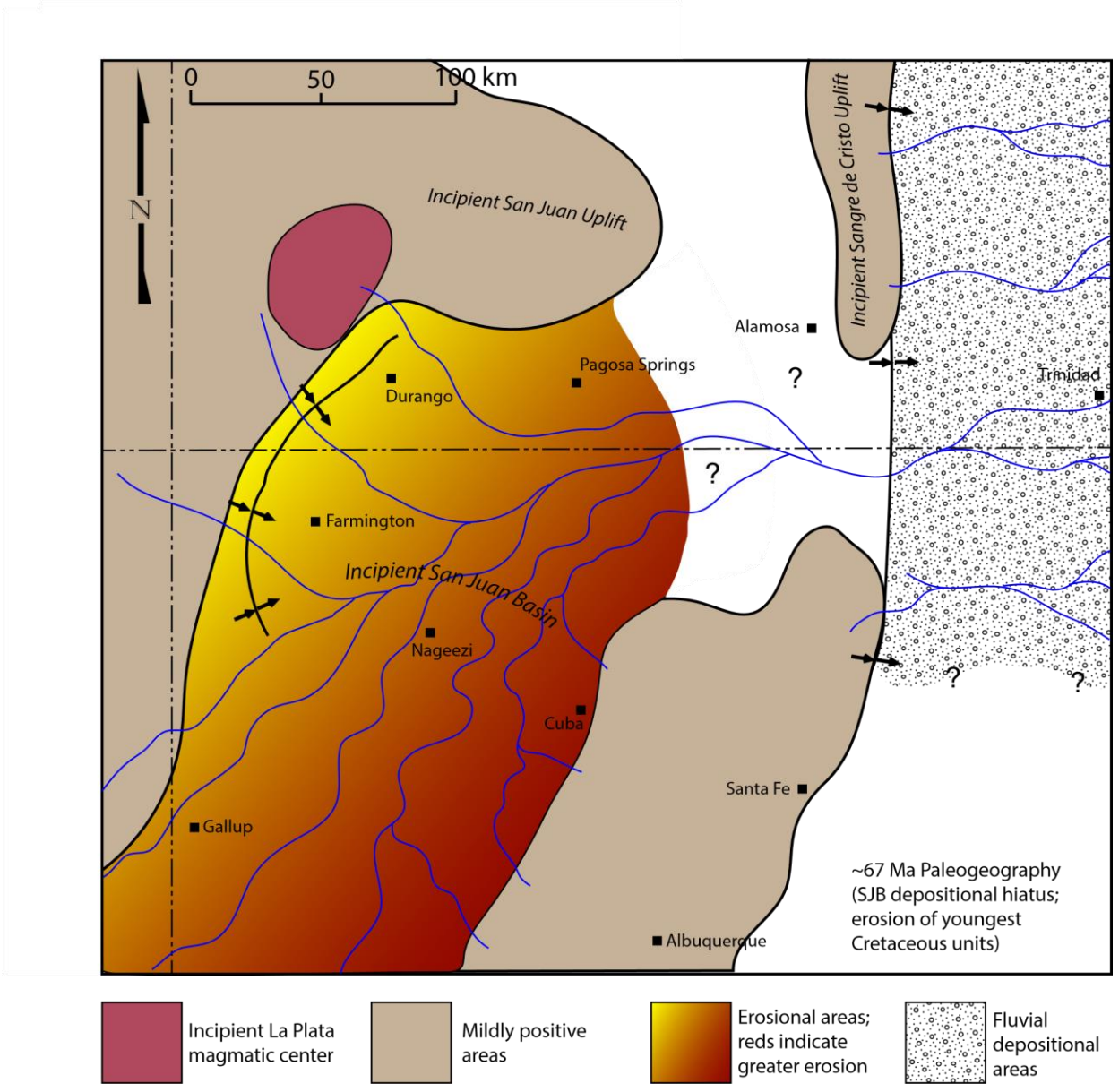

Figure 14. Paleogeographic interpretation of the San Juan Basin and surrounding areas during the late Maastrichtian. Deposition of the lower members of the Kirtland Shale had ceased, and erosional streams removed lower Maastrichtian and possibly upper Campanian deposits. Erosion was greatest in the southeastern SJB, potentially due relatively greater uplift in that area associated with the incipient Sierra Nacimiento Uplift. In the central San Juan Basin, northeast flowing streams became entrenched, creating a non-planar erosion surface onto which uppermost Maastrichtian and Paleocene sediments would be deposited. Maastrichtian-aged detrital zircons in upper Maastrichtian SJB deposits (Naashoibito Member of the Kirtland Shale) suggest that shallow intrusive igneous rocks of the La Plata Magmatic Center were uplifted and eroded shortly after cooling (Donahue, 2016).

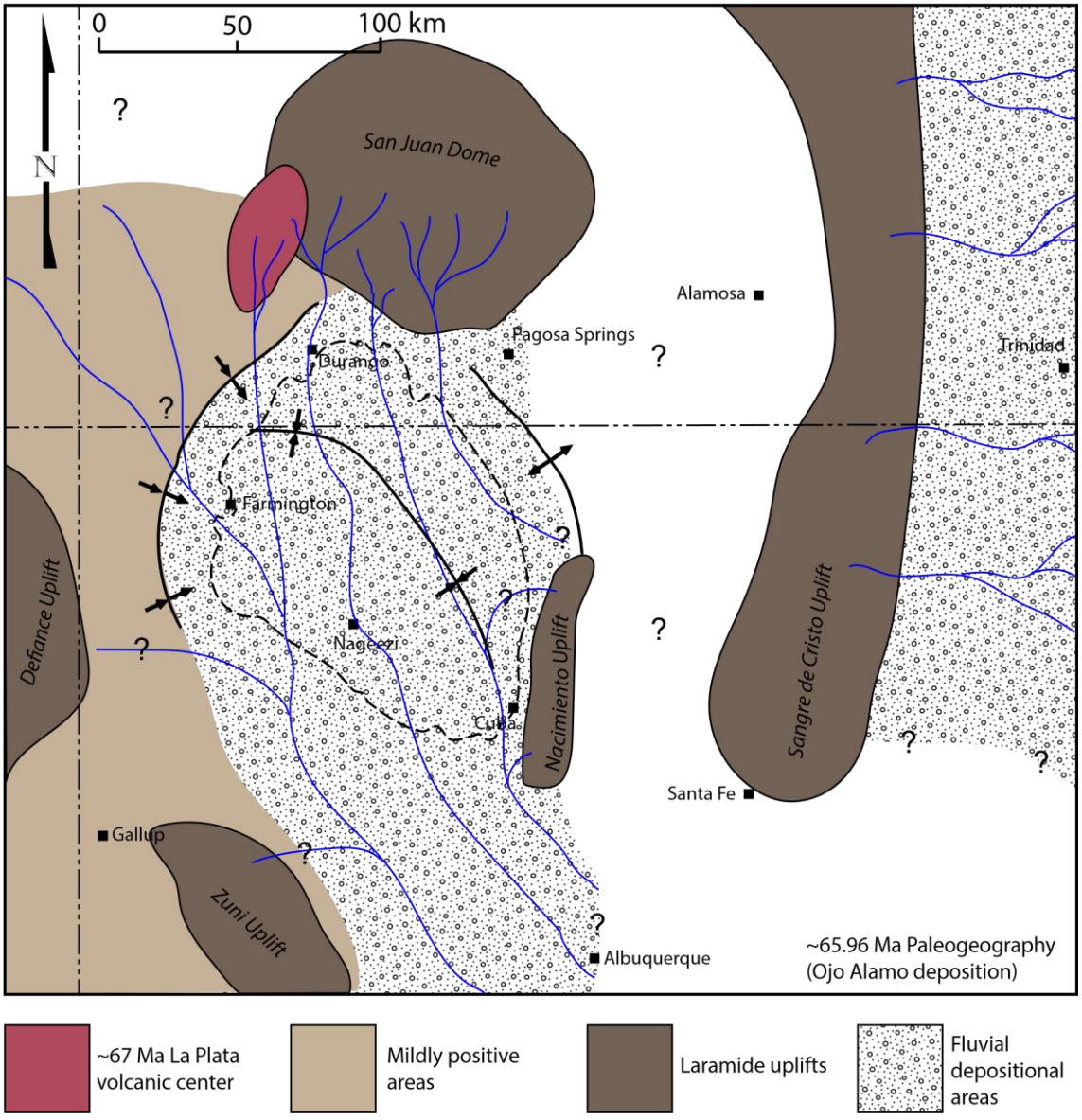

Figure 15. Paleogeographic interpretation of the San Juan Basin and surrounding areas during the earliest Paleocene. Early Laramide uplift of the Defiance, Zuni, and San Juan Uplifts reorganized regional drainage patterns, causing area streams to flow south/southeast. Subsidence of the San Juan Basin provided accommodation for the sediment these streams eroded from the emerging highlands. Volcanism in the La Plata Magmatic Center contributed sediment via erosion of shallow intrusive and volcanic rocks in the source area and via tephra fall. Uplift of the Sangre de Cristo highlands separated the fluvial systems of the Raton Basin from SJB fluvial systems for the first time since the retreat of the Cretaceous Interior Seaway (Bush et al. 2015), leading to sediment accumulation and storage in Laramide basins rather than on the retreating Gulf of Mexico coastal plain (Galloway et al., 2011; Blum & Pecha, 2014).

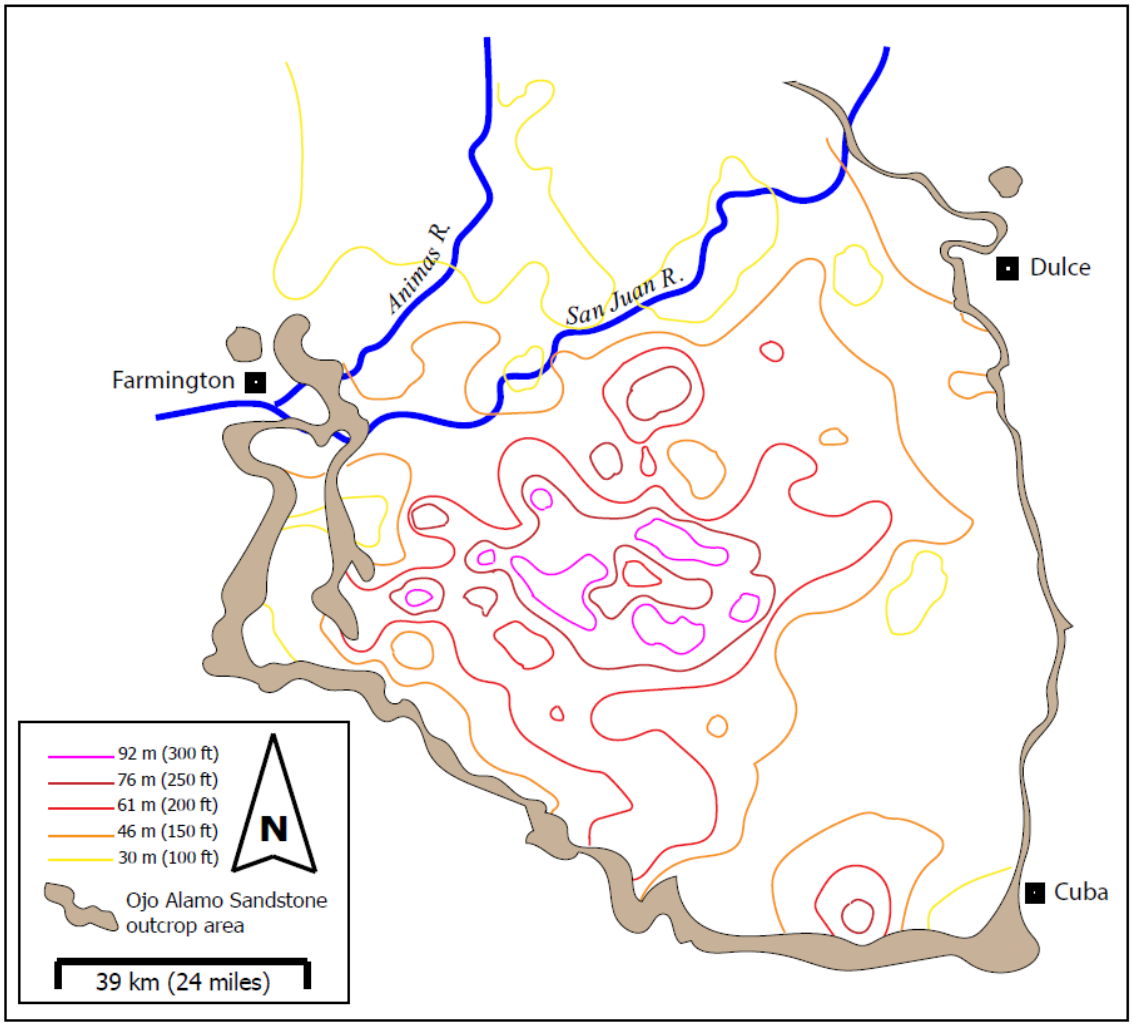

Figure 16. Isopach map of Ojo Alamo Sandstone. Modified from Russell (2008).

Figure 17. Thickness relationships of Ojo Alamo Sandstone along five cross-sections.

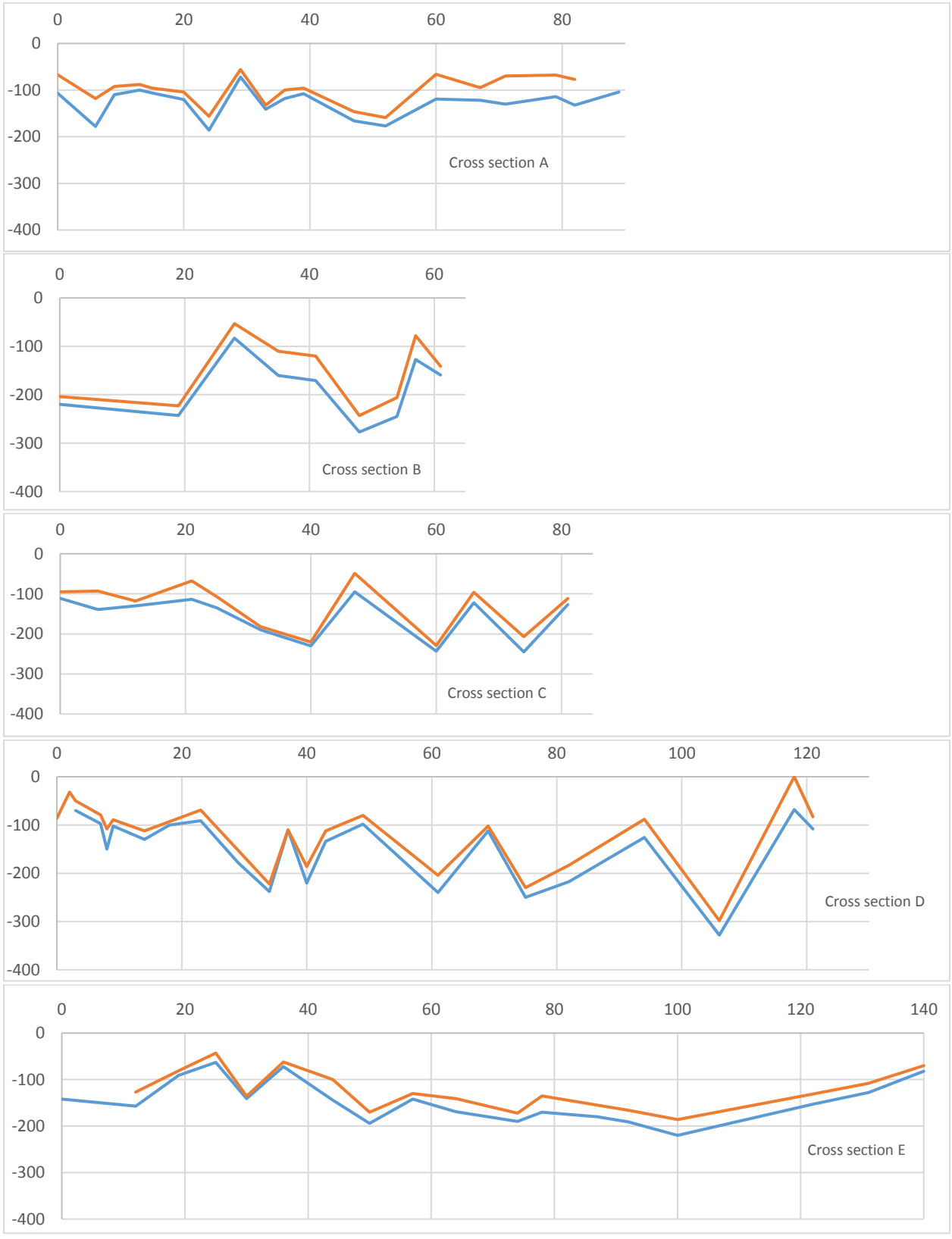

Figure 17 (previous page). Thickness relationships of the Ojo Alamo Sandstone and the basal sandstone therein along five cross sections through the San Juan Basin. Location of cross-sections given in Figure 4. X-axis shows distance from the western end of cross section, in km. Y-axis shows thickness in feet. Blue line indicates the depth of the lower contact of the Ojo Alamo Sandstone below the upper contact of the Ojo Alamo Sandstone. Red line indicates the top of the basal sandstone of the Ojo Alamo Sandstone. Data collected from well e-logs.

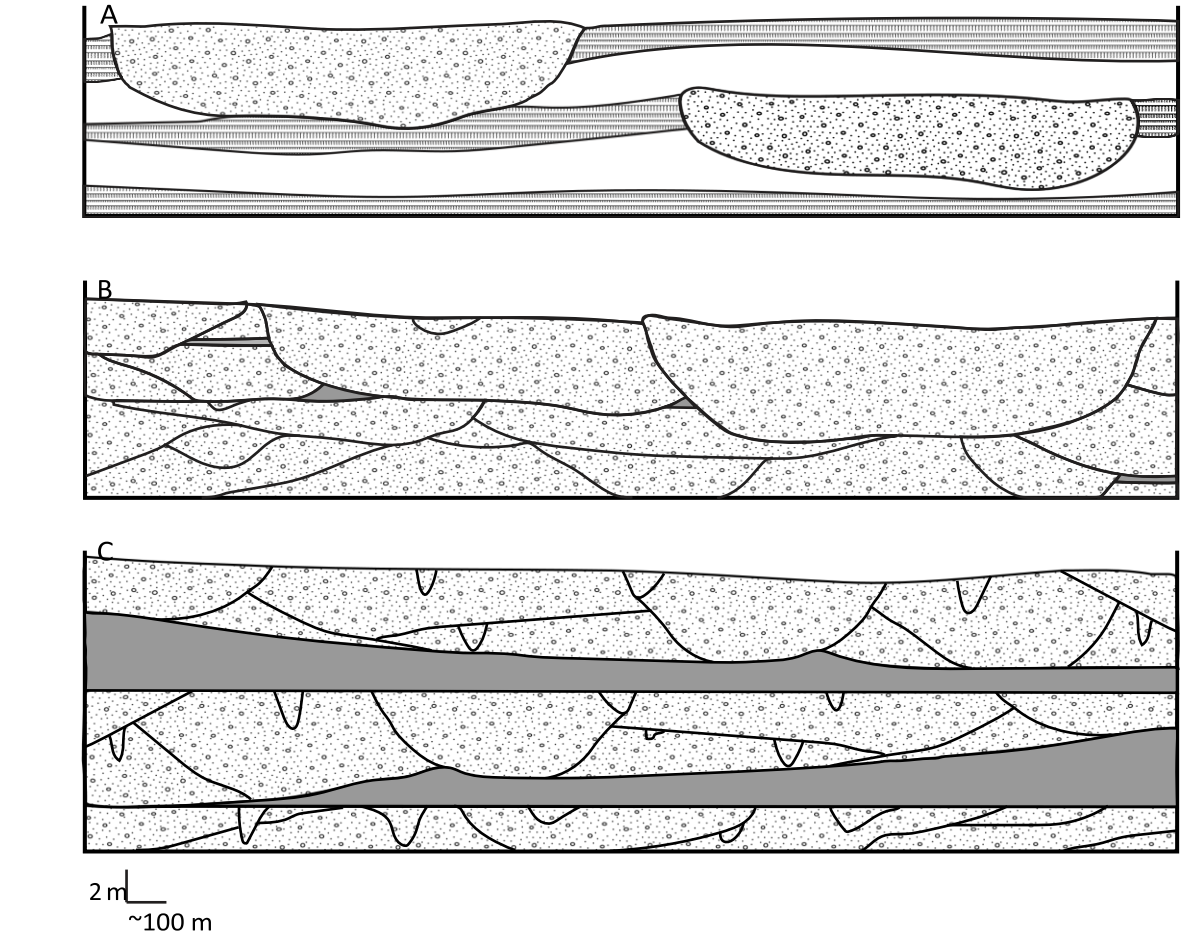

Figure 18. Cross-sections showing sedimentary architecture of alluvial deposits. A: Architecture in the Paleocene upper Willwood Formation, Bighorn Basin, Wyoming, showing well-developed paleosols, heterolithic sheet sandstones, and channel sandstones. Meters-wide ribbon sandstones are common within the heterolithic sheet sandstones and may incise into paleosols. Paleosols formed during intervals of subaerial exposure and depositional hiatus prior to avulsion. Sheet sandstones and ribbon sandstones are interpreted as avulsion deposits preceding the migration of a large channel (modified from Kraus & Wells (1999)). B: Typical architecture in the Ojo Alamo Sandstone throughout most of its outcrop area. Large channel bodies are laterally and vertically amalgamated. Ribbon sandstones and smaller channel deposits are uncommon. Overbank mudstones are uncommon and laterally truncated by channel sandstones. C: Architecture of the Ojo Alamo Sandstone at Mesa Portales. Single- and multi-story channel bodies are laterally and vertically amalgamated into 4-10 m-thick units separated by overbank mudstones. In some cases, channel body units scour completely through underlying overbank mudstones and into vertically adjacent sandstones of older channel sand bodies (*e.g.*, Fig. 5). Ribbon sandstones and smaller channel (bar-top channel?) deposits common.

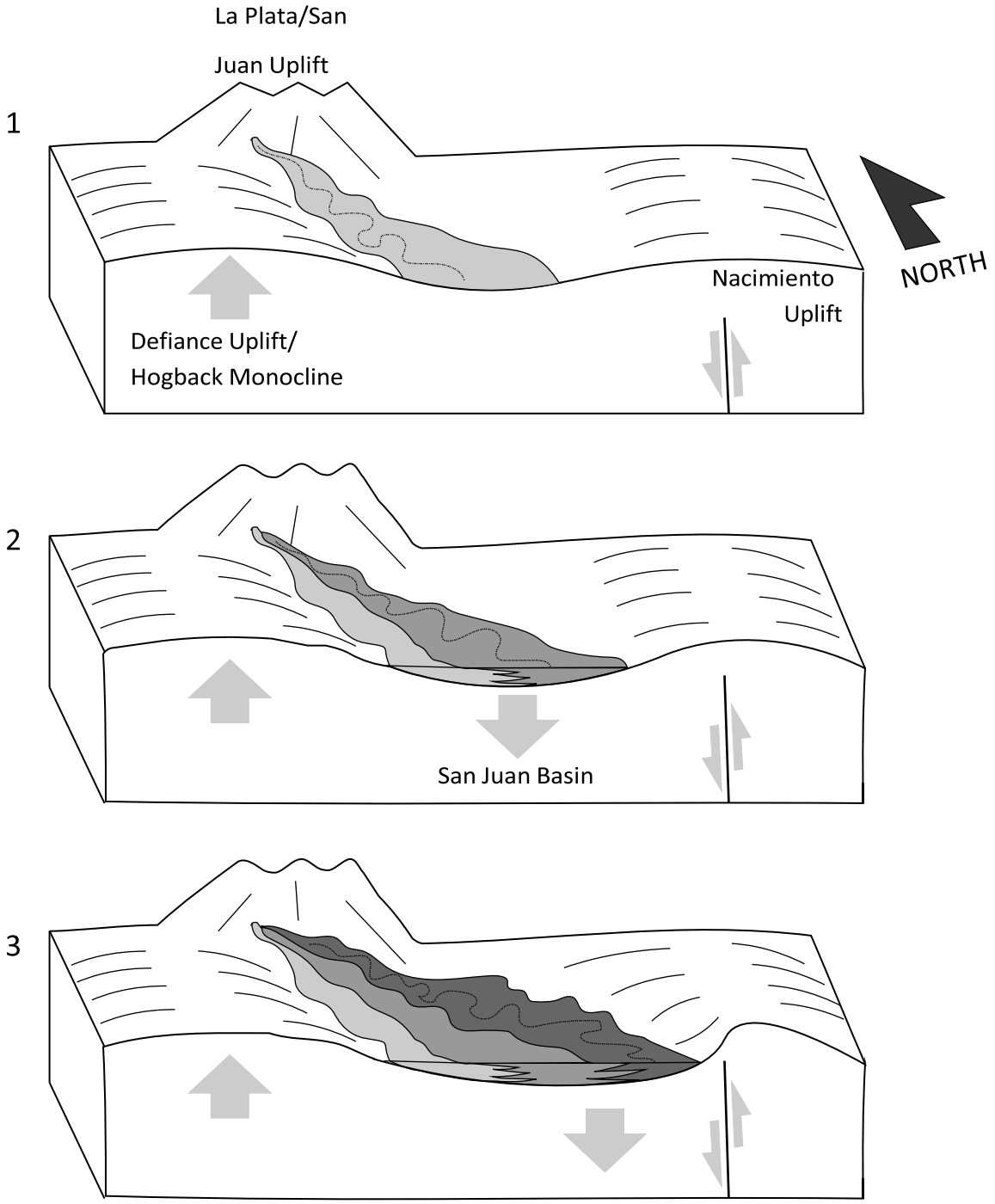

Figure 19. Schematic diagram showing eastward progression of the Ojo Alamo fluvial system depositional area due to increased uplift in the west and/or increased subsidence and accommodation in the east.

TABLES

Table 1. Bulk geochemical composition of sandstones sampled from the Kirtland Shale (Kk), Ojo Alamo Sandstone (Toa), and Nacimiento Formation (Tn).

Formation	Sample	Na2O	MgO	Al2O3	SiO2	P2O5	K2O	CaO	TiO2	MnO	Fe2O3	Total (%)
	Name	mass%	mass%	mass%	mass%	mass%	mass%	mass%	mass%	mass%	mass%	Majors
Kk	KISH-001	1.94	1.11	13.8	45.4	0.15	1.84	25.60	0.79	1.03	7.13	98.8
Kk	KISH-002	1.75	1.38	18.8	66.4	0.25	3.20	1.59	1.18	0.04	4.91	99.5
Kk	KISH-003	1.52	1.12	18.5	68.3	0.04	2.73	1.36	1.00	0.02	4.91	99.5
Kk	KISH-004	1.08	1.36	17.8	59.3	0.22	4.30	2.93	1.05	0.21	9.66	97.9
Kk	KISH-011	1.35	0.96	11.8	39.6	0.14	1.86	34.80	0.78	1.62	6.26	99.2
Kk	KISH-012	1.88	1.35	19.3	65.1	0.27	3.10	2.33	1.42	0.04	4.59	99.4
Kk	KISH-013	1.48	1.23	19.1	67.5	0.04	2.61	1.09	0.99	0.02	5.64	99.7
Kk	KISH-023	1.47	1.16	18.6	68.1	0.04	2.61	1.70	0.90	0.02	4.63	99.2
Kk	KISH-024	1.12	1.44	18.3	60.4	0.21	4.21	2.58	1.02	0.12	9.17	98.6
Kk	KIFA-001	1.28	0.99	14.8	59.6	0.10	2.46	12.80	0.81	1.12	5.06	99.0
Kk	KIFA-002	1.07	1.11	17.9	62.1	0.21	2.61	10.70	0.90	0.09	2.63	99.3
Kk	KIFA-003	1.32	1.19	14.5	64.2	0.04	1.99	9.33	1.00	0.43	4.91	98.9
Kk	KIFA-004	1.31	1.20	16.1	60.1	0.11	2.33	9.90	0.89	0.06	6.63	98.6
Kk	NASH-02	2.35	1.13	15.8	59.0	0.04	2.11	1.23	0.69	0.04	8.05	90.5
Toa	OJAL-102	0.55	0.95	25.8	59.7	0.06	1.48	1.63	1.23	0.00	7.92	99.3
Toa	OJAL-104	0.41	1.05	23.5	60.5	0.07	3.49	1.51	1.03	0.06	8.15	99.8
Toa	OJAS-001	0.72	1.43	20.7	62.2	0.10	4.93	1.18	1.12	0.06	7.15	99.6
Toa	OJAS-002	0.35	1.13	20.1	62.4	0.08	4.05	1.58	0.98	0.17	8.98	99.8
Toa	OJAS-003	1.21	0.32	13.3	74.1	0.11	6.49	0.58	0.47	0.04	2.69	99.3
Toa	OJAS-005	0.88	1.21	19.9	63.0	0.13	4.83	1.03	1.16	0.11	7.32	99.6
Toa	OJAS-011	0.68	1.43	21.3	62.1	0.11	4.76	1.18	1.16	0.05	6.89	99.7
Toa	OAES-01	1.01	1.11	21.5	59.5	0.12	7.69	2.51	1.01	0.10	5.25	99.8
Toa	OAES-02	0.61	0.80	20.4	63.4	0.10	5.91	1.46	1.21	0.07	4.99	99.0
Toa	OALP-02	0.69	0.95	22.9	62.9	0.08	6.09	1.19	0.96	0.04	4.10	99.9
Toa	OALP-03	0.39	1.08	23.1	61.1	0.09	6.19	1.61	1.08	0.07	4.98	99.7
Toa	OALP-04	0.65	0.42	20.0	66.7	0.11	6.89	0.68	0.88	0.04	2.69	99.1
Toa	OADN-01	0.67	1.01	22.7	62.1	0.10	6.91	1.59	0.92	0.10	3.46	99.6
Toa	OADN-03	0.95	1.13	23.3	61.5	0.12	5.73	1.37	1.10	0.13	3.95	99.3
Tn	CUME-02	0.75	0.60	19.7	61.8	0.10	2.22	7.61	1.32	0.78	4.12	99.0
Tn	CUME-06	1.06	0.61	11.0	76.7	0.02	1.55	0.31	0.91	0.02	2.75	94.9
Tn	CUME-08	0.70	0.07	19.2	62.0	0.07	2.17	6.71	1.10	0.58	5.90	98.5
Tn	CUME-14	1.23	1.09	15.0	57.9	0.05	2.03	0.59	0.66	0.05	13.65	92.2
Tn	CUME-18	0.96	0.73	21.4	64.5	0.08	2.36	1.93	1.15	0.03	5.92	99.1
Tn	CUME-19	0.10	0.79	19.2	64.8	0.07	2.19	4.69	0.99	0.85	4.96	98.6
Tn	BLAN-05	0.87	0.69	19.9	59.9	0.09	2.11	5.81	1.19	1.00	7.39	99.0

Formation	Sample	Na2O	MgO	Al2O3	SiO2	P2O5	K2O	CaO	TiO2	MnO	Fe2O3	Total (%)
	Name	mass%	mass%	mass%	mass%	mass%	mass%	mass%	mass%	mass%	mass%	Majors
Tn	MEPO-001	0.57	0.77	20.4	65.3	0.07	1.86	1.34	1.24	0.03	8.22	99.8
Tn	MEPO-002	0.79	0.53	18.5	69.7	0.04	2.42	0.08	1.38	0.03	5.39	98.9
Tn	MEPO-003	0.92	0.53	15.6	47.6	0.06	2.08	26.40	0.64	1.52	3.52	98.9
Tn	LIPL-01	1.18	1.31	22.9	60.1	0.21	4.53	1.11	0.96	0.09	7.32	99.7
Tn	LIPL-02	1.01	1.10	23.4	64.1	0.10	5.60	0.09	1.01	0.06	3.16	99.6
Tn	LIPL-03	0.59	0.99	21.2	60.9	0.08	6.91	2.29	1.06	0.10	3.16	97.3
Tn	LIPL-04	0.93	1.13	22.5	61.7	0.13	5.68	1.16	1.01	0.08	4.55	98.9
Tn	LIPL-07	0.85	0.87	19.9	60.9	0.02	3.89	5.91	0.90	0.05	6.54	99.8
Tn	WFKW-001	1.89	0.76	15.0	58.9	0.06	2.51	1.89	0.60	0.02	3.80	85.4
Tn	BIPO007	0.92	2.28	17.5	56.3	0.07	2.43	1.91	0.82	0.03	9.82	92.1
Tn	WFKW-002	2.28	0.86	16.5	66.0	0.06	2.57	1.75	0.58	0.04	4.45	95.0
Tn	KWFT08	1.55	1.40	16.9	64.8	0.02	0.82	0.67	1.10	0.03	5.72	93.0
Tn	CROW05	0.13	0.16	7.2	81.8	0.01	0.07	0.11	0.96	0.01	0.83	91.3
Tn	CROW04	0.32	0.43	20.1	63.3	0.02	0.10	0.55	1.03	0.01	3.98	89.8
Tn	JACA05	1.28	1.09	20.4	60.0	0.01	1.10	0.88	0.79	0.03	5.16	90.7
Tn	BETS-04	1.33	0.80	16.9	63.8	0.21	2.19	1.28	0.65	0.02	6.89	94.1
Tn	BDNZ-53	1.18	1.02	19.7	56.1	0.04	1.92	0.54	0.79	0.02	9.33	90.6
Tn	BDNZ-50	1.07	0.96	17.7	63.3	0.04	1.47	0.55	0.72	0.01	4.95	90.8
Tn	BDNZ-35	1.38	1.05	22.1	56.2	0.02	0.50	1.08	0.78	0.04	5.78	89.0
Tn	BDNZ-41	1.52	1.61	14.9	58.8	0.10	2.23	0.95	0.66	0.04	9.13	89.9
Tn	ANGE-06	1.17	1.06	15.6	61.3	0.05	2.15	1.16	0.69	0.02	9.37	92.5
Tn	ANGE-05	1.17	1.07	15.6	61.7	0.05	2.16	1.17	0.69	0.02	9.40	93.1

Table 2. Sedimentation rate estimates for the Ojo Alamo Sandstone.

Thickness of Ojo Alamo Sandstone (m)	Inferred duration of sedimentation (ky)	Sedimentation rate (m/ky)
120 (maximum thickness)	307 (minimum estimate of Sprain et al. (2015))	0.39
120	511 (maximum estimate of Sprain et al. (2015))	0.23
65 (average thickness)	307	0.21
65	511	0.13
6 (minimum thickness)	307	0.02
6	511	0.01

Chapter 2

Pyroclastic silcretes in the Paleocene Nacimiento Formation, New Mexico: a new genetic origin for silcretes

Kevin M. Hobbs[1], Peter J. Fawcett [1]

[1]*Earth and Planetary Sciences Department, University of New Mexico, Albuquerque, New Mexico, 87131 USA*

ABSTRACT

Silica-cemented sediments and soils, commonly called silcretes, are thought to form via one of three processes: (1) by long-term (>10^6 y) pedogenic silica accumulation in stable landscapes; (2) by interstitial silica precipitation by shallow groundwater downgradient from aluminosilicate weathering zones during landscape incision; or (3) in evaporitic alkaline ephemeral lakes in endorheic basins. Each of these genetic settings produces an associated specific set of silcrete characteristics. In contrast, the abundant silcretes in the Paleogene Nacimiento Formation (NFm) of New Mexico formed in the <10^6 y interval between deposition of underlying sediment and burial by overlying sediment during Laramide sedimentation, precluding long-term pedogenic origin. NFm silcrete stratigraphic relationships and mineralogic composition preclude both groundwater and alkaline ephemeral lake origins. Here we present evidence suggesting that NFm silcretes formed in the Paleocene from the rapid concentration of silica during alteration of volcanic tephra under supergene conditions, a new fourth process for silcrete genesis. These conclusions show that current understanding of silcrete genesis is incomplete, and that the role of fine-grained pyroclasts in sedimentary basins deserves further emphasis.

INTRODUCTION

Silcretes are indurated silica-cemented sediments and soils containing >85 wt.% SiO_2 (Summerfield, 1983; Nash & Ullyott, 2007). Most silcrete research has focused upon those from Australia and southern Africa, where they form from the long-term accumulation of silica in duricrusts in stable landscapes (*e.g.*, Thiry & Milnes 1990; Hill et al., 2003; Thiry et al., 2006); and from Cenozoic deposits of western Europe, where they represent paleosol duripans or more recent groundwater precipitation horizons (*e.g.*, Thiry, 1999; Bustillo & Bustillo, 2000; Ullyot et al., 2015; Huggett & Longstaffe, 2016). More localized silcrete formation is known from North America (*e.g.*, Wehrfritz, 1978; Nimlos & Ortiz-Solorio, 1987; Williamson et al., 1992), South America (*e.g.*, Scherer & Lavina, 2006; Batezelli & Ladeira, 2016), southwest Asia (Khalaf, 1988), and New Zealand (Lindqvist, 1990). Silcretes are known in rocks ranging in age from Precambrian to recent (Mustard & Donaldson, 1990; Dubroeucq & Thiry, 1994); the majority are hosted by Cenozoic sediments (Thiry, 1999; Nash & Ullyott, 2007).

Silcrete mineralogic composition is dominated by opal, chalcedony, and quartz (Bustillo & Bustillo, 2000; Nash & Ullyott, 2007). Matrices are composed of opal, chalcedony, and microquartz (<20 μm). Grain overgrowths and large void-fillings are commonly megaquartz (>20 μm). The detrital component of silcretes is usually quartz (Nash & Ullyott, 2007). There is a well-documented sequence of silica ordering in silcrete cements, with amorphous opal being replaced progressively by chalcedony, microquartz, and megaquartz (Thiry & Millot, 1987). This sequence is present in pedogenic silcretes, where more ordered silica is present near the top of the profile (Ballasteros et al., 1997), and in groundwater silcrete vug fills, where silica order increases towards the center of voids (Thiry & Milnes, 1991). Alumina content is usually

<1%, with higher concentrations reported in some pedogenic silcretes (Armenteros et al., 1995; Nash & Ullyott, 2007). The silica in most silcretes is derived from weathered silicate minerals. This leads to solute silica in surface and subsurface waters. Silica solubility is affected by a number of factors (Rimstidt, 1997; Lee & Gilkes, 2005; Maly et al., 2006), but under most conditions is greatest in waters above pH 9 (Dove & Rimstidt, 1994). Under most surficial and shallow groundwater conditions, quartz remains relatively insoluble, making quartzose sediments unlikely sources for solute silica in surface and subsurface waters (Nash & Ullyott 2007). Argillization and clay diagenesis are important silica sources (Birkeland, 1974; Wopfner, 1983) and usually occur in low pH environments associated with high bioactivity or precipitation of metal oxyhydroxides. Silica can have biogenic sources in monocotyledonous plants (Meunier et al. 1999) and diatoms (Battarbee et al. 2001). Pedogenic and evaporitic silcretes involve vertical translocation of silica, resulting in vertical gradations in silica form and/or content (Nash & Ullyott, 2007).

Current models for silcrete formation include pedogenic, groundwater, and evaporitic origins, each associated with a specific set of physical and chemical characteristics (Nash & Ullyott, 2007). Pedogenic silcretes form over long periods ($>10^6$ y) on basement rocks or basement-adjacent sediments, and indicate an unconformity (Wopfner, 1983; Thiry, 1999). They require the downward percolation of silica solutions and subsequent precipitation of silica lower in the solum, leading to an upper elluviated horizon and lower illuvated horizon (duripan) (Milnes & Thiry, 1992). Macromorphological features in pedogenic silcretes vary but usually include columnar structures, roots, and bioturbation structures (Nash & Ullyott, 2007). Groundwater

silcretes form at the water table or at groundwater outflow zones (Nash & Ullyott, 2007) in arenaceous sediments and limestones. These silcretes form downgradient from aluminosilicate weathering zones, where silica is liberated from primary minerals and clays during hydrolysis and subsequently delivered to silicification zones. Silica precipitation is triggered by changes in solution chemistry, leading to micro-scale concentric zones of silica phases or ordering (Thiry & Millot, 1987). Evaporitic silcretes, also called pan/lacustrine silcretes, form in or adjacent to lakes in endorheic basins (Summerfield, 1983; Nash & Ullyott, 2007). Changes of silica mobility related to salinity and pH in these environments lead to precipitation of silica from solution. Evaporitic silcretes are nodular or irregularly shaped, contain a wide variety of matrix minerals, and are geographically associated with other mineral phases reflecting the solute ions and/or molecules present in the evaporating water (Armenteros et al., 1995; Nash & Ullyott, 2007). Properties of pedogenic and groundwater silcretes are listed in Table 1.

THE NACIMIENTO FORMATION

The Nacimiento Formation (NFm) in the San Juan Basin (SJB) (Fig. 1) contains siliciclastic sandstone and mudstone deposited by southeast-flowing rivers in the Danian through Thanetian Ages of the Paleocene Epoch (Williamson, 1996). Deposition was concurrent with structural deformation caused by development of the San Juan Basin, San Juan Dome, La Plata Magmatic Center, and other Laramide Orogeny features in the early Paleocene (Smith, 1988; Cather, 2004; Donahue, 2016). Due to its rich and diverse fossil vertebrate fauna, much work has been devoted to NFm paleontology and biostratigraphy since the late 19th Century (Williamson, 1996, and references therein). Relatively little work has focused on the stratigraphy of the unfossiliferous portions of

the NFm, and even less has focused on the paleoclimatology, sedimentology, fluvial history, and paleoenvironmental interpretation of this unit.

The NFm contains numerous 10-50 cm thick, weathering resistant, indurated silica-rich beds. These beds are interbedded with assorted facies, including sandstone, mudstone, and paleosols. Rains (1981) applied the term silcrete to describe these beds. Due to their relatively resistance to weathering as compared to other NFm rocks, silcretes are noticeable features in the landscape as they cap mesas, form prominent bluffs and breakaways in hillslopes, and create talus-mantled slopes and plains below vertical outcrops. Despite their prominence in the landscape and their abundance in the NFm, SJB silcretes remain poorly understood.

Two previous studies have offered interpretation of the chemical and mineral composition, stratigraphic relationships, and genesis of NFm silcretes. Rains (1981) investigated the occurrence and nature of SJB silcretes in an effort to determine the environments and processes responsible for them. On the basis of field observations and petrographic and X-ray diffraction analyses, he concluded that the silcretes were the "result of extensive chemical weathering under complex and variable climate conditions" and that "these conditions are very similar to those under which major Australian silcretes developed" (p. 69). It should be noted that Australian silcretes are highly variable in observed form and suggested genesis (*e.g.*, Thiry and Milnes, 1990; Hill et al., 2003; Borger et al., 2004; Lee and Gilkes, 2005; Thiry et al., 2006). Seizing upon the shared characteristics of SJB and Australian silcretes, Rains interpreted SJB silcretes to have formed under similarly warm and seasonally wet conditions. In addition to detailed lithologic and petrographic descriptions, Rains (1981) provided detailed stratigraphic

measurements of silcrete-bearing sections of the Nacimiento Formation. Rains' field observations include silcretes that are laterally continuous on the km scale as well as silcretes displaying a bifurcating form in outcrop. Rains' petrographic analyses yield an average of 91% silica (quartz and cryptocrystalline silica matrix), 3% potassium feldspar, 3% clay/mica matrix, and 3% other; his X-ray diffraction analyses indicate the presence of quartz, amorphous silica, potassium feldspar, kaolin-group clays, and interstratified smectite-group clays.

Williamson et al. (1992) presented a description and interpretation of Nacimiento Formation silcretes, noting the similarities to and differences from silcretes in other settings. They remark upon the wide variability in the form of silcretes in different geographic, geologic, and temporal settings, and state that such variability likely represents different genetic conditions. Like Rains (1981), Williamson et al. (1992) conclude that SJB silcretes likely have their origin in pedogenic or surficial weathering processes, rather than groundwater diagenetic processes.

METHODS

Silcretes and adjacent strata were mapped and measured in the NFM outcrop area in San Juan and Sandoval Counties, New Mexico (Fig. 1). For optical petrographic analyses, thin sections were prepared with standard techniques. In order to determine grain size, composition, and texture, petrographic identification and point counts were performed with a petrographic microscope. Minerals were identified with X-ray diffraction analyses on a Panalytical X'Pert Pro diffractometer at the New Mexico Bureau of Geology and Mineral Resources. Bulk geochemical composition of silcretes and adjacent strata was determined with X-ray fluorescence analyses on a Rigaku ZSX Primus II wavelength-dispersive spectrometer in the Analytical Chemistry Laboratory at

the University of New Mexico. Elemental compositions of individual grains, matrix components, and clays were obtained on a JEOL 8200 electron microprobe analyzer in the Electron Microbeam Facility at the University of New Mexico.

Here, we present new data and interpretations in order better to understand how these silcretes relate to the tectonic, sedimentary, volcanic, and geomorphic evolution of the SJB during accumulation of NFm sediments in the Paleocene. Out work shows that NFm silcretes cannot be explained with conventional models of silcrete genesis. Using geochemical, petrographic, and stratigraphic investigations, we show the silcretes in this study are likely the result of alteration of volcanic ashfall deposits.

RESULTS

Silcretes of the NFm crop out in the southwest SJB (Fig. 1). Although they cannot accurately be correlated stratigraphically across the area, silcretes are more common in the lower 50 m and upper 100 m of the ~450 m-thick NFm. Stratigraphic correlation of NFm silcretes shows that there are at least 30 unique silcretes; the actual number is likely higher but difficult to ascertain due to difficulties in lateral correlation between outcrop areas. Silcretes are 10-50 cm thick with distinct planar upper contacts and distinct irregular to planar lower contacts. Individual silcrete beds are vertically homogenous. Silcretes overlie claystones, siltstones, sandstones, and paleosols, and are overlain by mudstones, siltstones, and sandstones. Subjacent and superjacent strata show no remarkable depletion or enrichment in Si, Al, or base cations. Silcretes are usually parallel to underlying strata, but can be observed cross-cutting lower units (Fig. 2). Root traces are present in 20% of observed silcretes. Burrows are present in 55% of observed silcretes and comprise two classes: straight, vertical ~3-5 mm-diameter cylindrical burrows; and subvertical 10-16 mm-diameter burrows. The larger burrows sometimes

become horizontal at the base of the silcrete stratum, suggesting that subjacent strata were less favorable for burrowing while bioturbation occurred. Individual silcrete beds can be traced laterally for up to 2 km. Silcretes laterally terminate against channel cuts (Fig. 2) or by pinching out. Laterally discontinuous silcretes pinch in and out over 10's to 100's of m.

The mineral composition, grain size, and sorting of NFm silcretes are substantially different from that of the superjacent and subjacent arkosic arenites, wackes, siltstones, and claystones encapsulating them. NFm silcretes contain moderately- to well-sorted, fine grained sand to silt predominated by strain-free monocrystalline quartz with minor amounts of microcrystalline quartz, chalcedony, feldspar, lithic fragments, and accessory minerals. Grains comprise 35-60% of the rock. Tephra shards are common (Fig. 3), making up 9-20% of the rock and were identified on the basis of biconcave shapes, arcuate clast margins, Y-shaped clasts, or preserved whole vesicles, all indicative of vesicularity. Many clasts are elongate and very angular. These have the same mineral and chemical composition as clasts that meet the criteria for shards, but we cannot be certain of their origin. By not counting them as shards, we almost certainly underestimate the total percentage of shards in NFm silcretes. These rocks are cemented by cryptocrystalline and microcrystalline silica matrix that comprises 40-65% of the rock (Fig. 4). Unlike many pedogenic and groundwater silcretes, there is no observed progression of silica ordering (*e.g.*, from low-order amorphous silica to high-order quartz) in grains, matrix, or vug fills of NFm silcretes. Clays make up <2% of the matrix and are often associated with bioturbation features. Unfilled pores make up <2% by volume of NFm silcretes, making these the lowest-porosity facies in the SJB Paleogene

section. By standard sedimentary classification, NFm silcretes are classified as silica-cemented submature quartz wackes. By the pyroclastic classification of Schmid (1981), NFm silcretes are tuffites. Using the micromorphological classification of Summerfield (1983), NFm silcretes are F-fabric silcretes (matrix-supported).

The average NFm silcrete contains 90% SiO_2, 6% Al_2O_3, and 4% other components by oxide weight percent (Table 2). Microprobe analysis shows that most detrital grains, tephra shards, and matrix materials are composed of quartz. Some grains and matrix materials contain lower-order silica forms, predominantly opal-CT. Detrital aluminosilicate minerals, including feldspars, and titanium oxides (presumably rutile) are also present. Matrix materials also include minor amounts of hydrated aluminosilicate clays. See the Appendices for full petrographic, bulk geochemical, and microprobe analytical data.

DISCUSSION

Volcanic Origin for NFm Silcretes

Nacimiento Formation silcretes share some mineral and physical properties with both pedogenic and groundwater silcretes (Table 1), but lack many of the properties needed to designate them as one or the other. For instance, the preservation of sedimentary structures is present in both groundwater and NFm silcretes; however, NFM silcretes lack the quartz overgrowths observed in groundwater silcretes. NFm silcretes are not associated with any evaporitic minerals and are limited in areal extent, precluding their interpretation as evaporitic silcretes. The moderate sedimentation rates in the Paleocene SJB of 0.01-0.12 mm/yr (Williamson, 1996) also preclude long-term pedogenic origin for NFM silcretes. We propose that NFm silcretes formed via neither long-term pedogenic silica accumulation nor silica precipitation in groundwater. Instead,

the alteration and cementation of aeolian-deposited silica-rich tephra were responsible for NFm silcretes. The abundance of very angular tephra shards (Fig. 3) suggest limited fluvial transport of these clasts after deposition. The nearest known igneous eruptive centers in the early Paleocene are ≥100 km from NFm silcretes (Cunningham et al., 1994), and tephra shards are likely to be destroyed or rounded if fluvially transported such a distance (Cas & Wright, 1988). The textural uniformity (fine sand to silt), sorting, lack of fluvial bedding structures, and stratigraphic relationships of NFm silcretes also suggest an ashfall origin. Some silcretes can be observed on either side of sand-filled channel cut structures, suggesting that the silcrete formation is related to original bed composition instead of a later water table position. The "bifurcating" silcretes of Rains (1981) at Ojo Encino, shown in Fig. 2, are in fact the result of erosion of a lower ashfall deposit by a channel cut and the subsequent deposition of a later ashfall deposit that draped topography. Some silcretes (BDNZ-21 and BDNZ-24; Repository data) show a higher proportion of feldspars, rounded quartz grains, and clay cements, suggesting some mixing of pyroclastic and epiclastic materials after the initial ashfall deposition of pyroclasts. In NFm fluvial sandstones, tephra shards are present but make up <1% of detrital grains, suggesting that aeolian pyroclastic deposition and/or reworking sometimes occurred in the Paleocene SJB but did not result in the creation of tuffite or subsequent silcrete.

Potential source volcanoes for pyroclasts in NFm silcretes are in the southwestern Colorado Mineral Belt, ~100 km NNW from NFm silcretes, and in the Colorado Plateau/Basin and Range transition zone of southeastern Arizona, ~400 km SW from NFm silcretes. Since there is no structural evidence for Cenozoic major crustal

contraction or extension in the area between the SJB and these magmatic centers, we assume these distances were similar during NFm deposition. Early Paleocene Colorado Mineral Belt igneous products are of intermediate chemical composition (Wegert & Parker, 2011), whereas coeval Arizona igneous products are felsic (Titley, 1995). Both Colorado and Arizona potential volcanic sources for NFm pyroclastic deposits are at a more westerly longitude than silcretes, meaning both were likely upwind of the Paleocene SJB if general global atmospheric circulation patterns are assumed, given the Paleocene SJB's location in the middle latitudes (Irving, 1979. The high silica content of NFm silcretes might suggest that the Arizona felsic (~70 wt. % SiO_2, Lang, 1991) eruptions are a more likely source of pyroclastics than are the Colorado intermediate (52-64 wt. % SiO_2, Wegert & Parker, 2011) eruptions. In either case, NFm silcretes, at 90 wt. % SiO_2, are more silica-rich than igneous sources. The chemical disparity between silcretes and potential igneous sources must be explained by post-depositional leaching of aluminum and base cations (*i.e.*, pyroclasts had the bulk chemical composition of their parent magma but were chemically altered after deposition), by chemical compositional sorting in an eruptive event (*i.e.*, silica-rich pyroclasts were preferentially deposited in the SJB due to sorting and/or chemical segregation processes), or by some combination of both. Pyroclastic aeolian deposits are known to be more felsic farther from the eruptive source, but even the most distal ash deposits rarely exceed ~79 wt % SiO_2 (Sarna-Wojcicki et al., 1981; Shane, 1991). Therefore, either Arizona or Colorado Paleocene magmatic centers are possible sources for NFm aeolian pyroclastic deposits.

NFm Silcrete Alteration

Even if the original bulk chemical composition of NFm aeolian pyroclastic deposits is assumed to be as silica-rich as the most silicic shards observed in recent

volcanic eruptions (75 wt. % SiO_2, 13 wt. % Al_2O_3, 12 wt. % other (Shane, 1991)), then post-deposition removal of Al and base cations is still required in order to attain the bulk chemical compositions observed in NFm silcretes (Table 2). This is problematic in regards to interpretation of NFm silcretes, as the geochemical stability of silicic pyroclastic materials is well documented (Dugmore et al., 1992; Pollard et al., 2003). At low pH, Si is relatively immobile (Alexander et al., 1954), but base cations are more mobile (Drever, 1994). Due to the presence of NFm silcretes immediately above and below arkosic sandstones with unaltered feldspars, the lack of remarkable loss or gain of Al or base cations in those sandstones, and the distinct boundaries between silcretes and subjacent and superjacent beds, it seems unlikely that low pH groundwater could have caused the leaching observed in silcretes. If it had, greater alteration of adjacent units and less distinct lithologic boundaries would be expected. Instead, the chemical environments and processes responsible for silcrete formation must have been strictly confined to the aeolian pyroclastic deposit beds themselves. A potential explanation is that porosity and permeability conditions within the aeolian pyroclastic deposits allowed acidic meteoric waters long enough residence time to leach most Al and base cations from the initially glassy pyroclasts and interstitial ash. Plants colonized these deposits, as is evidenced by preserved roots traces, and their contribution of organic acids and ligands likely increased Al solubility (Žutić and Stumm, 1984; Drever & Stillings, 1997), an effect seen in modern plant-rich soils (Johnson et al., 1981). Modern soil formed in acidic materials or under acid-producing plant communities can create spodic horizons wherein Al and base cations are removed. While NFm silcretes lack the accumulation of Al and base cations deeper in the profile as is observed in modern Spodosols, perhaps similar interactions

between acidic materials, plant communities, and Al-humus complexes allowed for the nearly complete removal of most non-silica elements from these horizons relatively rapidly after deposition. Though the exact cause and process of leaching in these deposits is unknown, it is evident that peculiar chemical conditions must have existed in order to produce the observed silcretes.

IMPLICATIONS AND CONCLUSIONS

New Consideration of Silcrete Genesis

NFm silcretes do not fit the currently accepted models for silcrete formation. Cross-cutting relations (Fig. 2) show that these beds were surficial or very shallow (shallower than the depth of channel incision) and that at least part of their development occurred while the sedimentary basin was undergoing fluvial depositional processes in the Paleocene. Since pedogenic silcretes are assumed to take hundreds of thousands to millions of years to form, there is not enough time elapsed during NFm deposition to account for all of the silcretes that it contains. In addition, NFm silcrete exhibit no vertical grading, association with elluviated horizons, or other pedogenic features found in pedogenic silcretes. Groundwater silcretes form via the interstitial precipitation of silica in arenaceous sediments downgradient of weathering zones during local/regional landscape incision. NFm silcrete do not fit with this model for several reasons. First, there are no known nearby weathering zones to supply silica-rich waters to the NFm. Second, NFm silcretes are not geographically associated with any major incision and can be found located downdip of local incisions, suggesting the discharge of silica-rich waters was not a factor in their origin. Third, groundwater silcretes disply overgrowths of silica minerals around detrital grains of the host sediment whereas NFm silcretes show complete replacement of host sediment with quartz and few to no silica overgrowths.

The indurated silica-rich beds described here fit the general accepted definition of silcretes but are incompatible with accepted methods of silcrete genesis. NFm silcretes are not relict features associated with long-term geomorphic stability in inactive landscapes. Instead, they represent relatively rapid induration in an active sedimentary basin. The presence of silica-rich ashfall deposits provided a unique stratigraphically constrained chemical and/or hydrological environment that generated the distinctive NFm silcretes. While the exact processes of NFm silcrete genesis are not fully understood, the role of fine-grained aeolian pyroclastic materials in the creation of silcretes deserves greater emphasis.

Paleoenvironments of the Nacimiento Formation

The presence of numerous ashfall deposits in the NFm demands a reconsideration of possible paleoenvironmental implications. NFm paleoclimatic conditions have been assumed as having high mean annual precipitation and temperatures, due in part to the interpretation of crocodilian and palm fossils as indicators of humid paleoclimate conditions (*e.g.*, Wing & Greenwood, 1993; Markwick, 1994). The abundance of preserved ashfall deposits in the NFm suggests that there was sufficient precipitation during NFm deposition to prevent the aeolian erosion of these deposits; rapid colonization by plants likely aided in this preservation process. Aeolian pyroclastic/ashfall deposits in other Cenozoic fluvial basins have been interpreted as having been deposited under subhumid to semiarid conditions and as having significant impacts on paleobiota and paleolandscape development (Hunt, 1990). The deposits we describe here prove that mineral material was delivered to the aggradational early Paleocene San Juan Basin via non-fluvial means. NFm silcretes show that portions of the NFm depositional system underwent periods of quiescence during which aeolian

pyroclastic deposits could not only accumulate, but also be colonized by biota and preserved.

REFERENCES CITED

Alexander, G.B., Heston, W.M., and Iler, H.K., 1954, The solubility of amorphous silica in water: Journal of Physical Chemistry, v. 58, p. 453-455.

Armenteros, I., Bustillo, M.A., and Blanco, J.A., 1995, Pedogenic and groundwater processes in a closed Miocene basin (northern Spain): Sedimentary Geology, v. 99, p. 17-36.

Ballasteros, E.M., Talegon, J.G., and Hernandez, M.A., 1997, Palaeoweathering profiles developed on the Iberian hercynian basement and their relationship to the oldest Tertiary surface in central and western Spain, *in* Widdowson, ed., Palaeosurfaces: Recognition, Reconstruction and Palaeoenvironmental Interpretation: Bath, England, Geological Society Publishing House, Special Publication 120, p. 175-185.

Battarbee, R.W., Jones, V.J., Flower, R.J., Cameron, N.G., Bennion, H., Carvalho, L., and Juggins, S., 2001, Diatoms, *in* Smol, J.P., Birks, H.J.B., and Last, W.M., eds., Tracking Environmental Change Using Lake Sediments, Volume 3: Terrestrial, Algal, and Siliceous Indicators: Dordrecht, The Netherlands, Kluwer Academic Publishers, p. 155-202.

Batezelli, A., and Ladeira, F.S.B., 2016, Stratigraphic Framework and evolution of the Cretaceous continental sequences of the Bauru, Sanfranciscana, and Parecis basins, Brazil: Journal of South American Earth Sciences, v. 65, p. 1-24.

Birkeland, P.W., 1974, Pedology, Weathering and Geomorphological Research: New York, Oxford University Press.

Borger, H., McFarland, M.J., and Ringrose, S., 2004, Processes of silicate karstification associated with pan formation in the Darwin-Koolpinya area of Northern Australia: Earth Surface Processes and Landforms, v. 29, p. 359-371.

Bustillo, M.A., and Bustillo, M., 2000, Miocene silcretes in argillaceous playa deposits, Madrid Basin, Spain: petrological and geochemical features: Sedimentology, v. 47, p. 1023-1037.

Cas, R.A.F., and Wright, J.V., 1988, Classification of modern and ancient volcaniclastic rocks of pyroclastic and epiclastic origins, *in* Volcanic Successions Modern and Ancient: Boston, Massachusetts, Allen and Unwin, 528 p.

Cather, S.M., 2004, Laramide orogeny in central and northern New Mexico and southern Colorado, *in* Mack, G.H., and Giles, K.A., eds., The Geology of New Mexico: A Geologic History: New Mexico Geological Society Special Publication 11, p. 203-248.

Cunningham, C.G., Naeser, C.W., Marvin, R.F., Luedke, R.G., and Wallace, A.R., 1994, Ages of selected intrusive rocks and associated ore deposits in the Colorado Mineral Belt: USGS Bulletin 2109, 31 p.

Donahue, M.S., 2016, Episodic uplift of the Rocky Mountains: Evidence from U-Pb detrital zircon geochronolgy and low-temperature thermochronology with a chapter on using mobile technology for geoscience education: Ph.D. dissertation, University of New Mexico, Albuquerque, 1177 p.

Dove, P.M., and Rimstidt, J.D., 1994, Silica-water interactions, *in* Heaney, P.J., Prewitt, C.T., and Gibbs, G.V., eds., Silica: Physical Behaviour, Geochemistry and Materials Applications: Washington, USA, Mineralogical Society of America, Reviews in Mineralogy 29, p. 259-308.

Drever, J.I., 1994, The effect of land plants on weathering rates of silicate minerals: Geochimica et Cosmochimica Acta, v. 58, n. 10, p. 2325-2332.

Drever, J.I., and Stillings, L.L., 1997, The role of organic acids in mineral weathering: Colloids and Surfaces A: Physicochemical and Engineering Aspects, v. 120, n. 1-3, p. 167-181.

Dubroeucq, D. and Thiry, M., 1994, Indurations silceuses dans les sols volcaniques. Comparaison avec des silcretes anciens: 15th World Congress of Soil Sciences, Acapulco, Mexico, July 10-16, 6a., p. 445-459.

Dugmore, A.J., Newton, A.J., Sugden, D.E., and Larsen, G., 1992, Geochemical stability of fine-grained silicic Holocene tephra in Iceland and Scotland: Journal of Quaternary Science, v. 7, n. 2, p. 173-183.

Gallagher, T.M., and Sheldon, N.D., 2013, A new paleothermometer for forest paleosols and its implications for Cenozoic climate: Geology, v. 41, n. 6, p. 647-650.

Hill, S.M., Eggleton, R.A., and Taylor, G., 2003, Neotectonic disruption of silicified palaeovalley systems in an intraplate, cratonic landscape: regolith and landscape evolution of the Mulculca range-front, Broken Hill Domain, New South Wales: Australian Journal of Earth Sciences, v. 50, p. 691-707.

Huggett, J., and Longstaffe, F.J., 2016, A brief account of new petrographic and isotopic insights into the Hertfordshire and Buckingham Puddingstones of SE England:

Proceedings of the Geologists' Association, http://dx.doi.org/10.1016/j.pgeola.2016.01.003.

Hunt, R.M., Jr., 1990, Taphonomy and sedimentology of Arikaree (lower Miocene) fluvial, eolian, and lacustrine paleoenvironments, Nebraska and Wyoming; A paleobiota entombed in fine-grained volcaniclastic rocks, *in* Lockley, M.G., and Rice, Al, eds., Volcanism and fossil biotas: Boulder, Colorado, Geological Society of America Special Paper 244, p. 69-112.

Irving, E., 1979, Paleopoles and paleolatitudes of North America and speculations about displaced terrains: Canadian Journal of Earth Science, v. 16, p. 669-694.

Johnson, N.M., Driscoll, C.T., Eaton, J.S., Likens, G.E., and McDowell, W.H., 1981, Acid rain, dissolved aluminum and chemical weathering at the Hubbard Brook Experimental Forest, New Hampshire: Geochimica et Cosmochimica Acta, v. 45, n. 9, p. 1421-1437.

Khalaf, F.I., 1988, Petrography and diagenesis of silcrete from Kuwait, Persian Gulf: Journal of Sedimentary Petrology, v. 58, n. 6, p. 1014-1022.

Lang, J.R., 1991, Isotopic and geochemical characteristics of Laramide igneous rocks in Arizona: Tucson, University of Arizona Ph.D. Dissertation, 201 p.

Lee, S.Y., and Gilkes, R.J., 2005, Groundwater geochemistry and composition of hardpans in southwestern Australia regolith: Geoderma, v. 126, p. 59-84.

Lindqvist, J.K., 1990, Deposition and diagenesis of Landslip Hill silcrete, Gore Lignite Measures (Miocene), New Zealand: New Zealand Journal of Geology and Geophysics, v. 33, p. 137-150.

Maly, K.D., Cajz, V., Adamovic, J., and Zacharias, J., 2006, Silicification of quartz arenites overlain by volcaniclastic deposits: an alternative to silcrete formation: Geologica Carpathica, v. 57, n. 6, p. 461-472.

Markwick, P.J., 1994, "Equability," continentality, and Tertiary "climate": The crocodilian perspective: Geology, v. 22, p. 613-616.

Milnes, A.R., and Thiry, M., 1992, Silcretes, *in* Martini, I.P., and Chesworth, W., eds., Weathering, Soils, and Palaeosols: Amsterdam, Elsevier, Developments in Earth Surface Processes 2, p. 349-377.

Mustard, P.S., and Donaldson, J.A., 1990, Paleokarst breccias, calcretes, silcretes and fault talus breccias at the base of Upper Proterozoic "Windermere' strata, northern Canadian Cordillera: Journal of Sedimentary Petrology, v. 60, p. 525-539.

Nash, D.J., and Ullyott, J.S., 2007, Silcrete, *in* Nash, D.J., McLaren, S.J., eds., Geochemical Sediments and Landscapes: Blackwell, Oxford, p. 95-143.

Nimlos, T.J., 1989, The density and strength of Mexican tepetate (duric materials): Soil Science, v. 147, n. 1, p. 23-27.

Nimlos, T.J., and Ortiz-Solorio, C., 1987, Tepetate, the rock mat: J. of Soil and Water Conservation, v. 42, n. 2, p. 83-86.

Pollard, A.M., Blockley, S.P.E., and Ward, K.R., 2003, Chemical alteration of tephra in the depositional environment: theoretical stability modelling: Journal of Quaternary Science, v. 18, n. 5, p. 385-394.

Rains, G.E., 1981, Paleocene silcrete beds in the San Juan Basin [M.S. Thesis]: Tucson, University of Arizona, 81 p.

Rimstidt, J.D., 1997, Quartz solubility at low temperatures: Geochimica et Cosmochimica Acta, v. 61, n. 13, p. 2553-2558.

Sarna-Wojcicki, A.M., Meyer, C.E., Woodward, M.J., and Lamothe, P.J., 1981, Composition of air-fall ash erupted on May 18, May 25, June 12, July 22, and August 7, *in* Lipman, P.W., and Mullineaux, D.R., eds., The 1980 eruptions of Mount St. Helens, Washington: USGS Professional Paper 1250, p. 667-681.

Scherer, C.M.S., and Lavina, E.L.C., 2006, Stratigraphic evolution of a fluvial-eolian succession: The example of the Upper Jurassic-Lower Cretaceous Guara and Botucatu formations, Parana Basin, Southernmost Brazil: Gondwana Research, v. 9, p. 475-484.

Schmid, R., 1981, Descriptive nomenclature and classification of pyroclastic deposits and fragments: Geology, v. 9, p. 41-43.

Shane, P.A.R., 1991, Remobilised silicic tuffs in middle Pleistocene fluvial sediments, southern North Island, New Zealand: New Zealand Journal of Geology and Geophysics, v. 34, p. 489-499.

Smith, L.N., 1988, Basin analysis of the lower Eocene San Jose Formation, San Juan Basin, New Mexico and Colorado [Ph.D. dissertation]: Albuquerque, University of New Mexico, 148 p.

Summerfield, M.A., 1983, Silcrete, *in* Goudie, A.S., and Pye, K., eds., Chemical Sediments and Geomorphology: Academic Press, London, p. 59-91.

Titley, S.R., 1995, Geological summary and perspective of porphyry copper deposits in southwestern North America, *in* Pierce, F.W., and Bolm, J.G., eds., Porphyry

Copper Deposits of the American Cordillera: Arizona Geological Society Digest, v. 20, p. 6-20.

Thiry, M., 1999, Diversity of continental silicification features: examples from the Cenozoic deposits in the Paris Basin and neibouring basement, *in* Thiry, M., and Simon-Coinçon, R., eds., Palaeoweathering, Palaeosurfaces and Related Continental Deposits, Special Publication 27, International Association of Sedimentologists: Blackwell, Oxford, p. 87-127.

Thiry, M., and Milnes, A.R., 1991, Pedogenic and groundwater silcretes at Stuart Creek Opal Field, South Australia: Journal of Sedimentary Petrology, v. 61, n. 1, p. 111-127.

Thiry, M., Milnes, A.R., Rayot, V., and Simon-Coincon, R., 2006, Interpretation of palaeoweathering features and successive silicifications in the Tertiary regolith of inland Australia: Journal of the Geological Society, London, v. 163, p. 723-736.

Ullyot, J.S., Nash, D.J., and Huggett, J.M., 2015, Cap structures as diagnostic indicators of silcrete origin: Sedimentary Geology, v. 325, p. 119-131.

Wegert, D., and Parker, D.F., 2011, Petrogenesis of the McDermott Formation trachyandesite, San Juan basin, Colorado and New Mexico: Rocky Mountain Geology, v. 46, n. 2, p. 183-196.

Wehrfritz, B.D., 1978, The Rhame Bed (Slope Formation, Paleocene), a silcrete and deep-weathering profile, in southwestern North Dakota [M.S. Thesis]: Grand Forks, University of North Dakota, 158 p.

Wing, S.L., and Greenwood, D.R., 1993, Fossils and fossil climate: The case for equable continental interiors in the Eocene: Philosophical Transactions of the Royal Society B, v. 341, p. 243-252.

Williamson, T.E., 1996, The beginning of the age of mammals in the San Juan Basin, New Mexico: Biostratigraphy and evolution of Paleocene mammals of the Nacimiento Formation: New Mexico Museum of Natural History and Science, Bulletin 8, 141 p.

Williamson, T.E., Crossey, L.J., and Lucas, S.G., 1992, Silcretes of the Paleocene Nacimiento Formation, *in* Lucas, S.G., Kues, B.S., Williamson, T.E., and Hunt, A.P., eds., San Juan Basin IV: New Mexico Geological Society Guidebook, v. 43, p. 38-42.

Wopfner, H., 1983, Environment of silcrete formation: a comparison of examples from Australia and the Cologne Embayment, West Germany, *in* Wilson, R.C.L., ed.,

Residual Deposits: Surface Related Weathering Processes and Materials: Geological Society of London, Special Publication 11, p. 151-157.

Žutić, V., and Stumm, W., 1984, Effect of organic acids and fluoride on the dissolution kinetics of hydrous alumina: a model study using the rotating disc electrode: Geochimica et Cosmochimica Acta, v. 48, n. 7, p. 1493-1503.

FIGURES

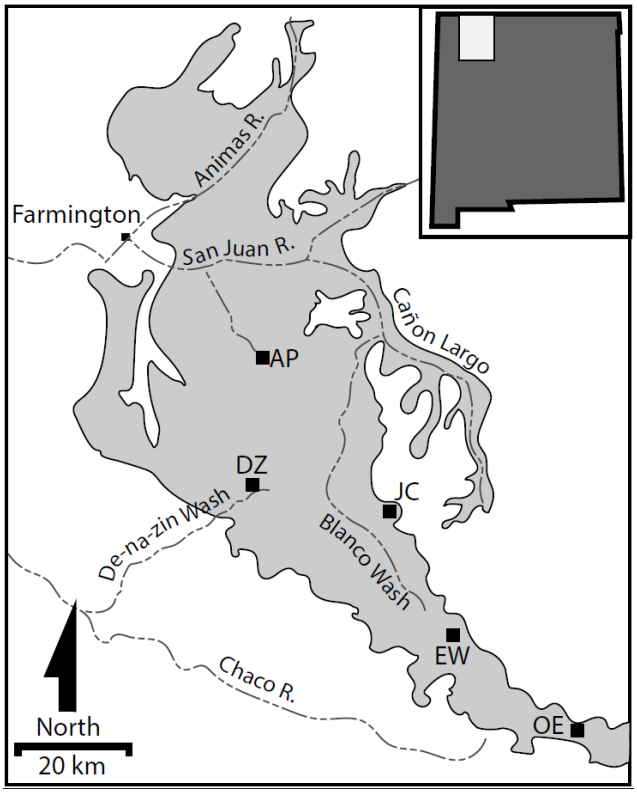

Figure 1. Location map of study area. Inset map shows location within New Mexico. Nacimiento Formation outcrop area marked by shaded area. AP: Angel Peak; DZ: De-na-zin Wash; JC: Jay Canyon; EW: Escavada Wash; OE: Ojo Encino.

Figure 2. Two silcretes at Ojo Encino. Arrows mark silcrete beds. Upper silcrete formed in aeolian pyroclastic material that was deposited in a channel cut through lower silcrete and adjacent siliciclastic strata. Scale varies; ~3 m vertical distance between the two silcretes near arrows.

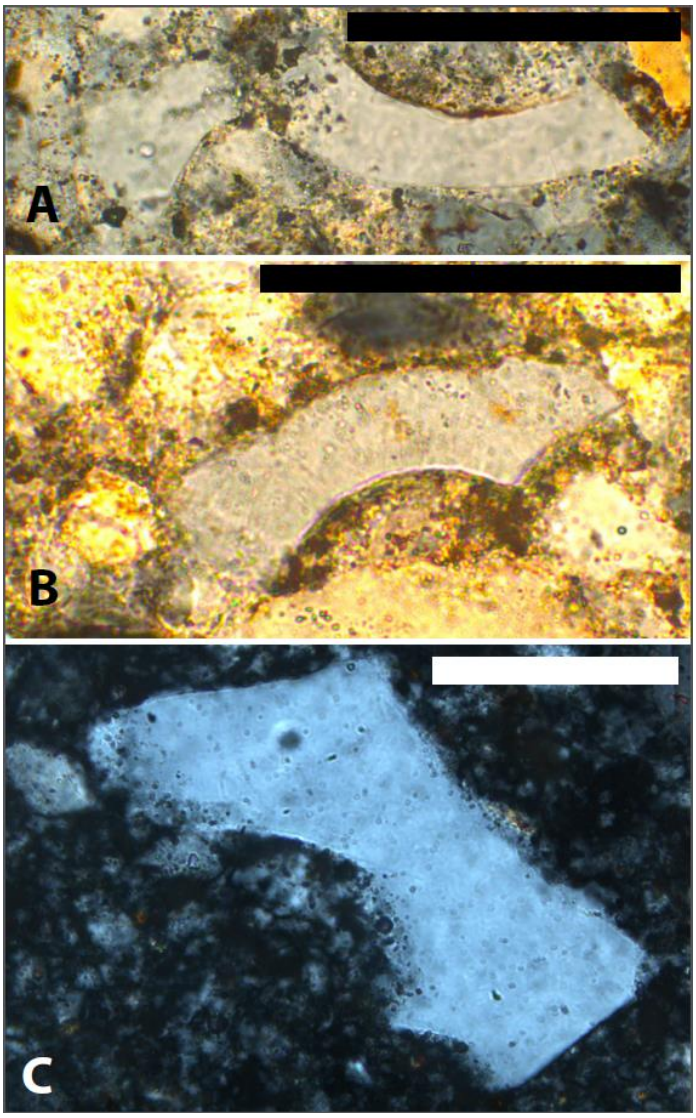

Figure 3. Photomicrographs of tephra shards in Nacimiento Formation silcretes. Scale bar in each is 0.1 mm. Sampling localities: A: Kutz Canyon. B: Escavada Wash. C: Jay Canyon.

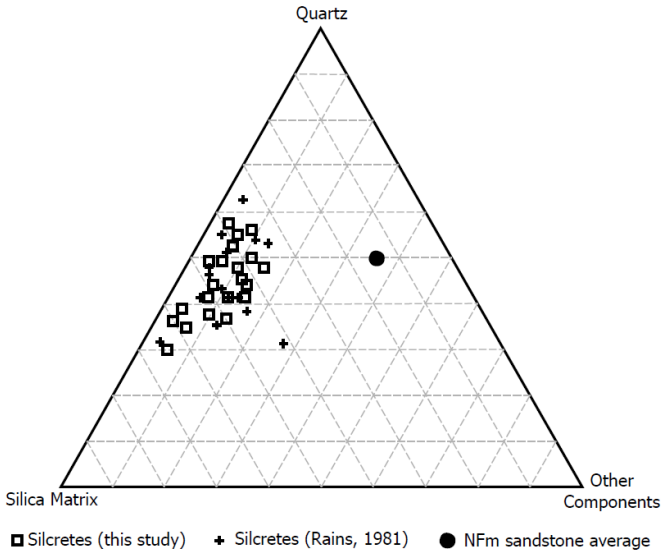

Figure 4. Ternary diagram showing relationships between quartz grains, silica matrix, and all other materials in Nacimiento Formation silcretes and average Nacimiento Formation sandstone.

TABLES

Pedogenic Silcretes	SJB Silcretes		Groundwater Silcretes
Sedimentary structures destroyed	X	✓	Sedimentary structures preserved
Microquartz dominant	✓	X	Quartz overgrowths dominant
Associated with kaolinitic weathering horizons	X	✓	Associated with arenaceous sediments
Indicate a depositional hiatus	✓	X	Unrelated to depositional processes
Columnar fractures	X	✓	Massive
Transect varous ages and types of substrate	✓	X	Associated with one stratum
Formed on stable basement rocks	X	✓	Formed in basin fill
Contain roots & bioturbation structures	✓	X	No pedofeatures present
Elluvial-over-illuvial vertical profile	X	✓	Little to no vertical grading
Require >10^6 y to form	?	?	Can form in <10^6 y
Form in subaerial weathering profile			Form in lithified sediment

Table 1. Properties of pedogenic and groundwater silcretes, taken from Nash & Ullyott (2007) and references therein. San Juan Basin (SJB) silcretes of this study, shown in middle column, share properties with both types of silcretes.

Sample	Wt % Na_2O	Wt % MgO	Wt % Al_2O_3	Wt % SiO_2	Wt % P_2O_5	Wt % K_2O	Wt % CaO	Wt % TiO_2	Wt % MnO	Wt % Fe_2O_3
BDNZ-24	1.852	0.402	13.134	79.059	0.019	3.132	0.472	0.717	0.017	1.196
ESCA-05	0.099	0.357	5.892	90.622	0.012	0.532	0.391	1.118	0.008	0.968
CROW-06	0.253	0.199	3.829	93.597	0.010	0.150	0.224	1.062	0.011	0.665
CROW-082	0.224	0.151	5.275	92.229	0.013	0.103	0.143	1.070	0.014	0.779
CROW-05	0.145	0.178	7.867	89.619	0.015	0.081	0.118	1.054	0.010	0.910
ANSI-01	0.297	0.194	4.022	91.191	0.019	1.599	0.197	1.009	0.018	0.991
JACA-17	0.220	0.246	5.009	90.879	0.013	0.816	0.431	1.150	0.013	0.897
Average	0.4	0.2	6.4	89.6	0.0	0.9	0.3	1.0	0.0	0.9

Table 2. Bulk geochemical data of SJB silcretes.

Appendix A. Petrographic Point Count Data

Sample	GRAINS								MATRIX			Grand Total
	Shard	Quartz Unknown	Detrital	Total	Chert	Feldspar	Other	Total	Silica	Clay	Total	
ANSI-01a	8	23	9	40	2	3	0	45	53	2	55	100
ANSI-01b	12	28	5	45	1	2	1	49	50	1	51	100
BDNZ-24	9	15	17	41	5	9	5	60	32	8	40	100
CROW-06A	4	34	3	41	2	1	1	45	55	0	55	100
CROW-06B	5	26	0	31	2	1	1	35	65	0	65	100
CROW-06C	5	29	3	37	1	1	1	40	59	1	60	100
CROW-082A	11	19	6	36	4	3	1	44	54	2	56	100
CROW-082B	8	22	5	35	2	2	2	41	58	1	59	100
CROW-082C	6	26	5	37	2	2	1	42	57	1	58	100
ESCA-05a	2	16	8	26	6	3	5	40	58	2	60	100
ESCA-05b	2	20	5	27	5	1	5	38	61	1	62	100
BDNZ-21	6	16	6	28	6	9	9	52	40	8	48	100
CROW-05	9	29	7	45	1	1	1	48	51	1	52	100
JACA-17	7	31	2	40	1	3	1	45	55	0	55	100
CROW-081A	8	26	1	35	1	0	4	40	59	1	60	100
CROW-081B	7	29	2	38	2	0	3	43	56	1	57	100
Average	6.8	24.3	5.3	36.4	2.7	2.6	2.6	44.2	53.9	1.9	55.8	100

Appendix B. Bulk Geochemical Data

Sample	Wt % Na_2O	Wt % MgO	Wt % Al_2O_3	Wt % SiO_2	Wt % P_2O_5	Wt % K_2O	Wt % CaO	Wt % TiO_2	Wt % MnO	Wt % Fe_2O_3	Total
BDNZ-24	1.852	0.402	13.134	79.059	0.019	3.132	0.472	0.717	0.017	1.196	100.0
ESCA-05	0.099	0.357	5.892	90.622	0.012	0.532	0.391	1.118	0.008	0.968	100.0
CROW-06	0.253	0.199	3.829	93.597	0.010	0.150	0.224	1.062	0.011	0.665	100.0
CROW-082	0.224	0.151	5.275	92.229	0.013	0.103	0.143	1.070	0.014	0.779	100.0
CROW-05	0.145	0.178	7.867	89.619	0.015	0.081	0.118	1.054	0.010	0.910	100.0
ANSI-01	0.297	0.194	4.022	91.191	0.019	1.599	0.197	1.009	0.018	0.991	99.5
JACA-17	0.220	0.246	5.009	90.879	0.013	0.816	0.431	1.150	0.013	0.897	99.7
Average	0.4	0.2	6.4	89.6	0.0	0.9	0.3	1.0	0.0	0.9	99.9

Appendix C. Microprobe Elemental Data

SAMPLE	SiO2	Al2O3	TiO2	Na2O	MgO	FeO	K2O	CaO	BaO	O	HO	TOTAL
ANSI01 Clast 1	98.2	0.0	0.0	0.0	0.0	0.0	0.0	0.0	0.0	0.0	1.8	100
ANSI01 Clast 10	63.4	18.5	0.0	2.6	0.0	0.0	7.2	0.1	0.7	0.0	7.3	100
ANSI01 Clast 10	68.0	19.9	0.0	2.6	0.0	0.1	6.1	0.0	0.7	0.0	2.6	100
ANSI01 Clast 11	2.4	2.9	64.0	0.0	0.2	18.3	0.0	0.4	0.3	0.0	11.4	100
ANSI01 Clast 11	4.0	3.1	65.0	0.0	0.1	17.1	0.0	0.5	0.2	0.0	10.0	100
ANSI01 Clast 12	102.0	0.0	0.0	0.0	0.0	0.0	0.0	0.0	0.0	0.0	0.0	102.02
ANSI01 Clast 13	33.7	32.3	0.2	2.1	2.4	14.3	0.0	0.1	0.0	0.0	14.9	100
ANSI01 Clast 13	35.3	32.0	0.4	2.3	3.4	13.2	0.0	0.1	0.0	0.0	13.4	100
ANSI01 Clast 2	95.3	1.3	0.0	0.0	0.0	0.2	0.1	0.0	0.4	0.0	2.6	100
ANSI01 Clast 3	98.1	0.0	0.0	0.0	0.0	0.0	0.0	0.0	0.0	0.0	1.8	100
ANSI01 Clast 4	97.8	0.0	0.0	0.0	0.0	0.0	0.0	0.0	0.0	0.0	2.2	100
ANSI01 Clast 5	97.7	0.0	0.0	0.0	0.0	0.0	0.0	0.0	0.0	0.0	2.3	100
ANSI01 Clast 6	98.4	0.0	0.0	0.0	0.0	0.0	0.0	0.0	0.0	0.0	1.5	100
ANSI01 Clast 7	67.8	19.4	0.6	0.1	1.1	3.4	1.3	0.3	0.0	0.0	5.9	100
ANSI01 Clast 8	36.3	0.0	0.0	0.0	0.0	0.0	0.0	0.0	0.0	0.0	63.6	100
ANSI01 Clast 9	0.5	0.9	94.8	0.0	0.0	1.1	0.0	0.1	0.0	0.0	2.5	100
ANSI01 Clast 9	0.5	0.9	94.7	0.0	0.0	1.1	0.0	0.1	0.0	0.0	2.6	100
ANSI01 Matrix 1	74.7	8.9	0.2	0.1	0.7	1.7	0.4	0.4	0.0	0.0	12.9	100
ANSI01 Matrix 2	77.7	9.3	0.2	0.1	0.7	1.6	0.3	0.3	0.0	0.0	9.6	100
ANSI01 Matrix 3	56.6	9.4	0.2	0.1	0.8	3.1	0.4	0.4	0.0	0.0	29.1	100
ANSI01 Matrix 3	98.3	0.8	0.0	0.0	0.0	0.0	0.1	0.0	0.0	0.0	0.9	100
ANSI01 Matrix 4	99.2	1.0	0.1	0.0	0.0	0.1	0.1	0.0	0.0	0.0	0.0	100.6
ANSI01 Matrix 5	102.3	0.0	0.0	0.0	0.0	0.0	0.0	0.0	0.0	0.0	0.0	102.35
ANSI01 Matrix 6	102.4	0.0	0.0	0.0	0.0	0.0	0.0	0.0	0.0	0.0	0.0	102.53
ANSI01 Matrix 7	102.8	0.0	0.0	0.0	0.0	0.0	0.0	0.0	0.0	0.0	0.0	102.77
ANSI01 Matrix 8	98.8	1.1	0.8	0.0	0.0	0.1	0.0	0.0	0.2	0.0	0.0	101.14
BDNZ24 clast 1	67.5	21.0	0.0	11.4	0.0	0.1	0.1	0.9	0.0	0.0	0.0	100.85
BDNZ24 clast 2	45.9	38.6	0.0	0.3	0.1	0.8	11.0	0.0	0.1	0.0	3.2	100
BDNZ24 clay	57.8	23.3	0.3	0.4	1.5	5.3	1.0	1.3	0.0	0.0	9.1	100
BDNZ24 clay 2	64.6	21.6	0.4	0.1	1.5	4.7	2.5	1.2	0.0	0.0	3.5	100
BDNZ24 matrix 3	46.6	21.6	3.4	0.1	1.1	4.3	1.2	1.4	0.0	0.0	20.4	100
BDNZ24 matrix 3	61.0	17.7	0.4	0.3	0.9	3.6	1.1	1.2	0.0	0.0	13.8	100
BDNZ24 matrix 3	65.6	19.5	0.2	0.2	0.5	1.9	1.0	0.6	0.0	0.0	10.6	100
BDNZ24 matrix 3	72.3	11.8	0.3	0.4	0.9	2.7	0.7	1.0	0.0	0.0	10.1	100
BDNZ24 matrix 4	46.9	18.4	0.4	0.2	1.0	5.8	2.3	1.6	0.0	0.0	23.3	100
BDNZ24 matrix 4	53.1	21.1	0.2	0.2	1.1	3.7	3.9	0.9	0.0	0.0	16.0	100
BDNZ24 matrix 4	97.1	2.3	0.0	0.2	0.1	0.2	0.3	0.1	0.0	0.0	0.0	100.25
BDNZ24 matrix1	49.7	20.1	0.0	1.5	0.3	1.3	6.2	0.2	0.4	0.0	20.3	100
BDNZ24 matrix2	46.1	20.0	0.1	1.9	1.1	3.5	1.7	0.8	0.0	0.0	24.7	100
BDNZ24 matrix2	51.0	23.3	0.1	0.2	0.9	3.5	1.5	0.7	0.0	0.0	18.8	100
BDNZ24 matrix2	63.2	15.2	0.2	0.4	0.8	3.0	2.9	0.8	0.0	0.0	13.7	100
BDNZ24 matrix2	71.3	12.3	0.2	0.2	0.6	2.5	1.4	0.6	0.0	0.0	10.9	100
BDNZ24 shard 16	102.7	0.0	0.0	0.0	0.0	0.0	0.0	0.0	0.0	0.0	0.0	102.8
BDNZ24 shard 16	102.7	0.0	0.0	0.0	0.0	0.0	0.0	0.0	0.0	0.0	0.0	102.83
BDNZ24 shard 17	64.9	18.8	0.0	0.5	0.0	0.0	16.1	0.0	0.7	0.0	0.0	101.02
BDNZ24 shard 6	100.7	0.0	0.0	0.0	0.0	0.0	0.0	0.0	0.0	0.0	0.0	100.76
BDNZ24 shard 7	100.3	0.0	0.0	0.0	0.0	0.0	0.0	0.0	0.0	0.0	0.0	100.31
BDNZ24 shard 8	101.0	0.0	0.0	0.0	0.0	0.0	0.0	0.0	0.0	0.0	0.0	101.02
BDNZ24 shard 9	101.5	0.0	0.0	0.0	0.0	0.0	0.0	0.0	0.0	0.0	0.0	101.48
BDNZ24 shard 9	101.5	0.0	0.0	0.0	0.0	0.0	0.0	0.0	0.0	0.0	0.0	101.52
BDNZ24 shard1	100.8	0.0	0.0	0.0	0.0	0.0	0.0	0.0	0.0	0.0	0.0	100.84
BDNZ24 shard2	100.9	0.0	0.0	0.0	0.0	0.0	0.0	0.0	0.0	0.0	0.0	100.92
BDNZ24 shard3	59.0	19.6	1.4	1.3	0.7	3.7	1.7	1.0	0.0	0.0	11.7	100
BDNZ24 shard3	65.5	18.5	0.0	0.4	0.0	0.1	16.6	0.0	0.0	0.0	0.0	101.11
BDNZ24 shard4	62.6	24.2	0.0	8.8	0.0	0.0	0.1	5.2	0.0	0.0	0.0	100.88
BDNZ24 shard5	102.2	0.0	0.0	0.0	0.0	0.0	0.0	0.0	0.0	0.0	0.0	102.24
Crow06 Clast 1	96.2	0.9	0.0	0.1	0.0	0.1	0.1	0.0	0.1	0.0	2.5	100
Crow06 clast 2	100.4	0.0	0.0	0.0	0.0	0.0	0.0	0.0	0.0	0.0	0.0	100.43
Crow06 clast 3	100.2	0.0	0.0	0.0	0.0	0.0	0.0	0.0	0.0	0.0	0.0	100.27
Crow06 clast 4	97.0	0.1	0.0	0.0	0.0	0.1	0.0	0.0	0.0	0.0	2.8	100
Crow06 clast 5	100.8	0.0	0.0	0.0	0.0	0.0	0.0	0.0	0.0	0.0	0.0	100.86

SAMPLE	SiO2	Al2O3	TiO2	Na2O	MgO	FeO	K2O	CaO	BaO	O	HO	TOTAL
Crow06 clast 6	100.8	0.0	0.0	0.0	0.0	0.0	0.0	0.0	0.0	0.0	0.0	100.83
Crow06 clast 7	97.2	0.0	0.0	0.0	0.0	0.0	0.0	0.0	0.0	0.0	2.7	100
Crow06 clast 8	97.7	0.0	0.0	0.0	0.0	0.0	0.0	0.0	0.0	0.0	2.3	100
Crow06 clast 9	97.5	0.0	0.0	0.0	0.0	0.0	0.0	0.0	0.0	0.0	2.5	100
Crow06 matrix 1	99.8	0.1	0.0	0.0	0.0	0.0	0.0	0.0	0.0	0.0	0.1	100
Crow06 matrix 2	97.0	0.1	0.0	0.0	0.0	0.0	0.0	0.0	0.0	0.0	2.9	100
Crow06 matrix 3	97.1	0.0	0.0	0.0	0.0	0.0	0.0	0.0	0.0	0.0	2.9	100
Crow082 clast 1	94.2	1.0	0.5	0.0	0.1	1.2	0.1	0.1	0.1	0.0	2.7	100
Crow082 clast 1	95.8	1.2	0.0	0.0	0.0	0.6	0.1	0.0	0.1	0.0	2.1	100
Crow082 clast 1	95.9	1.0	0.0	0.0	0.0	0.4	0.1	0.1	0.0	0.0	2.4	100
Crow082 clast 1	96.1	0.9	0.0	0.0	0.0	1.7	0.0	0.0	0.0	0.0	1.2	100
Crow082 clast 10	99.5	0.0	0.0	0.0	0.0	0.0	0.0	0.0	0.0	0.0	0.5	100
Crow082 clast 11	100.4	0.0	0.0	0.0	0.0	0.0	0.0	0.0	0.0	0.0	0.0	100.45
Crow082 clast 11b	97.6	0.0	0.0	0.0	0.0	0.0	0.0	0.0	0.0	0.0	2.3	100
Crow082 clast 12	100.0	0.1	0.0	0.0	0.0	0.0	0.0	0.0	0.0	0.0	0.0	100.06
Crow082 clast 12b	87.4	0.1	8.0	0.0	0.0	2.9	0.0	0.0	0.0	0.0	1.7	100
Crow082 clast 13	99.3	0.0	0.0	0.0	0.0	0.0	0.0	0.0	0.0	0.0	0.7	100
Crow082 clast 14	98.4	0.0	0.0	0.0	0.0	0.0	0.0	0.0	0.0	0.0	1.6	100
Crow082 clast 2	98.9	0.0	0.0	0.0	0.0	0.0	0.0	0.0	0.0	0.0	1.1	100
Crow082 clast 3	98.1	0.0	0.0	0.0	0.0	0.0	0.0	0.0	0.0	0.0	1.8	100
Crow082 clast 4	99.5	0.0	0.0	0.0	0.0	0.0	0.0	0.0	0.0	0.0	0.4	100
Crow082 clast 5	98.0	0.0	0.0	0.0	0.0	0.0	0.0	0.0	0.0	0.0	1.9	100
Crow082 clast 6	99.1	0.0	0.0	0.0	0.0	0.0	0.0	0.0	0.0	0.0	0.8	100
Crow082 clast 7	99.5	0.0	0.0	0.0	0.0	0.0	0.0	0.0	0.0	0.0	0.4	100
Crow082 clast 8	97.3	0.0	0.0	0.0	0.0	0.0	0.0	0.0	0.0	0.0	2.6	100
Crow082 clast 9	99.0	0.0	0.0	0.0	0.0	0.0	0.0	0.0	0.0	0.0	1.0	100
Crow082 matrix 1	97.4	0.5	0.0	0.0	0.0	0.0	0.0	0.0	0.0	0.0	2.0	100
ESCA05 Clast 1	102.7	0.0	0.0	0.0	0.0	0.0	0.0	0.0	0.0	0.0	0.0	102.71
ESCA05 Clast 2	101.3	0.0	0.0	0.0	0.0	0.0	0.0	0.0	0.0	0.0	0.0	101.37
ESCA05 Clast 3	71.3	18.1	0.7	0.1	0.7	2.5	0.6	0.7	0.0	0.0	5.3	100
ESCA05 clast 4	100.8	0.0	0.0	0.0	0.0	0.0	0.0	0.0	0.0	0.0	0.0	100.82
ESCA05 clast 5	99.0	0.0	0.0	0.0	0.0	0.0	0.0	0.0	0.0	0.0	1.0	100
ESCA05 clast 6	84.8	0.0	0.0	0.0	0.0	0.0	0.0	0.0	0.0	0.0	15.2	100
ESCA05 clast 6	101.7	0.0	0.0	0.0	0.0	0.0	0.0	0.0	0.0	0.0	0.0	101.76
ESCA05 clast 7	103.0	0.0	0.0	0.0	0.0	0.0	0.0	0.0	0.0	0.0	0.0	103.05
ESCA05 clast 8a	102.8	0.0	0.0	0.0	0.0	0.0	0.0	0.0	0.0	0.0	0.0	102.83
ESCA05 clast 8b	102.4	0.0	0.0	0.0	0.0	0.0	0.0	0.0	0.0	0.0	0.0	102.39
ESCA05 clast 8c	102.2	0.0	0.0	0.0	0.0	0.0	0.0	0.0	0.0	0.0	0.0	102.22
ESCA05 clast 8d	102.6	0.0	0.0	0.0	0.0	0.0	0.0	0.0	0.0	0.0	0.0	102.61
ESCA05 Clay 1	67.1	16.8	0.7	0.1	1.2	3.2	0.8	0.6	0.0	0.0	9.6	100
ESCA05 Clay 2	70.0	19.0	0.5	0.1	0.9	2.7	0.5	0.6	0.0	0.0	5.6	100
ESCA05 Matrix 4	78.6	3.0	2.0	0.1	0.0	0.4	0.1	0.1	0.0	0.0	15.7	100
Qtz Std Test	100.7	0.0	0.0	0.0	0.0	0.0	0.0	0.0	0.0	0.0	0.0	100.7

Chapter 3

Paleoenvironmental and paleoclimatic conditions recorded by paleosols of the Paleocene Nacimiento Formation, New Mexico, USA

Kevin M. Hobbs[1]

[1]*Earth and Planetary Sciences Department, University of New Mexico, Albuquerque, New Mexico 87131 USA*

ABSTRACT

The environmental factors affecting pedogenesis are relatively well-understood in modern systems. However, meaningful interpretation of the paleoenvironmental significance of paleosols in a complex stratigraphic record requires understanding of the interplay between climate, sedimentation, erosion, hydrological processes, and tectonics during the accumulation and pedogenic alteration of sediments. Here, we study pedogenic features, stratigraphic position, geochemistry, and petrography of paleosols in the Nacimiento Formation in order to gain insight into the paleoenvironmental conditions of the Paleocene in the San Juan Basin. Paleotaxonomical indicators in the Nacimiento Formation suggest humid subtropical paleoclimatic conditions, but physical and mineral properties of some of the formation's paleosols indicate seasonal or long-term aridity. Other paleosols are suggestive of temperate subhumid conditions. In this study, we investigate paleosols through the San Juan Basin Paleocene section to understand better the paleoenvironmental conditions during depositional hiatuses. Physical properties were used to categorize paleosols into pedotypes indicative of unique soil moisture conditions. The general stratigraphic distribution of these pedotypes shows an increase in soil drainage conditions through the Nacimiento Formation that cannot be correlated with known climate changes. We suggest that fluvial system evolution was the major control on pedogenic conditions. Widely-used paleosol geochemical climate analyses were

applied to Nacimiento Formation paleosols and provide estimates that are in disaccord with estimates derived from paleotaxonomical indicators. We show that in alluvial depositional systems with sources areas in weathered sedimentary rocks, these analyses can be difficult to interpret and likely lead to estimates that do not reflect true pedogenic conditions. Petrographic analysis of Nacimiento Formation paleosols shows that some likely formed under semiarid to subhumid conditions that allowed pedogenic accumulation and illuviation of smectite clays yet did not substantially chemically alter primary detrital plagioclase feldspar grains in paleosol B horizons.

INTRODUCTION

The early Paleogene Nacimiento Formation of the San Juan Basin is renowned for its preservation of one of the richest, most taxonomically diverse, early Paleocene fossil mammalian faunas (Williamson & Lucas, 1992; Williamson, 1996). Because of its paleofaunal content, the Nacimiento Formation has been the focus of numerous studies that attempt to understand the composition of and changes to mammalian faunas in the first few millions of years of the Paleocene Epoch (*e.g.*, Williamson, 1996; Lofgren et al., 2004; Silcox & Williamson, 2012; Williamson et al., 2012). These studies have documented the evolution, immigration, and extinction trends of the rapidly diversifying Paleocene mammalian fauna, but few have offered interpretation of the suite of complex paleoenvironmental factors that were coeval with earliest Cenozoic mammals. These factors include paleotemperatures, paleoprecipitation, paleopedology, seasonality, and sedimentation timing and history.

In this study, the paleoenvironmental conditions present during deposition of the Nacimiento Formation are reconstructed based on the physical and chemical properties of paleosols preserved in the stratigraphic section. Detailed study of pedogenic features,

geochemical trends, mineral composition, and stratigraphic relationships allows for new interpretations of paleoenvironmental parameters that have not been addressed by previous studies. When considered in context of stratigraphic position, Nacimiento Formation paleosols provide a record of paleoenvironmental changes through the formation. In this study, we aim to determine the paleoenvironmental conditions present during pedogenesis in the San Juan Basin in the Paleocene and to put those conditions in a context of stratigraphic, paleontologic, and regional paleolandscape understanding.

Of the factors affecting soil formation, climate often exerts the strongest long-term influence. Climate conditions during pedogenesis affect the physical, mineral, and chemical properties of soils. Assuming no subsequent diagenetic alteration, these effects are preserved in paleosols, as well. Many characteristics of paleosols can be correlated with an associated function of climate during pedogenesis. A stratigraphic record of multiple paleosols within a section, unit, or basin can therefore be interpreted as representative of climate conditions during hiatuses between depositional events during sediment accumulation. Well-developed paleosols such as those in the Nacimiento Formation are unique among paleoclimate indicators in that they represent the long-term average of climate conditions during pedogenesis, making them less likely to be influenced by short-duration climate shifts.

Because of the potential value of paleosols as paleoclimate proxies, many methods use the well-established relationships between climate and soil properties to provide estimates of past climate conditions. Relationships of particular interest to this study are the long-term trends of soluble element loss in weathered soils (Chadwick et al., 2003), the increase in chemical weathering intensity with increasing annual temperature

and annual precipitation (Gallagher & Sheldon, 2013; Sheldon et al., 2002), and the relationship between soil clay species and annual precipitation (Tabor et al., 2008; 2004; Tabor & Montanez, 2004). Here, we use the above relationships and their interpretations not only to gain insight into Paleocene climate conditions in the San Juan Basin, but also to test the applicability of such methods in a complex sedimentary basin.

GEOLOGIC SETTING

The San Juan Basin (SJB) is a Laramide perimeter basin with gentle structural relief. Sediments accumulated in the SJB from the Late Cretaceous until at least the early Oligocene; the youngest remaining sedimentary units in the majority of the basin are those of the early Eocene San Jose Formation. The SJB is asymmetric with its highest subsidence on the northeast side of the basin (Dickinson et al., 1988). Bound on the east by the Nacimiento Fault and Archuleta Anticlinorium, the south by the Zuni and Lucero Uplifts, the west by the Defiance Uplift, and the north by the San Juan Uplift (Cather 2004), the SJB received most of its sediments from highlands to the north and the early San Juan Uplift (Baltz, 1967; Donahue, 2016), although source areas in the Nacimiento, Zuni, and Defiance Uplifts are suspected. The fluvial strata of the SJB indicate a general southeast paleocurrent direction in the Paleogene (Smith 1988).

The Nacimiento Formation is up to 525 m thick and contains mudstone and interbedded poorly-cemented fine to coarse sandstones (Baltz, 1967). The shales and sandstones are of two different lithologic facies across the San Juan Basin. However, the lateral changes between facies are so gradual that no lateral lithologic boundaries have been proposed. Most lithologic descriptions of the Nacimiento Formation are based on observations made in the southern portion of the SJB due to better access to and exposure of outcrops there. Descriptions from the northern portions of the basin are based on well

logs. The lowermost Nacimiento Formation interfingers or shares a gradational contact with the underlying Ojo Alamo Sandstone (Baltz, 1967), an observation often cited as evidence for placing the Ojo Alamo in the Paleogene as opposed to the Cretaceous. The Nacimiento Formation also interfingers with the coeval sandy Animas Formation to the north.

The Nacimiento Formation was deposited in terrestrial fluvial environments in the San Juan Basin (Williamson & Lucas, 1992). The San Juan Basin is one of a number of Laramide sedimentary basins in the western U.S. (Dickinson et al., 1988; Smith, 1988) that received sediments from the Jurassic through the Neogene (Baltz, 1967). Dickinson et al. (1988) suggest that the Paleocene/Eocene was a period of continued sedimentation in many Laramide basins, including the San Juan Basin. The onset of the Laramide orogeny in the Late Cretaceous/early Paleogene not only initiated the retreat of the interior seaway that had defined baselevel for much of the Cretaceous (eustatic effects likely played a role in sealevel changes, as well), but also caused greater relief and steeper gradients in the incipient basins. In the San Juan Basin, Paleocene paleoflow was primarily north to south; the Nacimiento Formation's coarsening northward and its interfingering with the coarser-grained Animas Formation to the north adds strength to the north-to-south paleoflow argument. Sandstones in the Arroyo Chijuillita Member contain angular orthoclase feldspar in the western portions of the outcrop area, likely indicating a source terrane of granitic Proterozoic rocks (Baltz, 1967) of the western San Juan Dome. In the eastern basin, however, pebbles of volcanic rocks are contained within the lower Arroyo Chijuillita Member, likely sourced from the early stages of the San Juan Volcanic Field. Much of the shale and siltstone in the Nacimiento Formation was likely

weathered from Cretaceous rocks nearby, given their similar lithologic compositions (Baltz, 1967). The eastern (Sierra Nacimiento uplift) and northwestern (Hogback Monocline) margins of the San Juan Basin were undergoing deformation during the latest Cretaceous and early Paleogene (Cather, 2004) and were potential source areas for recently-deposited sediments from within or near the basin. In general, sorting is poorer in the northern Nacimiento Formation than in the south. Baltz (1967) attributed this poor sorting to fan deposition in the northwestern San Juan Basin in the early Paleocene. The aforementioned north-to-south paleoflow would have deposited lower-energy fine-grained sediments farther south. The fluvial siliciclastic sediments of the Nacimiento Formation were deposited as the by south-flowing fans and/or fluvial systems emerging from the San Juan Dome, incipient San Juan Volcanic Field, Sierra Nacimiento highlands, or an unknown granitic highland.

METHODS

Paleosols were documented at 10 locations in the western San Juan Basin (Fig. 1). Where possible, paleosol-bearing sections were correlated to the lithologic and/or biostratigraphic zones of Williamson (1996). The author chose Williamson's (1996) zonation because of its areal and stratigraphic coverage and its documentation of recognizable lithostratigraphic features that can be used for correlation. The sections exposed at the 10 study locations span the entire Nacimiento Formation stratigraphic interval, though no one location provides a complete section of the entire formation. Paleosols were identified based on the presence of pedogenic horizons recognizable in the field, root traces, root haloes, and macroscopic pedogenic features such as gradational lower contacts and pseudoslickenlines. Pedogenic features documented in the field included horizon thickness, Munsell color, lithologic composition, physical pedogenic

features, paleontologic features, and stratigraphic position and relationships. Due to the variegated and millimeter-scale nature of some coloration features in Nacimiento Formation paleosols, all colors could not evaluated; in these cases, horizon-representative colors were listed.

Paleosol materials collected for geochemical analyses were taken from a depth of at least 10 cm normal to present land surface in order to minimize effects of recent weathering and/or climate conditions. After collection, materials were dried for 12 hours at 90°C before further physical or chemical analyses. Bulk geochemical composition of samples was determined on lithium tetraborate-fused paleosol samples with a Rigaku ZSX Primus II X-ray fluorescence (XRF) spectrometer by the Analytical Chemistry Laboratory in the Department of Earth and Planetary Sciences at the University of New Mexico. Fine portions of sandy paleosols were passed through 230-mesh (63 μm) sieves for X-ray diffraction (XRD) analysis in order to determine mineral composition. XRD analysis was performed at the New Mexico Bureau of Geology and Mineral Resources on a Panalytical X'Pert Pro diffractometer emitting Cu K-alpha radiation with 1.54 Å wavelength. Where paleosol materials were of high enough strength in the field, samples were collected for thin section analysis from at least 10 cm depth normal to present land surface. These materials were cemented by Petropoxy 154 and cured for 10 minutes at 135°C.

Geochemical climate analyses on paleosol B horizon materials were performed with methods of Sheldon et al. (2002), Nordt & Driese (2010), and Gallagher & Sheldon (2013). A strong correlation exists between precipitation and chemical index of alteration

(CIA) of a soil, allowing MAP during pedogenesis to be estimated from paleosols as follows:

$$MAP\ (mm) = 221.12\exp^{0.0197(CIA\text{-}K)}$$

where *CIA-K* is defined as (100)*[(Al_2O_3)/(Al_2O_3 + CaO + Na_2O)] using molecular percentages from whole-rock XRF analysis (Sheldon et al., 2002). The standard error on the above MAP estimation equation is ±182 mm. For paleosols with vertic properties, MAP during pedogenesis was estimated with the CALMAG proxy:

$$MAP\ (mm) = 22.69(CALMAG) - 435.8$$

Where *CALMAG* is defined as (Al_2O_3/(Al_2O_3 + CaO + MgO)*100) using molecular percentages from whole-rock XRF analysis. The standard error on the CALMAG MAP estimates is ±108 mm (Nordt & Driese, 2010). Mean annual precipitations (MAT) during pedogenesis can also be estimated from a paleosol using geochemical data with the equation:

$$MAT\ (°C) = -2.74 * \ln(PWI) + 21.39$$

where *PWI*, paleosol weathering index, is defined as (100 * [(4.20*Na) + (1.66*Mg) + (5.54*K) + (2.05*Ca)] using molecular percentages from whole-rock XRF analysis (Gallagher and Sheldon, 2013). Due to uncertainties concerning sedimentary strata thickness and their relationship to paleosol parent material composition, constitutive

mass-balance methods of paleosol geochemical analysis (*e.g.*, Chadwick et al., 1990) were not applied.

Nacimiento Formation paleosols were classified into pedotypes based upon physical and compositional characteristics. Using the interpretations of Mack et al. (1993) and Retallack (1994) as an example, these pedotypes are inferred to represent groups of paleosols that formed under similar environmental conditions. These pedotype-classified paleosols were put into stratigraphic context by position in the published Nacimiento Formation stratigraphy of Williamson (1996) and the stratigraphic sections measured for this study.

RESULTS

Twenty-nine paleosol profiles were identified in the study area and classified into six pedotypes. Individual profiles tend to exhibit upwards fining and are often separated from one another by sandstone sheets, muddy overbank deposits, or silcretes. Using Mack et al.'s (1993) paleosol classification, Nacimiento Formation paleosols fall into the categories of argillisols, protosols, and vertisols. Some pedogenically-altered profiles are stacked and form composite profiles (Fig. 2) *sensu* Kraus & Brown (1986) and Kraus (1999). Some paleosols were truncated by channel cuts. No paleosols were observed that appeared to have formed across different parent materials. Lateral extent of individual paleosols is difficult to determine due to access, recent colluvium, and stratigraphic relationships; however, two paleosols at Jay Canyon extend laterally with no remarkable physical variation for at least 1.1 km. Relative stratigraphic positions and pedotypes of observed paleosols are shown in Figures 3 and 4.

Pedotypes

Pedotype I: Low-chroma drab paleosols with carbonaceous root fossils

This pedotype contains low-chroma (chroma = 1 or 2) brown, tan, or gray profiles. There is little horizonation. Parent materials include silty sands, muddy sands, muddy silty sands, silts, and muddy silts. Carbonaceous root fossils are present in the upper portions of these paleosols. Because of these paleosols' low strength and fractured, crumbly nature, it was not possible to collect representative material for petrographic thin section analysis. XRD analyses indicate the presence of smectite-group clays.

Pedotype II: Mid- to high-value green paleosols with absence of clay coatings

This pedotype contains mid- to high-value (value = 6-8) greenish gray and light greenish gray profiles. Drab root haloes are present. Parent materials are silty sands. These paleosols are sometimes capped with silcrete, but show no remarkable increase in Si content relative to parent material or non-silcrete bearing paleosols of the same pedotype. Both smectite-group and kaolin-group clays are present.

Pedotype III: Mottled red-and-drab paleosols

This pedotype contains paleosols with strongly mottled red and grey/green horizons. Carbonaceous root fossils are sometimes present in the horizons above the mottling. Grain size varies. The mottled horizon is the only well-developed diagnostic horizon.

Pedotype IV: Smectite-rich paleosols with pseudoslickenlines, low-value gray and red colors, and poor geochemical differentiation

This pedotype contains dark (low-value) gray and/or red profiles. Carbonaceous root fossils are sometimes present. Pseudoslickenlines up to 50 cm length are indicative of paleosol material volume change related to smectite-group clays. Composition of parent materials is difficult to ascertain but is assumed to be mud and muddy silt. These

paleosols are poorly horizonated, likely due to the physical mixing associated with development of vertic properties during pedogenesis.

Pedotype V: High-chroma paleosols formed on lower-chroma basal units

This pedotype contain upper horizons with high-chroma oranges and reds atop lower-chroma parent materials. Clay coatings are present and comprise smectite-group clays or a combination of smectite-group and kaolin-group clays. Parent materials include silts, silty sands, muddy silty sands, and sands. Well-developed horizonation is present.

Pedotype VI: Pedogenically-altered sandstone with upward decrease in grain size and well-developed horizonation

This pedotypes contains profiles that often display upwards reddening, though some paleosols contain gray and grayish green horizons. Clay coatings are present and comprise smectite-group clays. Parent materials include silty sands and sands. Horizons are well developed and persist laterally for up to hundreds of meters with no remarkable variation. Like pedotypes 2 and 4, paleosols of this pedotypes show no enrichment in Si when overlain by silcrete strata.

Correlated stratigraphic sections showing the distribution of paleosols and biostratigraphic and lithostratigraphic zones is illustrated in Figures 3 and 4.

Geochemical Climate Analyses

Chemical weathering indices of 30 paleosols' Bt horizon materials were used to produce estimates of the paleotemperature and paleoprecipitation conditions under which the paleosols formed. Summary geochemical data and paleoclimate estimates are presented in Table 1. Full geochemical data are presented in Appendix A. Geochemically derived MAT estimates range from 9-16°C; MAP estimates range from 890-1380 mm.

X-ray Diffraction Analyses

Diffractograms from the fine (mud and silt) portions of 20 Nacimiento Formation paleosols are shown in Appendix B. Quartz and interstratified smectite-group clay minerals are present in each analyzed sample. Illite, kaolin-group clay minerals, and gypsum are present in some analyzed samples. The relative proportions of the three clay minerals was determined by summing and comparing the number of counts at each mineral's 001 crystal plane spacing associate peak (~6.5° 2θ for interstratified smectite-group clay minerals; 8.9° 2θ for illite; and 12.4° 2θ for kaolinite); these results are shown in Table 2 and Figure 6.

DISCUSSION

Paleoenvironmental Interpretation of Pedotypes

Pedotypes I, IV, V, and VI are represented by multiple paleosols in different stratigraphic positions throughout the study area in the southern and western SJB. Pedotypes II and III each have only one representative paleosol in the study area; however, their characteristics are so unique as to warrant their own pedotypes.

The suites of pedogenic features used for pedotype classification indicate the presence of poorly drained pedotypes I and II), moderately drained/seasonally variable (pedotypes III and IV), and well-drained (pedotypes V and VI) paleopedogenic conditions in the Paleocene SJB. Nacimiento Formation paleosols exhibit both high-chroma and low-chroma colors, aiding interpretation of hydromorphic and well-drained paleosol horizons (*e.g.*, Kraus, 1999). Paleosols indicative of both poorly-drained and well-drained paleopedogenic conditions are present throughout the Nacimiento Formation section; however, there is a general trend towards better-drained paleosols upsection (Fig. 4). Overall paleosol chemical and physical characteristics suggest temperate paleoclimate conditions.

Pedotype I is interpreted as resulting from poorly-drained paleopedogenic conditions due to its low-chroma colors, generally weakly developed horizonation, and carbonaceous root fossils. This pedotype is fairly evenly distributed throughout the Nacimiento Formation, with four representative paleosols in the Arroyo Chijuillita Member, three representative paleosols in the Ojo Encino Member, and two representative paleosols in the Escavada Member. Given the presence of decimeters-thick B horizons in some representatives of this pedotype, it is unlikely that the low-chroma colors are the result of a short pedogenetic duration; instead, it is more probable that paleosols of this pedotype formed in the absence of prevalent oxidizing conditions (Quinney et al., 2013; Therrien et al., 2009; Mack et al., 1993). Modern alluvial soils formed in saturated conditions or over shallow water tables in temperate environments exhibit organic-rich B horizons, gleyed colors (chroma = 1), and low-contrast mottling (Daniels et al., 1971), and are likely analogues for Nacimiento Formation paleosols with similar characteristics.

The green coloration in the BC horizon of pedotype II is interpreted as indicative of saturated and/or reducing conditions in that portion of the solum during pedogenesis. The upper horizons of pedotype II paleosols are redder and indicative of oxidizing conditions, suggesting that pedogenesis occurred over a shallow, stable water table.

Pedotypes V and VI are interpreted as the results of pedogenesis in well-drained (non-aquic) temperate conditions. One of the 12 paleosols of pedotypes V and VI is found in the Arroyo Chijuillita Member; 11 representative paleosols are found in the Escavada Member. Pedotypes V and VI paleosols are not found in the Ojo Encino Member. High-chroma horizons, well-developed horizonation, lack of carbonaceous root

fossils, and illuviated clay-rich horizons are indicative of prevalent non-saturated conditions throughout the solum for the majority of pedogenic duration (Retallack, 1988; Kraus, 1999). The presence of smectite and illite clay coatings, along with the relatively small proportion of kaolinite in the fine portions of these paleosols, suggests pedogenesis in semi-arid or dry-summer continental climate (Tan, 1982). Many sandy BC horizons of pedotypes V and VI paleosols contain unaltered primary aluminosilicate minerals (Fig. 7), further suggesting ustic, aridic, or xeric soil moisture conditions during pedogenesis since wetter paleopedogenic conditions likely would have produced less active clays such as kaolinite or oxides such as gibbsite (Berner & Holdgren, 1979; Vasquez, 1981).

Pedotypes III and IV are interpreted as indicative of variable water table depth and/or seasonal wetting and drying during pedogenesis. The representative pedotype III paleosol, located within the Arroyo Chijuillita Member at De-na-zin Wash, exhibits strong red/gray mottling with increasing redness up-profile, suggesting free drainage and oxidizing conditions above variable-depth saturated zone dominated by reducing conditions (Daniels et al., 1971).

The seven representative paleosols of pedotype IV are found in the upper half of the Arroyo Chijuillita Member and throughout the Ojo Encino Member. They are not present in the Escavada Member. These paleosols lack strong horizonation, are rich in smectite clays, and exhibit pseudoslickenlines up to 50 cm in length (Carritt, 2014), suggesting vertisol-like processes during pedogenesis. Modern vertic soils form under semi-arid to humid subtropical conditions (Nordt & Driese, 2010) and require seasonal wetting and drying in order to develop the solum volume changes related to loss of interlayer water in 2:1 clays. This wetting and drying can be related to wet-season/dry-

season precipitation trends, as seen in Indian and north African modern vertic soils, or to some combination of flooding and seasonal precipitation, as seen in modern alluvial vertic soils (Aslan & Autin, 1998). In either case, vertic properties in modern soils seem to require a minimum of 90 consecutive days of limited soil moisture during which clay constituents shrink. Indicators of vertisol-like properties in Nacimiento Formation pedotype IV paleosols suggest that these paleosols formed under better-drained conditions than pedotype I and II paleosols but under more poorly-drained conditions than pedotype V and VI paleosols.

Paleoenvironmental Changes Through the Nacimiento Formation Represented by Stratigraphic Distribution of Pedotypes

The six pedotypes presented here represent qualified categories on a continuum of soil moisture and/or water table conditions during pedogenesis of Nacimiento Formation sediments, with pedotype I representing the most poorly drained/shallow water table conditions and pedotypes V and VI representing the most freely drained/deeper water table conditions. When the distribution of pedotypes is viewed in relative stratigraphic context, as shown in Figure 4, there is seen a marked change in soil drainage conditions through the Nacimiento Formation.

Poorly drained and moderately drained pedogenic conditions prevailed during deposition and pedogenesis of the Early Paleocene Arroyo Chijuillita Member. Eleven of the 12 Arroyo Chijuillita Member paleosols are indicative of stable, high water tables or seasonally fluctuating water tables. Pedotype IV paleosols with vertic properties, indicative of seasonally fluctuating water tables, become more common upsection in the Arroyo Chijuillita Member, suggesting a general drop in water tables or increasing seasonality of soil moisture. There is one well-drained pedotype VI paleosol low in the

Arroyo Chijuillita Member at Betonnie Tsosie Wash, indicating variability in the general observed trend. With only one paleosol representative of well-drained conditions in the Arroyo Chijuillita Member, it is difficult to interpret whether geographic, temporal, or other factors were responsible for the well-drained pedogenic conditions.

Paleosols preserved in the Ojo Encino Member are indicative of poorly drained reducing conditions and seasonally wet vertisol-like conditions. While there are no apparent trends of pedogenic change in the Ojo Encino Member, the lack of well-drained paleosols suggests that water tables were permanently or seasonally high throughout the deposition and pedogenesis of the Ojo Encino Member.

Beginning at the base of the Escavada Member, paleosols indicative of well-drained pedogenic conditions dominate the paleosol record for the remainder of Nacimiento Formation deposition and pedogenesis. Eleven of the 13 paleosols observed in the Escavada Member formed in freely drained oxidizing conditions, suggesting deeper water tables than were present earlier in Nacimiento Formation deposition and pedogenesis. The presence of two pedotype I paleosols, indicative of high water tables and reducing conditions, within the Escavada Member are indicative of poorly drained pedogenic conditions that were either short-lived, geographically restricted, or both.

The observed trend of Nacimiento Formation paleosols becoming better-drained through time could be representative of increasing climate aridity, increasing depth to water table in the depositional/pedogenic system, changes of the location of preserved paleosols, unknown factors, or some combination of factors. Relationships between incision, deposition, and burial/preservation of soils in the overall aggradational Paleocene San Juan Basin fluvial system likely play a role, as well. There is no apparent

correlation between the pedotype (with the inferred associated paleosol moisture conditions) of a paleosol and its estimated MAP value (Table 1), suggesting that precipitation conditions were not solely responsible for the observed apparent drying trend seen in Nacimiento Formation paleosols. Quinney et al. (2013) reported a similar lack of correlation between paleosol geochemically derived paleoprecipitation estimates and the inferred paleosol moisture conditions in a Cretaceous fluvial sedimentary system, suggesting that precipitation conditions alone are not responsible for many physical properties of paleosols in active sedimentary basins. Because of the proximity to the Cretaceous Interior Seaway and the presence of minor marine deposits in their study interval, Quinney et al. (2013) suggested that changes in baselevel related to sealevel changes were responsible for the variation in soil moisture conditions in the Late Cretaceous fluvial sediments in their study. No marine deposits are known from the Paleogene section of the San Juan Basin, and the epieric sea was at least hundreds of kilometers from the San Juan Basin during the deposition and pedogenesis of the Nacimiento Formation (Cather, 2004; Blum & Pecha, 2014), suggesting that minor sealevel changes likely were not responsible for the paleosol moisture trends observed there.

Hartley et al. (2013) and Weissmann et al. (2013; 2015) report a pattern of well-drained soils proximal to sedimentary source and poorly drained soils distal to sedimentary source in modern fluvial-dominated siliciclastic sedimentary basins. As a fluvial system progrades, older poorly drained distal soils might be buried by sediments on which better-drained and more proximal soils develop (Weissmann et al., 2013), leading to an upsection trend of increasing soil drainage similar to that observed in

Nacimiento Formation paleosols (Fig. 4). This trend and the interpretation of the pedogenic and stratigraphic components therein obviously is complicated by intraformational unconformities, poor dating constraints, and outcrop exposure and access; however, the trend is likely to persist even in the presence of climate changes and minor incision during net progradation of the fluvial system. Given the lack of observed reliable indicators of major paleoclimate shifts related to Nacimiento Formation paleosols or stratigraphy, combined with the lack of evidence of marine influence in the Paleogene San Juan Basin, the most likely potential explanation for the observed trend in paleosol drainage is that water table conditions and the associated alluvial pedogenic conditions were controlled at least in part by the progradation of the Nacimiento Formation fluvial system (Fig. 5).

Geochemical Climate Analyses of Mean Annual Temperature (MAT)

The paleosol-derived MAT estimates shown in Table 1 range from 11-16°C ± 2.1°C using the PWI proxy of Gallagher & Sheldon (2013). Using the S proxy of Sheldon et al. (2002), the range is 9-17°C ±4.4°C. While there are not many published robust quantitative paleotemperature estimates from the Nacimiento Formation, our MAT estimates are similar to preliminary geochemical climate analysis estimates from other researchers in the Arroyo Chijuillita Member (Davis et al., 2015). However, the MAT estimates presented here are difficult to reconcile with the MAT estimates demanded by the presence of fossils that constrain minimum paleotemperature estimates. Crocodilian fossils are present in the Nacimiento Formation (Lucas, 1992). The most cold-adapted and highest-latitude extant crocodilians are geographically restricted to areas with MAT >16°C (Markwick, 1994) and a cold month mean (CMM) T of >4.4°C (Hutchison, 1982), setting a lower MAT and CMM constraint for paleoenvironments associated with

crocodilian fossils. The Nacimiento Formation also contains fossil palms, a taxon whose living representatives are restricted to areas with a CMM of 5-7°C (Sakai & Larcher, 1987; Wing & Greenwood, 1993), further raising the lower temperature constraints for paleoenvironments present in the Paleocene San Juan Basin. These warm-adapted fossil taxa are stratigraphically well-distributed through the Nacimiento Formation, but are not found within the paleosols in this study. Therefore, if the paleosol-derived MAT estimates are assumed to be accurate, then there must have been frequent and substantial episodes of MAT shifts during the deposition of the Nacimiento Formation. While short-lived warming events (termed "hyperthermals") are known from the Paleocene (Bralower et al., 2002; Quillévéré et al., 2008; Bornemann et al., 2009), it is unlikely that the 'cold paleosol/warm taxa' paradox is representative of numerous, high-magnitude (at least 5°C) MAT shifts in the Paleocene San Juan Basin, as there are no known causal mechanisms for so many hyperthermals as well as no associated record of similar numerous high-magnitude hyperthermals from coeval Paleocene paleoclimate records. This suggests that the MAT estimates shown in Table 1 are systemically low. That Nacimiento Formation paleosol-derived MAT estimates are inaccurate is also supported by comparison to Paleocene benthic marine temperatures. Zachos et al. (2008) show that simultaneous to deposition of the Nacimiento Formation, average benthic marine temperatures were 8-10°C. It is unlikely that a mid-latitude continental environment such as the Paleocene San Juan Basin experienced average temperatures as little as 1°C warmer than coeval benthic marine environments. In the Denver Basin, ~250 km northeast of the San Juan Basin, a paleoflora coeval to the Nacimiento Formation is indicative of tropical temperature regimes (Ellis et al., 2003), further suggesting that

warm temperatures were likely to have existed in the Paleocene San Juan Basin. Nacimiento Formation paleosol-derived MAT estimates must be questioned.

Multiple workers have applied the PWI proxy of Gallagher & Sheldon (2013) to obtain MAT estimates that are in accord with coeval independently-derived estimates in the same study intervals (*e.g.*, Hyland, 2014; Smith et al., 2015; Hobbs & Parrish, 2016) with both residual and alluvial paleosols. The S proxy of Sheldon et al. (2002) is equally successfully applied (*e.g.*, Therrien, 2005; Kraus & Riggins, 2007; Hyland, 2014). However, the aforementioned paradoxes of Nacimiento Formation paleosol MAT estimates being lower than other climate estimates suggest that these paleosol-derived MAT estimate proxies cannot be applied accurately in some situations. To explore potential reasons for inaccurate Nacimiento Formation MAT estimates obtained with the PWI proxy, the PWI values of Nacimiento Formation paleosols (Table 1) were compared with those calculated for Nacimiento Formation parent materials, other San Juan Basin fluvial siliciclastic rocks, and composite materials from the upper crust, North American shales, and igneous rocks (Fig. 8). One of the potential problems associated with paleosol geochemistry-derived paleoclimate estimates is that they assume that paleosols formed from the in situ weathering of primary minerals in unweathered parent materials. However, as shown in Table 3, the mixture of primary unweathered geological materials with even small amounts of clay minerals will lead to PWI values that fall within the range of modern soil B horizons. In fluvial siliciclastic environments, such admixture of allogenic clays is likely if the source area or transport area includes either sedimentary units containing clays or weathering horizons formed under previous climate conditions or by deposition of aeolian materials on stable surfaces within a fluvial system. The PWI

values for Nacimiento Formation sandstones and mudstones fall within the range of PWI values of moderately to highly weathered soils (alfisols and ultisols), even though these units are demonstrably not paleosols. This suggests that while geochemically derived paleosol paleoclimate estimate techniques such as the PWI proxy can be applied successfully on unaltered residual or clay-free alluvial parent materials, their application to siliciclastic materials with some proportion of allogenic clays is problematic. At the bulk sampling scale that is necessary for analysis and application of these proxies, it is often impossible to ascertain what portion of clays is authigenic and what portion is allogenic, as it was for this study. Without knowing the admixture of component clays, PWI values from alluvial paleosols should likely be treated as maximum constraints; MAT estimates derived from them should be treated as minimum constraints given the inverse relationship between PWI and MAT. In complex sedimentary systems such as the Paleocene San Juan Basin, the accretionary or cumulic nature of pedogenesis likely precludes the accurate application of paleosol-based geochemical climate proxies. The use of these methods in sedimentary systems where the input of even minor amounts of alluvial, eolian, or pyroclastic input cannot be quantified is inadvisable.

A potentially important effect of the comparisons illustrated in Figure 8 is the recognition that the relative "weathering" as inferred from PWI values of Cretaceous and Paleogene sandstones in the San Juan Basin increases through time. A similar trend is seen in mudstones from the same units. This suggests that an increasing amount of weathered materials was being incorporated into the sediments accumulating in the San Juan Basin during deposition of the Late Cretaceous Kirtland Shale and Paleocene Ojo Alamo Sandstone and Nacimiento Formation. By the time of Nacimiento Formation

deposition, up to 12 km of Paleozoic and Mesozoic sedimentary cover had been removed from the source areas of the paleorivers feed in the San Juan, with up to 5 km of that comprising often clay-rich Cretaceous sediments (Fassett, 1974; Donahue, 2016). Detrital zircon evidence suggests that the San Juan Basin's sedimentary source areas in the western Colorado Mineral Belt and the San Juan Dome were actively uplifting across the K/Pg boundary (Donahue, 2016), unroofing crystalline basement rocks in the process. That unroofing potentially is represented by the upsection decreasing PWI (increasing "weathering") observed in the fluvial siliciclastic rocks of the San Juan Basin: as more source area uplift occurred, more clay-rich sedimentary cover was incorporated into the sediment load of rivers depositing sediments in the San Juan Basin. More work is needed to gain higher-resolution data on the PWI values of pedogenically unaltered San Juan Basin siliciclastic units, especially to extend the timespan back into the Campanian and forward into the Eocene.

Mean Annual Precipitation in the Paleocene San Juan Basin

The paleosol-derived MAP estimates shown in Table 1 range from 907-1383 mm/yr ±182 mm/yr. The CALMAG proxy of Nordt & Driese (2010), developed for soils and paleosols with vertic properties, was applied to paleosols of pedotype IV. The CIA-K proxy of Sheldon et al. (2002) was applied to all other paleosols. Both MAP proxies utilize the relative abundances of base cations to estimate weathering conditions. Like the MAT proxies discussed above, these MAP proxies require non-accretionary conditions during pedogenesis because they are calibrated in simple mass-balance pedogenic conditions found in residual soils. However, as shown above, accretionary conditions must be assumed during at least some portion of Nacimiento Formation sedimentation

and pedogenesis due to their formation in an active alluvial environment as well as the input of eolian and volcanic materials (Chapter 2, this volume). Therefore, the MAP values listed in Table 1 are suspect. While independently derived MAT estimates can be compared to the paleosol-derived MAT estimates discussed above, there is little published information on MAP conditions from the Nacimiento Formation. However, given the likely complications arising from unknown allogenic/authigenic clay ratios and evidence for eolian additions to the Nacimiento Formation (Chapter 2, this volume), we are not confident that our MAP estimates are accurate. That they are fairly evenly distributed across a reasonable range of MAP values with no significant outliers suggests that inaccuracy-causing changes affected all paleosols relatively equally or that these non-climatic changes were relatively minor. Further work is needed to understand better the factors affecting geochemical weathering indexes and their application as MAP proxies in complex accretionary alluvial paleosol settings.

While quantitative MAP estimates from Nacimiento Formation paleosols are inconclusive, the physical and petrographic properties of some of the paleosols do provide insight into the moisture conditions under which they form. The B horizons of pedotype V and IV paleosols contain unaltered plagioclase feldspar grains with argillans of illuviated smectite and illite clays (Fig. 7). Similar pedogenic micromorphology is observed in modern aridic soils formed in climates with MAP >700 mm (Eswaran et al., 2002; Persico et al., 2011). The combination of well-developed horizonation, unaltered detrital feldspar, and illuviated predominately smectite clays in these paleosols suggests that they did not form under wet conditions. Even if the inaccurate paleosol-derived MAT values are assumed as representative of the temperature conditions under which these

paleosols formed, long-term pedogenesis in humid climates would chemically alter feldspars to kaolinite and hydroxides of iron and aluminum (Al-Hawas, 1989; Carnicelli et al., 2015). Warmer conditions such as those indicated by crocodilian and palm taxa would increase the weathering rate of primary minerals and decrease the likelihood of their preservation in paleosol B horizons.

The indicators of seemingly semiarid-to-subhumid precipitation conditions in some Nacimiento Formation paleosols contrasts with the formation's fish, turtle, and crocodilian fossils (Matthew, 1937; Williamson, 1996) that are indicative of riparian and/or perennial fluvial environments. This contrast can be reconciled when each moisture indicator (paleosols and fossils) is considered in the context of the depositional system as a whole. For instance, abandoned floodplains/channels distal to an active channel can undergo long periods of pedogenesis (Carnicelli et al, 2015), even in basins that are undergoing net aggradation. If channel incision, distance from active channel, or long-term precipitation conditions cause a water table depth greater than the depth of the solum, and if the long-term precipitation conditions are semiarid to subhumid, then it is reasonable to expect development of soils representative of prevailing precipitation conditions even in fairly close proximity to an active channel in which might be preserved wetlands-indicative species. The exclusive use of faunal and floral megafossils as a paleomoisture proxy in a basin might lead to a riparian bias in interpretation of basin-scale paleoclimate conditions. Nacimiento Formation paleosols suggest that in the Nacimiento depositional system, humid conditions were not always present, especially on the stable geomorphic surfaces away from active channels that probably made up the majority of the area of the basin at any given point in time.

CONCLUSIONS

Geochemical, mineral, and physical analyses of the paleosols of the Nacimiento Formation show that environmental changes occurred during the deposition and pedogenesis of its sediments in the Paleocene. Changes in paleosol drainage indicators generally coincide with the lithological changes that define the three members of the formation, with older poorly drained paleosols being subsequently overlain by younger better-drained paleosols. We interpret this as evidence for basin-scale hydrological changes associated with the progradation of a fluvial system. Quantitative paleosol-derived paleoclimate proxies fall within a narrow range but are likely inaccurate due to incorporation of clays from ancient weathering profiles and/or clay-cemented sedimentary rocks in the San Juan Basin upland source area into the sediments of the Nacimiento Formation. The addition of aeolian materials, either dust or volcanic ashfall deposits, into the depositional environment is another likely cause for the inaccuracies inferred from interpretation of these proxies. Mineralogic and petrographic properties of these paleosols suggest that some formed under conditions considerably drier than have been inferred previously from megafossil-based paleoenvironmental moisture estimates.

REFERENCES CITED

Al-Hawas, I.A.M., 1989, Clay mineralogy and soil classification of alluvial and upland soils associated with Blackwater and Nottoway Rivers in southeastern Virginia: M.S. Thesis, Virginia Polytechnic Institute and State University, Blacksburg, 136 p.

Aslan, A., and Autin, W.J., 1998, Holocene flood-plain soil formation in the southern lower Mississippi Valley: implications for interpreting alluvial paleosols: Geological Society of America Bulletin, v. 110, p. 433-449.

Baltz, E.H., 1967, Stratigraphy and regional tectonic implications of part of Upper Cretaceous and Tertiary rocks, East-Central San Juan Basin, New Mexico: U.S. Geo. Surv. Prof. Pap. 552, 101 p.

Berner, R.A., and Holdgren, G.R., Jr., 1979, Mechanism of feldspar weathering II: Observations of feldspars from soils: Geochimica et Cosmochimica Acta, v. 43, p. 1173-1186.

Blum, M., and Pecha, M., 2014, Mid-Cretaceous to Paleocene North American drainage reorganization from detrital zircons: Geology, v. 42, n. 7, p. 607-610.

Bornemann, A., Schulte, P., Sprong, J., Steurbaut, E., Youssef, M., and Speijer, R.P., 2009, Latest Danian carbon isotope anomaly and associated environmental change in the Southern Tethys (Nile Basin, Egypt): Journal of the Geological Society, v. 166, p. 1135-1142.

Bralower, T.J., Premoli Silva, L., and Malone, M.J., 2002, New evidence for abrupt climate change in the Cretaceous and Paleogene: an Ocean Drilling Program expedition to Shatsky Rise, northwest Pacific: GSA Today, v. 12, p. 4-10.

Carnicelli, S., Benvenuti, M., Andreucci, S., and Ciampalini, R., 2015, Late Pleistocene relic Ultisols and Alfisols in an alluvial fan complex in coastal Tuscany: Quaternary International, v. 376, p. 163-172.

Carritt, J.A., 2014, Characterization of fluvial facies distributions and cyclicity using terrestrial LiDAR: Paleocene Nacimiento Formation, Kutz Canyon, New Mexico: M.S. Thesis, University of New Mexico, Albuquerque, 84 p.

Cather, S.M. 2004. Laramide orogeny in central and northern New Mexico and southern Colorado. p. 203–248. *In* G.H. Mack and K.A. Giles (ed.) The geology of New Mexico, a geologic history. Spec. Publ. 11. New Mexico Geol. Soc., New Mexico.

Condie, K.C., 1993, Chemical composition and evolution of the upper continental crust: Contrasting results from surface samples and shales: Chemical Geology, v. 104, p. 1-37.

Chadwick, O.A., Gavenda, R.T., Kelly, E.A., Ziegler, K., Olson, C.G., Elliott, W.C., and Hendricks, D.M., 2003, The impact of climate on the biogeochemical functioning of volcanic soils: Chemical Geology, V. 202, p. 195-223, doi: 10.1016/j.chemgeo.2002.09.001.

Chadwick, O.A., Brimhall, G.H., and Hendricks, D.M., 1990, From a black to a gray box – a mass balance interpretation of pedogenesis: Geomorphology, v. 3, p. 369-390.

Daniels, R.B., Gamble, E.E., and Nelson, L.A., 1971, Relations between soil morphology and water-table levels on a dissected North Carolina coastal plain: Soil Science Society of America Journal, v. 35, p. 781-784.

Davis, A.J., Atchley, S., Peppe, D., Flynn, A., and Williamson, T.E., 2015, Giving context to early Paleocene mammal evolution: Climate and landscape reconstruction of the

Arroyo Chijuillita Member of the Nacimiento Formation, San Juan Basin, New Mexico: Geological Society of America Abstracts with Programs, v. 47, n. 5, p. 588.

Donahue, M.S., 2016, Donahue, M.S., 2016, Episodic uplift of the Rocky Mountains: Evidence from U-Pb detrital zircon geochronolgy and low-temperature thermochronology with a chapter on using mobile technology for geoscience education: Ph.D. dissertation, University of New Mexico, Albuquerque, 1177 p.

Ellis, B., Johnson, K.R., and Dunn, R.E., 2003, Evidence for an in situ early Paleocene rainforest from Castle Rock, Colorado: Rocky Mountain Geology, v. 38, n. 1., p. 73-100.

Eswaran, H., Rice, T., Ahrens, R., Stewart, B.A., eds., 2002, Soil classification : A global desk reference: CRC Press, Boca Raton, Florida, 264 p.

Fassett, J.E., 1974, Cretaceous and Tertiary rocks of the eastern San Juan Basin, New Mexico and Colorado: New Mexico Geological Society Guidebook, v. 25, p. 225-230.

Gallagher, T.M., and Sheldon, N.D., 2013, A new paleothermometer for forest paleosols and its implications for Cenozoic climate: Geology, v. 41, n. 6, p. 647-650.

Gardner, J.H., 1910, The Puerco and Torrejon Formations of the Nacimiento Group: The Journal of Geology, v. 18, n. 8, p. 702-741.

Gromet, L.P., Dymek, R.F., Haskin, L.A., and Korotev, R.L., 1984, The "North American shale composite": Its compilation, major and trace element characeristics: Geochimica et Cosmochimica Acta, v. 48, p. 2469-2482.

Hartley, A.J., Weissmann, G.S., Bhattacharayya, P., Nichols, G.J., Scuderi, L.A., Davidson, S.K., Leleu, S., Chakraborty, T., Ghosh, P., and Mather, A.E., 2012, Soil development on modern distributive fluvial systems: Preliminary observations with implcations for interpretation of paleosols in the rock record: SEPM Special Publication 104, p. 149-158.

Hobbs, K.M., and Parrish, J.T., 2016, Global change recorded in Columbia River basalt-hosted paleosols: Geological Society of America Bulletin, doi: 10.1130/B31437.1.

Hutchison, J.H., 1982, Turtle, crocodilian, and champsosaur diversity changes in the Cenozoic of the north-central region of western United States: Palaeogeography, Palaeoclimatology, Palaeoecology, v. 37, p. 149-164.

Hyland, E.G., 2014, Multiproxy terrestrial records of climatic and ecological change during the early Eocene climatic optimum: Ph.D. Dissertation, University of Michigan, Ann Arbor, 158 p.

Kraus, M.J., 1999, Paleosols in clastic sedimentary rocks: their geologic applications: Earth-Science Reviews, v. 42, p. 387-406.

Kraus, M.J., and Brown, T.M., 1986, Paleosols and time resolution in alluvial stratigraphy, *in* Wright, P.V., ed., Paleosols: Their Recognition and Interpretation: Princeton Uniersity press, Princeton, New Jersey, p. 180-207.

Kraus, M.J., and Riggins, S., 2007, Transient drying during the Paleocene-Eocene Thermal Maximum (PETM): Analysis of paleosols in the Bighorn Basin, Wyoming: Palaeogeography, Palaeoclimatology, Palaeoecology, v. 245, p. 444-461.

Lindsay, E.H., Butler, R.F., and Johnson, N.M., 1981, Magnetic polarity zonation and biostratigraphy of Late Cretaceous and Paleocene continental deposits, San Juan Basin, New Mexico: American Journal of Science, v. 281, p. 390-435.

Lofgren, D.L., Lillegraven, J.A., Clemens, W.A., Gingerich, P.D., and Williamson, T.E., 2004, Paleocene biochronology; the Puercan through Clarkforkian land mammal ages, *in* Woodburne, M.O., ed., Late Cretaceous and Cenozoic mammals of North America: Columbia University Press, New York, p. 43-105.

Lucas, S.G., and Ingersoll, R.V., 1981, Cenozoic continental deposits of New Mexico: an overview: Geol. Soc. of Amer. Bulletin, v. 91, p. 917-932.

Lucas, S.G., 1992, Cretaceous-Eocene crocodilians from the San Juan Basin, New Mexico, New Mexico Geological Society Guidebook, v. 43, p. 257-264.

Mack, G.H., James, C.W., and Monger, C., 1993, Classification of paleosols: Geological Society of America Bulletin, v. 105, p. 129-136.

Markwick, P.J., 1994, "Equability", continentality, and Tertiary "climate": The crocodilian perspective: Geology, v. 22, p. 613-616.

Matthew, W.D., 1937 Paleocene faunas of the San Juan Basin, New Mexico: Transactions of the American Philosophical Society, v. 30, p. 1-510.

Nordt, L.C., and Driese, S.D., 2010, New weathering index improves paleorainfall estimates from Vertisols: Geology, v. 38, n. 5, p. 407-410.

Pearson, M.J., 1978, Quantitative clay mineralogical analyses from the bulk geochemistry of sedimentary rocks: Clays and Clay Minerals, v. 26, p. 423-433.

Persico, L.P., McFadden, L.D., Frechette, J.D., and Meyer, G.M., 2011, Rock type and dust influx control accretionary soil development on hillslopes in the Sandia Mountains, New Mexico, USA: Quaternary Research, v. 76, p. 411-416.

Quillévéré, F., Norris, R.D., Kroon, D., and Wilson, P.A., 2008, Transient ocean warming and shifts in carbon reservoirs during the early Danian: Earth and Planetary Science Letters, v. 265, p. 600-615.

Quinney, A., Therrien, F., Zelenitsky, D.K., and Eberth, D.A., 2013, Palaeoenvironmental and palaeoclimatic reconstruction of the Upper Cretaceous (late Campanian-early Maastrichtian) Horseshoe Canyon formation, Alberta, Canada: Palaeogeography, Palaeoclimatology, Palaeoecology, v. 371, p. 26-44.

Retallack, G.J., 1988, Field recognition of paleosols, *in* Reinhardt, J., and Sigleo, eds., Paleosols and Weathering Through Geologic Time—Principles and Aplications: Geological Society of America Special Paper 216, p. 1-20.

Retallack, G., 1994, A pedotype approach to latest Cretaceous and earliest Tertiary paleosols in eastern Montana: Geological Society of America Bulletin, v. 196, p. 1377-1397.

Sakai, A., and Larcher, W., 1987, Frost survival of plants: responses and adaptation to freezing stress: Berlin, Springer-Verlag, 321 p.

Sheldon, N.D., Retallack, G.J., and Tanaka, S., 2002, Geochemical climofunctions of North American soils and application to paleosols across the Eocene-Oligocene Boundary in Oregon: The Journal of Geology, v. 110, p. 687-696.

Silcox, M.T., and Williamson, T.E., 2012, New discoveries of early Paleocene (Torrejonian) primates from the Nacimiento Formation, San Juan Basin, New Mexico: Journal of Human Evolution, v. 63, n. 6, p. 805-833.

Smith, S.Y., Manchester, S.R., Samant, B., Mohabey, D.M., Wheeler, E., Baas, P., Kapgate, D., Srivastava, R., and Sheldon, N.D., 2015, Integrating paleobotanical, paleosol, and stratigraphic data to study critical transitions: a case study from the Late Cretaceous-Paleocene of India, *in* Polly, D.P., Head, J.J., and Fox, D.L., eds., Earth-life transitions: Paleobiology in the context of Earth system evolution: The Paleontological Society Papers, v. 21, p. 137-166.

Tabor, N.J., and Montañez, I.P., 2004, Morphology and distribution of fossil soils in the Permo-Pennsylvanian Wichita and Bowie Groups, north-central Texas, USA: Implications for western equatorial Pangean paleoclimate during icehouse-greenhouse transition: Sedimentology, v. 51, p. 851–884, doi:10.1111/j.1365-3091.2004.00655.x.

Tabor, N.J., Montañez, I.P., Scotese, C.R., Poulsen, C.J., and Mack, G.H., 2008, Paleosol archives of environmental and climatic history in paleotropical western Pangea during the latest Pennsylvanian through Early Permian, *in* Fielding, C.R., Frank, T.D., and Isbell, J.L., eds., Resolving the Late Paleozoic Ice Age in Time and Space: Geological Society of America Special Paper 441, p. 291–303, doi:10.1130/2008.2441(20).

Tabor, N.J., Montañez, I.P., Zierenber, R., and Currie, B.S., 2004, Mineralogical and geochemical evolution of a basalt-hosted fossil soil (Late Triassic, Ischigualasto Formation, northwest Argentina): Potential for paleoenvironmental reconstruction: Geological Society of America Bulletin, v. 116, no. 9–10, p. 1280–1293, doi:10.1130/B25222.1.

Tan, K.H., 1982, Principles of soil chemistry: New York, Dekker Publishing, 267 p.

Therrien, F., 2005, Palaeoenvironments of the latest Cretaceous (Maastrichtian) dinosaurs of Romania: insights from fluvial deposits and paleosols of the Transylvanian and Haţeg basins: Palaeogeography, Palaeoclimatology, Palaeoecology, v. 218, p. 15-56.

Therrien, F., Zelenitsky, D.K., Weishampel, D.B., 2009, Paleoenvironmental reconstruction of the Late Cretaceous Sanpetru Formation (Hateg Basin, Romania) using paleosols and implications for the "disappearance" of dinosaurs: Palaeogeography, Palaeoclimatology, Palaeoecology, v. 272, p. 37-52.

Vasquez, F.M., 1981, Formation of Gibbsite in soils and saprolites of temperate-humid zones: Clay Minerals, v. 16, p. 43-52.

Weissmann, G.S., Hartley, A.J., Scuderi, L.A., Nichols, G.J., Davidson, S.K., Owen, A., Atchely, S.C., Bhattacharayya, P., Chakraborty, T., Ghosh, P., Nordt, L.C., Michel, L., and Tabor, N.J., 2013, Prograding distributive fluvial systems – geomorphic models and ancient examples, *in* Driese, S.G., and Nordt, L.C., eds., New Frontiers in Paleopedology and Terrestrial Paleoclimatology, SEPM Special Publication 104, p. 131-147.

Weissmann, G.S., Hartley, A.J., Scuderi, LA., Nichols, G.J., Owen, A., Wright, S., Felicia, A.L., Holland, F., and Anaya, F.M.L., 2015, Fluvial geomorphic elements in modern sedimentary basins and their potential preservation in the rock record: Geomorphology, v. 250, p. 187-219.

Williamson, T.E., 1996, The beginning of the age of mammals in the San Juan Basin, New Mexico: Biostratigraphy and evolution of Paleocene mammals of the Nacimiento Formation: New Mexico Museum of Natural History and Science, Bulletin 8, 141 p.

Williamson, T.E., Brusatte, S.L., Carr, T.D., Weil, A., and Standhardt, B.R., 2012, The phylogeny and evolution of Cretaceous-Paleogene metatherians: cladistics analysis and description of new early Paleocene specimens from the Nacimiento Formation, New Mexico: Journal of Systematic Paleontology, v. 10, n. 4, p. 625-651.

Williamson, T.E., Brusatte, S.L., Peppe, D.J., Secord, R., and Weil, A., 2012, No evidence for conformable contact between the Ojo Alamo Sandstone and the Nacimiento Formation: New Mexico Geology, v. 34.

Williamson, T.E., and Lucas, S.G., 1992, Stratigraphy and mammalian biostratigraphy of the Paleocene Nacimiento Formation, southern San Juan Basin, New Mexico: New Mexico Geological Society Guidebook, v. 43, p. 265-296.

Wing, S.L., and Greenwood, D.R., 1993, Fossils and fossil climate: the case for equable continental interiors in the Eocene: Philosophical Transactions of the Royal Society of London B, v. 341, p. 243-252.

Zachos, J.C., Dickens, G.R., and Zeebe, R.E., 2008, An early Cenozoic perspective on greenhouse warming and carbon-cycle dynamics: Nature, v. 451, p. 279-283.

FIGURES

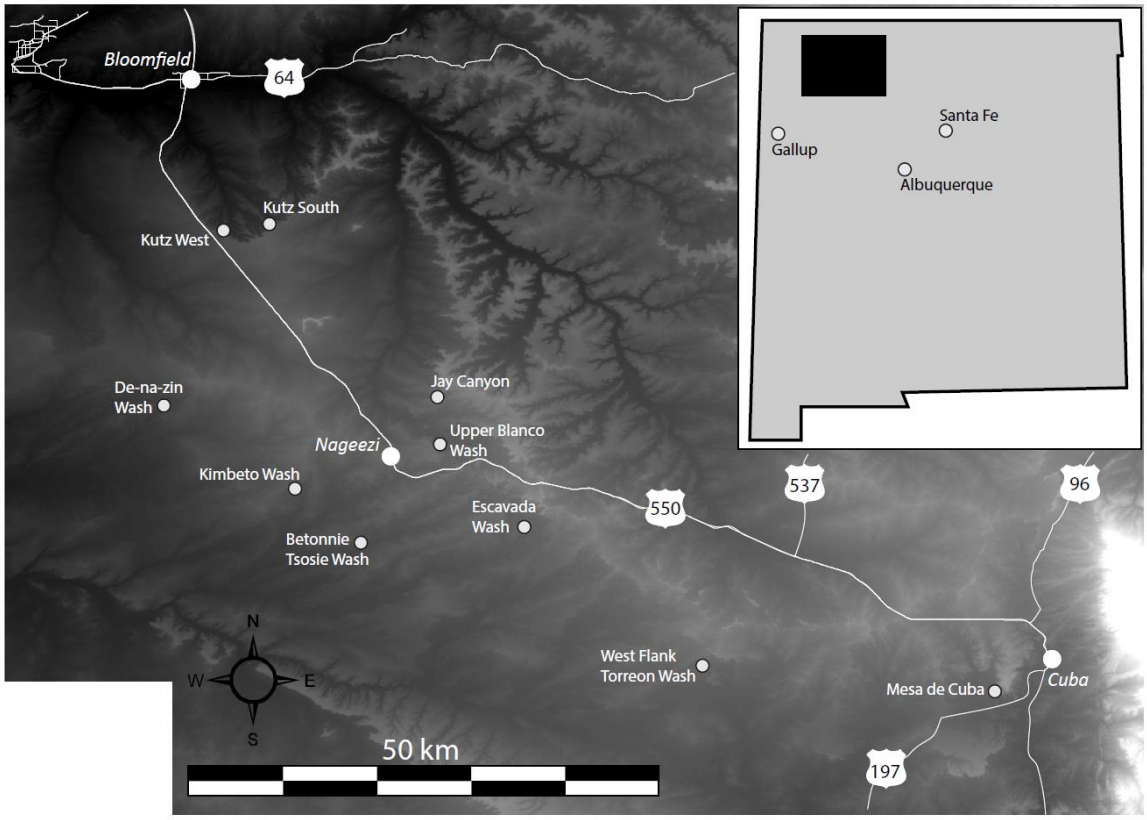

Figure 1. Location of study sites within the San Juan Basin. Inset illustrates location of study area in northwest New Mexico, USA.

Figure 2. Stacked paleosols at Kutz Canyon. Both upper and lower reddened Bt horizons exhibit drab root haloes. A horizon truncated before deposition of overlying sediments in both paleosols. Staff in upper left is 1.5 m long.

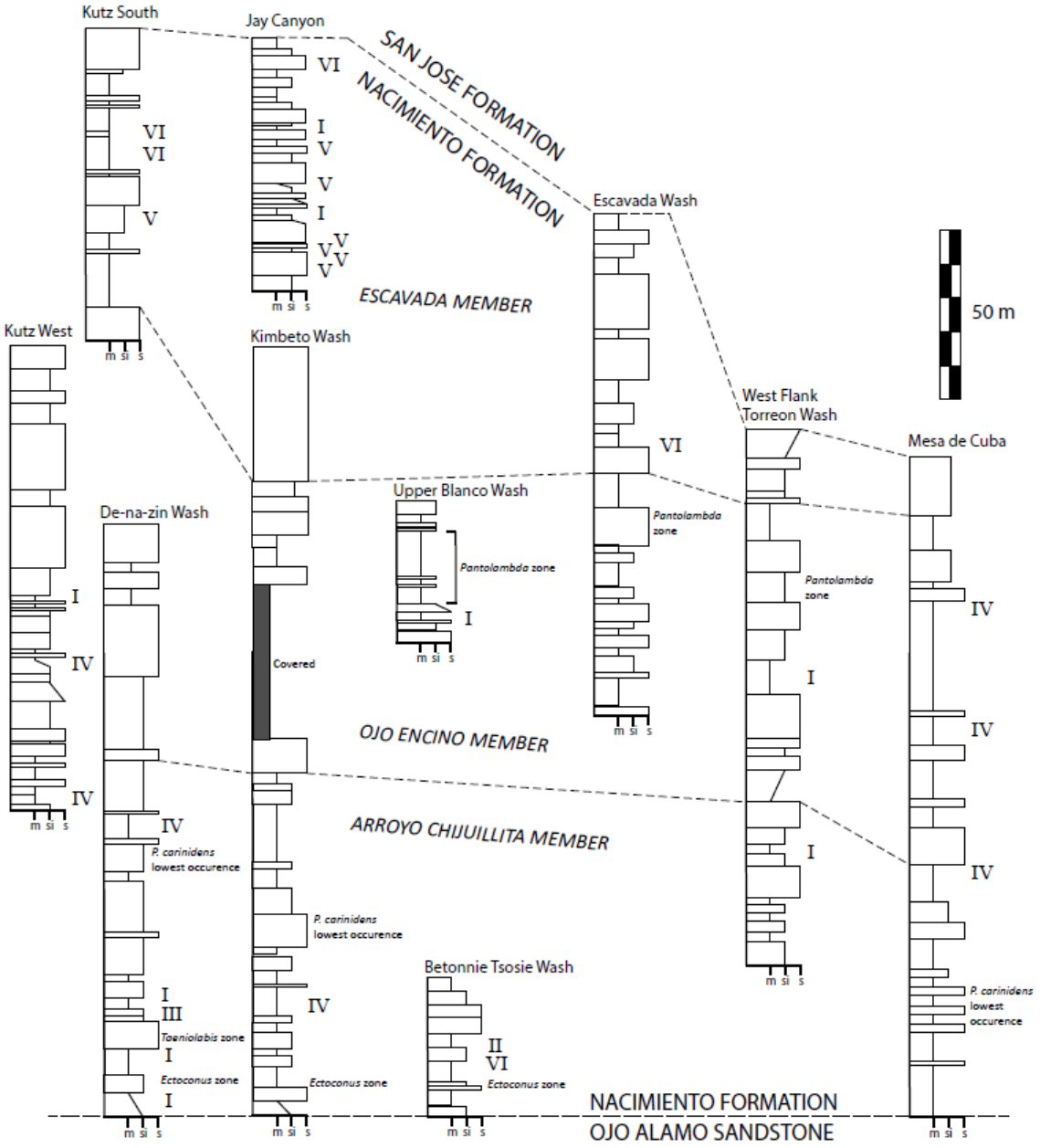

Figure 3. Correlated sections illustrating the stratigraphic distribution of Nacimiento Formation paleosol pedotypes in this study. Roman numerals to the right of each section represent the stratigraphic location and pedotype (I-VI) of studied paleosols. Dashed lines represent member boundaries. The Arroyo Chijuillita and Ojo Encino Members are difficult to correlate to Kutz Canyon; at those sections, general stratigraphic correlation was attempted. Sections for Kutz West, Jay Canyon, and Upper Blanco Wash were measured for this study; all other sections, member boundaries, and biozones modified from Williamson (1996).

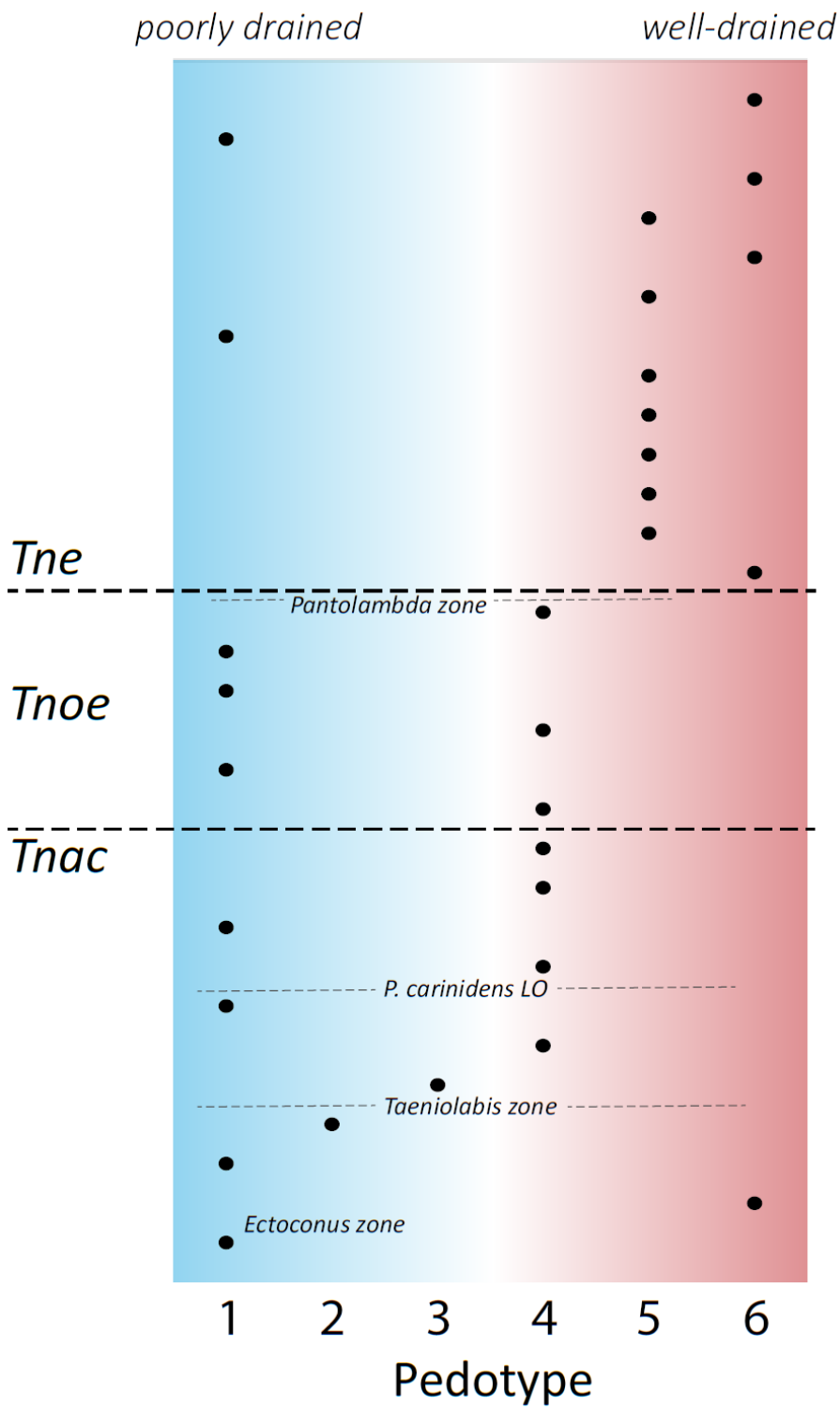

Figure 4. Pedotypes of Nacimiento Formation paleosols in stratigraphic order. No vertical scale implied. Biozones from Williams (1996). *Tnac:* Arroyo Chijuillita Member. *Tnoe*: Ojo Encino Member. *Tne*: Escavada Member. *LO*: lowest occurrence.

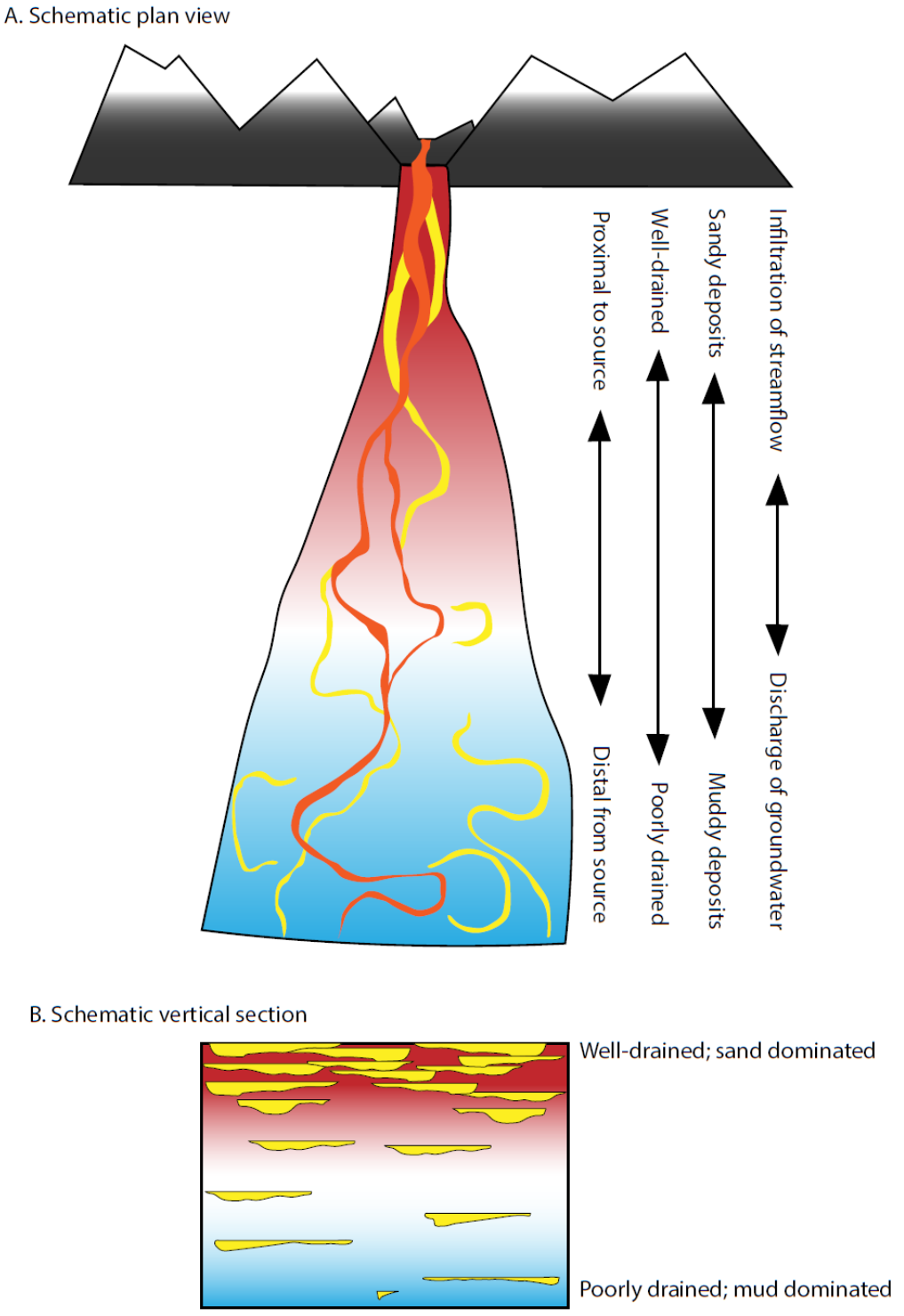

Figure 5. A: Schematic plan view of a prograding active fluvial system. Soil drainage regimes represented by same color gradient as Figure 4. Orange represents active channel; yellow represents abandoned channels. B: Schematic cross section of prograding fluvial system succession. Note upsection increase in sand percentage and paleosol drainage conditions. Modified from Weissmann et al. (2013).

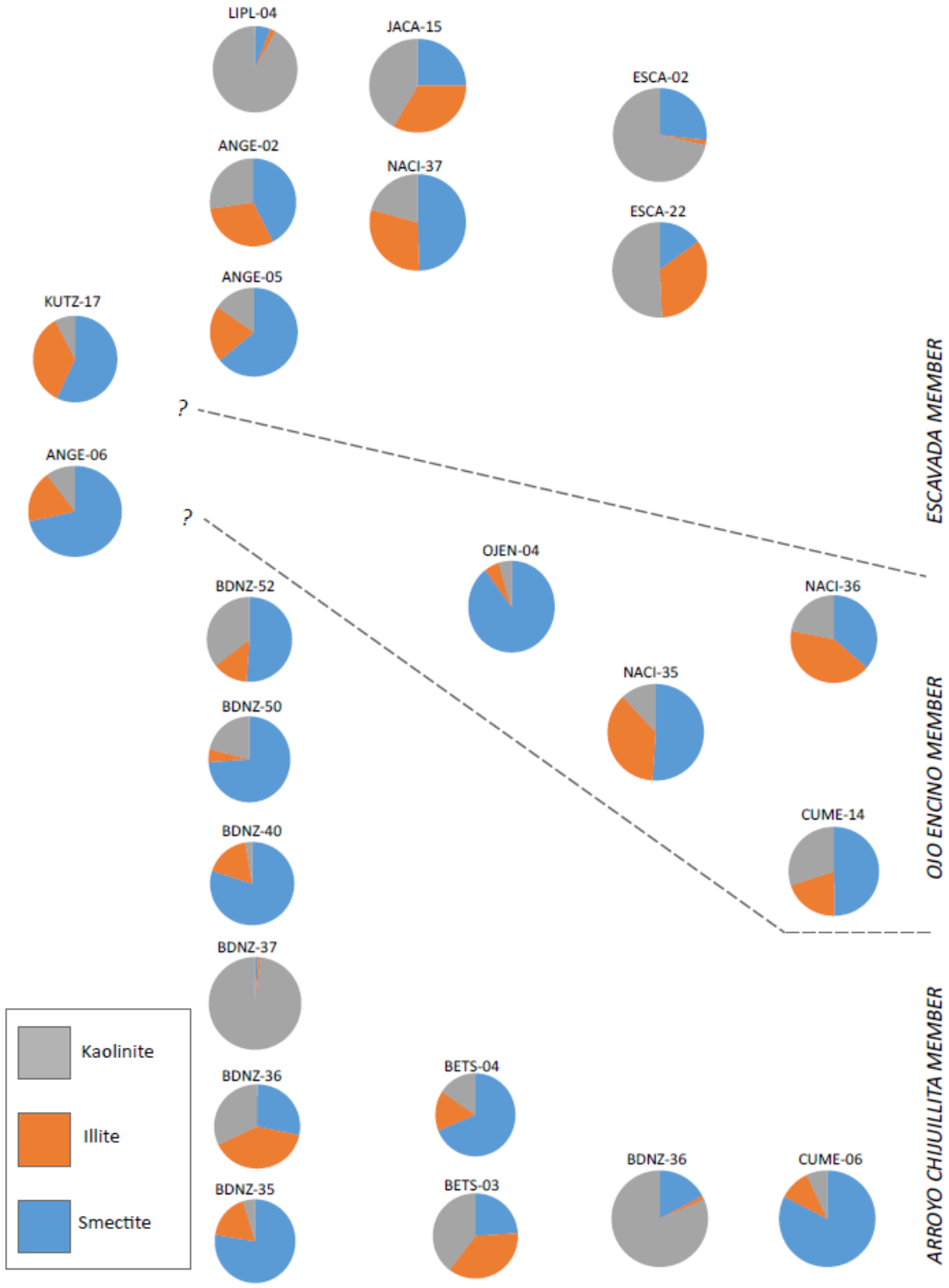

Figure 6. Proportions of smectite (blue), illite (red), and kaolinite (gray) clays in fine fractions of B horizons of Nacimiento Formation paleosols. Numerical proportions in Table 2.

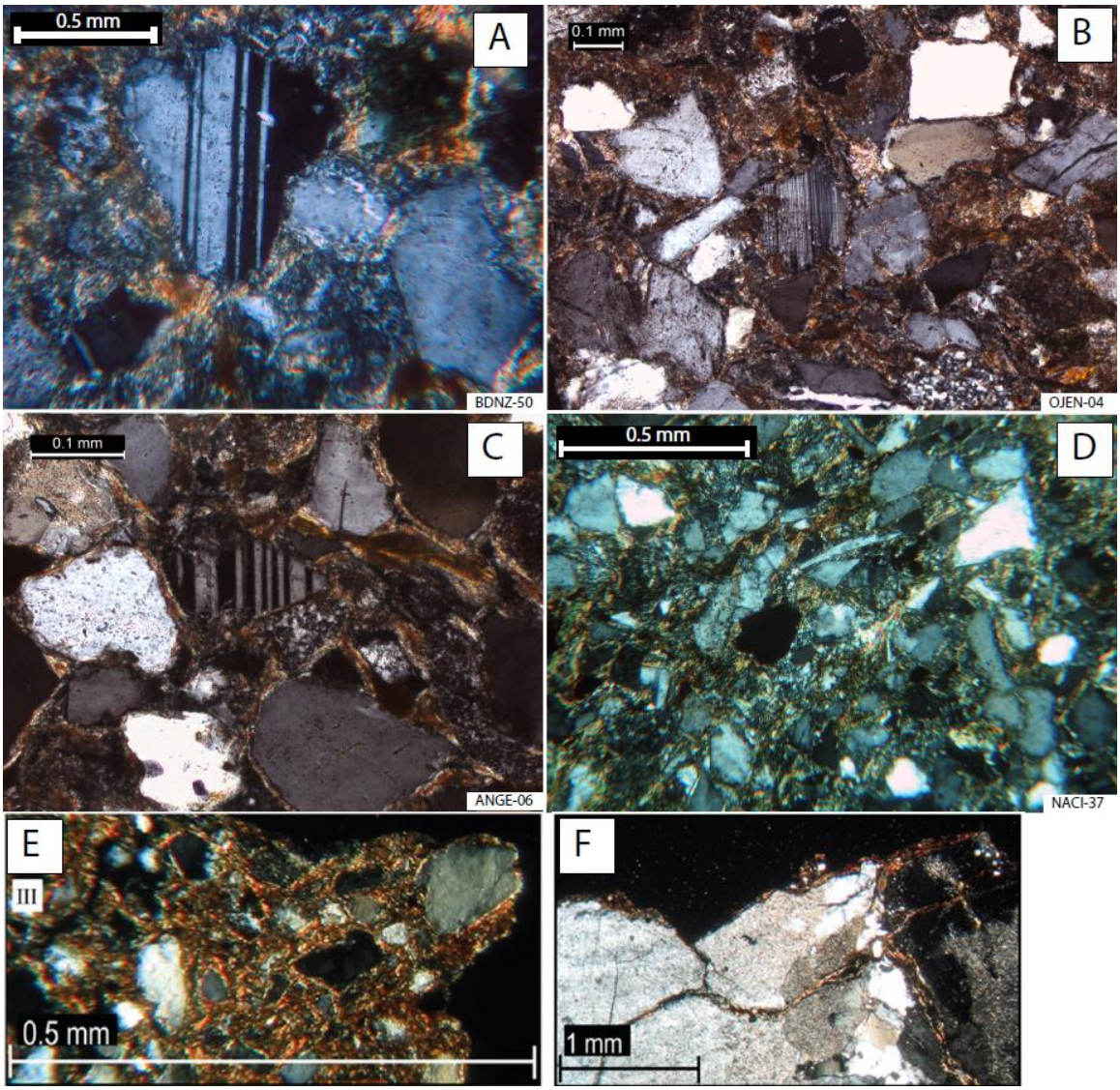

Figure 7. **A-D:** Photomicrographs of paleosol sandy B horizon materials showing illuviated clay argillans coating unaltered detrital grains. A: Plagioclase feldspar with predominately smectite argillans, De-na-zin Wash. B: Plagioclase feldspar and quartz grains with predominately smectite argillans; Upper Blanco Wash. C: Plagioclase feldspar, quartz, and chert grains with predominately smectite argillans, Kutz West. D: Assorted detrial grains with smectite, illite, and kaolinite argillans, Jay Canyon. **E-F:** Illuviated active clays from recent aridisols, showing petrographic and micromorphologic similarities to Nacimiento Formation argillans inferred to have formed under semiarid to subhumid climate conditions, modified from Persico et al. (2011).

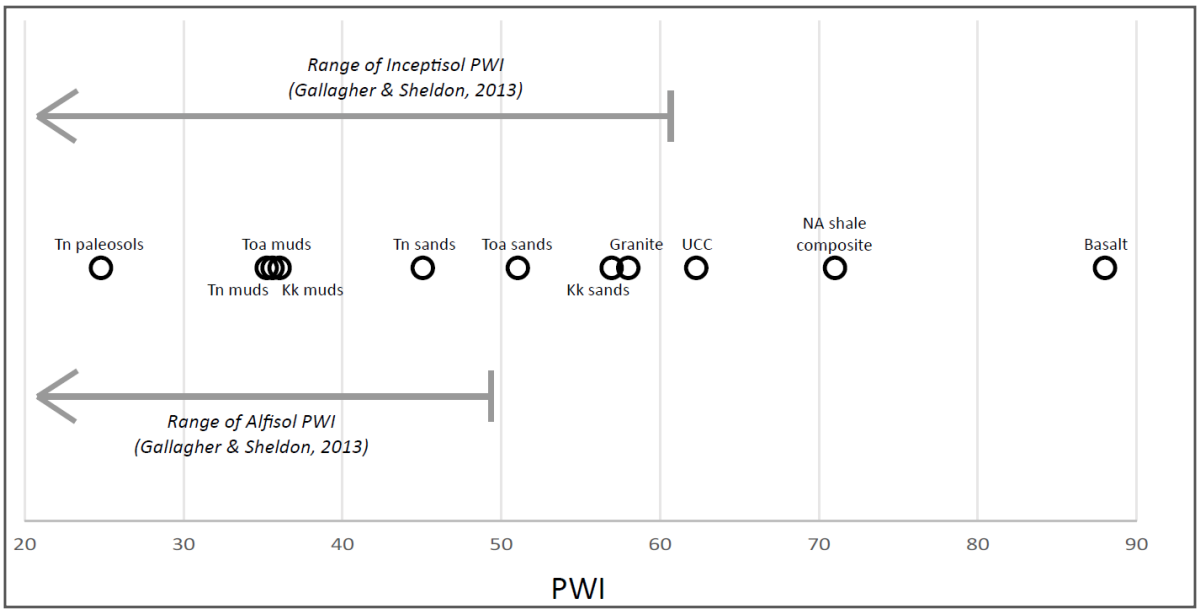

Figure 8. Comparison of paleosol weathering index (PWI) values for Nacimiento Formation paleosols, San Juan Basin K/Pg fluvial siliciclastic units, North American shale composite, upper continental crust (UCC) composite, granite, and basalt. Range of PWI values for modern forest soils from Gallagher & Sheldon (2013) shown with arrows. Non-San Juan Basin values from Condie (1993) and Gromet et al. (1984).

Sample Name	CIA-K	S	PWI	MAP, mm	MAT S, °C	MAT PWI, °C	Pedotype
LIPL-04	85.050	0.216	26.5	1078	11.4	12.4	VI
JACA15	90.852	0.147	18.0	1324	14.6	13.5	V
JACA13	90.219	0.072	11.1	1308	16.0	14.8	V
JACA11	90.088	0.173	19.1	1304	14.1	13.3	V
JACA08	83.840	0.245	31.8	1153	12.8	11.9	V
JACA06	83.720	0.258	32.4	1150	12.5	11.9	I
JACA05	85.172	0.154	22.8	1184	14.4	12.8	I
JACA04	89.829	0.160	17.4	1298	14.3	13.6	V
JACA01	92.631	0.053	7.5	1371	16.3	15.9	V
JACA03	89.392	0.175	19.9	1286	14.1	13.2	V
CROW04	93.083	0.030	6.5	1383	16.8	16.2	VI
ANGE-02	79.642	0.264	29.1	950	10.0	12.2	V
KH28	82.465	0.243	28.3	1123	12.8	12.2	IV
ESCA-22	89.354	0.088	12.2	1200	15.0	14.5	VI
NACI-37	87.548	0.186	22.6	1148	12.2	12.9	
ESCA-02	77.728	0.219	35.0	910	11.3	11.7	VI
ANGE-05	79.396	79.396	29.3	1056	12.3	12.1	V
KUTZ-17	93.157	0.044	7.2	1323	16.1	16.0	IV
ANGE-06	79.447	79.447	29.1	1058	12.3	12.2	I
KWFT24	75.991	0.332	38.1	988	11.2	11.4	I
OJEN-04	79.557	0.220	32.4	949	11.2	11.9	
NACI-36	82.325	0.246	26.8	1009	10.6	12.4	IV
KWFT08	82.552	0.192	23.5	1124	13.8	12.7	I
NACI-35	78.070	0.318	33.1	913	8.7	11.8	I
CUME-14	82.907	82.907	26.9	1132	12.1	12.4	IV
BDNZ-53	87.160	87.160	25.4	1231	13.5	12.5	IV
BDNZ-52	88.055	88.055	24.0	1253	13.6	12.7	IV
BDNZ-51	88.393	88.393	19.0	1261	14.0	13.3	IV
BIPO007	78.265	0.230	36.9	1033	13.0	11.5	IV
BDNZ-50	86.539	86.539	21.9	1216	13.8	12.9	IV
BDNZ-41	77.897	77.897	33.5	1026	11.2	11.8	I
BDNZ-40	78.006	78.006	35.4	1028	10.5	11.6	I
BDNZ-39	71.667	71.667	43.6	907	8.7	11.0	I
CUME-06	82.664	82.664	19.9	1127	11.5	13.2	IV
BDNZ-36	85.761	85.761	33.1	1198	11.9	11.8	I
BETS-04	78.920	78.920	29.9	1047	12.3	12.1	II
BDNZ-35	83.988	83.988	20.5	1157	15.0	13.1	I
BETS-03	88.361	0.082	12.4	1171	15.1	14.5	II

Table 1. Summary of geochemical proxy values for samples in this study. Abbreviation sources: CIA-K; S = Sheldon et al. (2002); PWI = Gallgher & Sheldon (2013). MAP = mean annual precipitation, mm/yr. MAT = mean annual temperature, °C. Full geochemical analytical results in Appendix A.

Sample	Smectite %	Illite %	Kaolinite %
ANGE-02	42	30	27
ANGE-05	64	21	15
ANGE-06	71	18	10
BDNZ-35	77	18	5
BDNZ-36	28	40	32
BDNZ-37	1	1	98
BDNZ-40	80	17	3
BDNZ-50	74	5	21
BDNZ-52	51	13	36
BETS-03	24	36	40
BETS-04	69	16	16
CUME-06	83	10	7
CUME-14	50	20	30
ESCA-02	27	2	71
ESCA-22	15	34	51
JACA-15	25	33	42
KUTZ-17	57	35	8
KWFT-20	17	1	81
LIPL-04	6	2	92
NACI-35	51	37	12
NACI-36	36	42	22
NACI-37	49	30	21
OJEN-04	90	6	5

Table 2. Proportions of smectite, illite, and kaolinite clays in fine fractions of Nacimiento Formation paleosol B horizons.

Sample Name	Na2O	MgO	Al2O3	SiO2	P2O5	K2O	CaO	TiO2	Fe2O3	
	mass%	mass%	mass%	mass%	mass%	mass%	mass%	mass%	mass%	PWI
UCC, Condie (1993)	3.4	2.21	15.21	65.72	0.14	2.84	3.94	0.66	5.04	63.2
NASC, Gromet et al. (1984)	4.36	1.57	17.66	60.41	0.5	2.93	5.02	1.09	6.26	71.6
Kaolinite, Pearson (1978)	0.17	0.08	39.07	45.77		0.31	0.26		0.04	4.3
Montmorillonite, Pearson (1978)	1.13		18.57	43.77						7.7
95% UCC/5% Kaol	3.2385	2.1035	16.403	64.723	0.133	2.7135	3.756	0.627	4.79	60.3
90% UCC/10% Kaol	3.077	1.997	17.596	63.725	0.126	2.587	3.572	0.594	4.54	57.3
85% UCC/15% Kaol	2.9155	1.8905	18.789	62.728	0.119	2.4605	3.388	0.561	4.29	54.4
80% UCC/20% Kaol	2.754	1.784	19.982	61.73	0.112	2.334	3.204	0.528	4.04	51.4
75% UCC/25% Kaol	2.5925	1.6775	21.175	60.733	0.105	2.2075	3.02	0.495	3.79	48.5
95% UCC/5% Montmorillonite	3.2865	2.0995	15.378	64.623	0.133	2.698	3.743	0.627	4.788	60.5
90% UCC/10% Montmorillonite	3.173	1.989	15.546	63.525	0.126	2.556	3.546	0.594	4.536	57.7
85% UCC/15% Montmorillonite	3.0595	1.8785	15.714	62.428	0.119	2.414	3.349	0.561	4.284	54.9
80% UCC/20% Montmorillonite	2.946	1.768	15.882	61.33	0.112	2.272	3.152	0.528	4.032	52.1
75% UCC/25% Montmorillonite	2.8325	1.6575	16.05	60.233	0.105	2.13	2.955	0.495	3.78	49.3
95% NASC/5% Kaol	4.1505	1.4955	18.731	59.678	0.475	2.799	4.782	1.0355	5.949	68.2
90% NASC/10% Kaol	3.941	1.421	19.801	58.946	0.45	2.668	4.544	0.981	5.638	64.9
85% NASC/15% Kaol	3.7315	1.3465	20.872	58.214	0.425	2.537	4.306	0.9265	5.327	61.5
80% NASC/20% Kaol	3.522	1.272	21.942	57.482	0.4	2.406	4.068	0.872	5.016	58.1
75% NASC/25% Kaol	3.3125	1.1975	23.013	56.75	0.375	2.275	3.83	0.8175	4.705	54.8
95% NASC/5% Montmorillonite	4.1985	1.4915	17.706	59.578	0.475	2.7835	4.769	1.0355	5.947	68.4
90% NASC/10% Montmorillonite	4.037	1.413	17.751	58.746	0.45	2.637	4.518	0.981	5.634	65.2
85% NASC/15% Montmorillonite	3.8755	1.3345	17.797	57.914	0.425	2.4905	4.267	0.9265	5.321	62.0
80% NASC/20% Montmorillonite	3.714	1.256	17.842	57.082	0.4	2.344	4.016	0.872	5.008	58.8
75% NASC/25% Montmorillonite	3.5525	1.1775	17.888	56.25	0.375	2.1975	3.765	0.8175	4.695	55.6

Table 3. PWI values of unweathered materials (UCC and NASC) and mixtures of these materials with increasing proportions of common clay minerals. Note decreasing PWI values as proportion of clays increases. UCC values from Condie (1993). NASC values from Gromet et al. (1984). Clay values from Pearson (1978).

Appendix A. Full geochemical data from analyzed materials.

Sample Name	Na2O mass%	MgO mass%	Al2O3 mass%	SiO2 mass%	P2O5 mass%	K2O mass%	CaO mass%	TiO2 mass%	MnO mass%	Fe2O3 mass%
ANGE-02	1.164	1.043	16.019	61.007	0.049	2.132	1.199	0.78	0.019	6.137
ANGE-05	1.174	1.066	15.646	61.685	0.053	2.161	1.171	0.69	0.02	9.404
ANGE-06	1.167	1.056	15.58	61.256	0.053	2.145	1.161	0.687	0.019	9.369
BDNZ-35	1.377	1.048	22.144	56.207	0.019	0.5	1.076	0.783	0.039	5.78
BDNZ-36	1.454	1.067	19.016	57.168	0.082	2.938	0.421	0.801	0.029	9.412
BDNZ-37	1.921	0.272	12.621	67.674	0.027	2.829	0.41	0.514	0.014	1.344
BDNZ-39	2.684	1.24	16.016	68.592	0.106	2.791	1.054	0.462	0.016	2.752
BDNZ-40	1.834	1.429	15.453	62.384	0.032	2.451	0.737	0.677	0.039	6.681
BDNZ-41	1.519	1.612	14.894	58.821	0.097	2.232	0.95	0.657	0.035	9.128
BDNZ-50	1.07	0.963	17.686	63.293	0.042	1.474	0.545	0.718	0.013	4.948
BDNZ-51	0.826	0.82	16.275	67.709	0.021	1.433	0.428	0.811	0.012	3.649
BDNZ-52	1.003	0.872	18.946	59.14	0.045	1.993	0.506	0.899	0.02	7.723
BDNZ-53	1.176	1.016	19.735	56.06	0.039	1.917	0.535	0.794	0.019	9.33
BETS-03	0.896	0.615	20.686	61.845	0.019	0.213	0.688	0.813	0.039	7.511
BETS-04	1.334	0.796	16.901	63.84	0.208	2.193	1.276	0.653	0.015	6.892
BIPO007	0.916	2.28	17.525	56.282	0.072	2.432	1.91	0.822	0.034	9.819
CROW04	0.32	0.427	20.085	63.271	0.016	0.101	0.553	1.033	0.012	3.977
CROW05	0.132	0.163	7.185	81.849	0.014	0.074	0.108	0.963	0.009	0.831
CUME-06	1.056	0.61	10.954	76.733	0.016	1.55	0.308	0.905	0.019	2.748
CUME-14	1.23	1.085	14.991	57.859	0.05	2.027	0.587	0.662	0.047	13.646
ESCA-02	1.102	2.19	18.129	59.994	0.069	1.987	1.86	0.831	0.029	7.438
ESCA-22	0.991	0.61	21.161	60.059	0.018	0.209	0.49	0.82	0.028	5.943
JACA01	0.614	0.338	19.908	66.416	0.016	0.117	0.357	1.247	0.012	6.179
JACA03	0.968	0.714	17.995	64.338	0.015	1.546	0.364	0.647	0.016	3.606
JACA04	0.927	0.58	17.617	65.477	0.012	1.293	0.321	0.504	0.013	3.661
JACA05	1.281	1.092	20.37	60.017	0.013	1.098	0.878	0.786	0.029	5.156
JACA06	1.44	1.479	18.359	65.076	0.021	2.349	0.758	0.838	0.032	6.488
JACA08	0.98	1.557	17.351	61.703	0.069	2.548	1.019	0.823	0.034	8.241
JACA11	1.02	0.597	18.359	65.708	0.012	1.493	0.257	0.595	0.013	2.93
JACA13	0.839	0.57	20.668	60.997	0.013	0.199	0.53	0.813	0.019	6.777
JACA15	0.911	0.553	19.894	59.16	0.013	1.42	0.339	0.503	0.013	3.284
JACA17	0.245	0.312	11.142	73.297	0.016	0.804	0.185	0.75	0.009	2.501
KH28	1.065	0.946	16.739	57.003	0.026	2.264	1.066	0.769	0.082	9.878
KUTZ-17	0.468	0.472	20.159	63.271	0.029	0.111	0.391	0.983	0.027	4.961
KWFT08	1.547	1.403	16.88	64.811	0.017	0.815	0.667	1.099	0.029	5.715
KWFT24	2.181	1.498	17.137	60.237	0.033	2.194	1.152	0.763	0.022	9.55
LIPL-04	1.467	1.001	19.874	61.278	0.041	1.744	0.594	0.697	0.019	4.911
NACI-35	1.915	1.216	16.846	59.019	0.029	2.032	0.87	0.788	0.041	7.129
NACI-36	1.642	1.043	17.84	59.951	0.087	1.555	0.621	0.549	0.027	5.591
NACI-37	0.919	0.897	18.465	60.297	0.054	1.768	0.613	0.797	0.04	6.715
OJEN-04	1.269	1.168	20.195	62.89	0.026	2.167	1.706	0.873	0.034	4.664

Appendix B. X-Ray diffractograms from XRD-analyzed fine fractions of Nacimiento Formation paleosol B horizon materials.

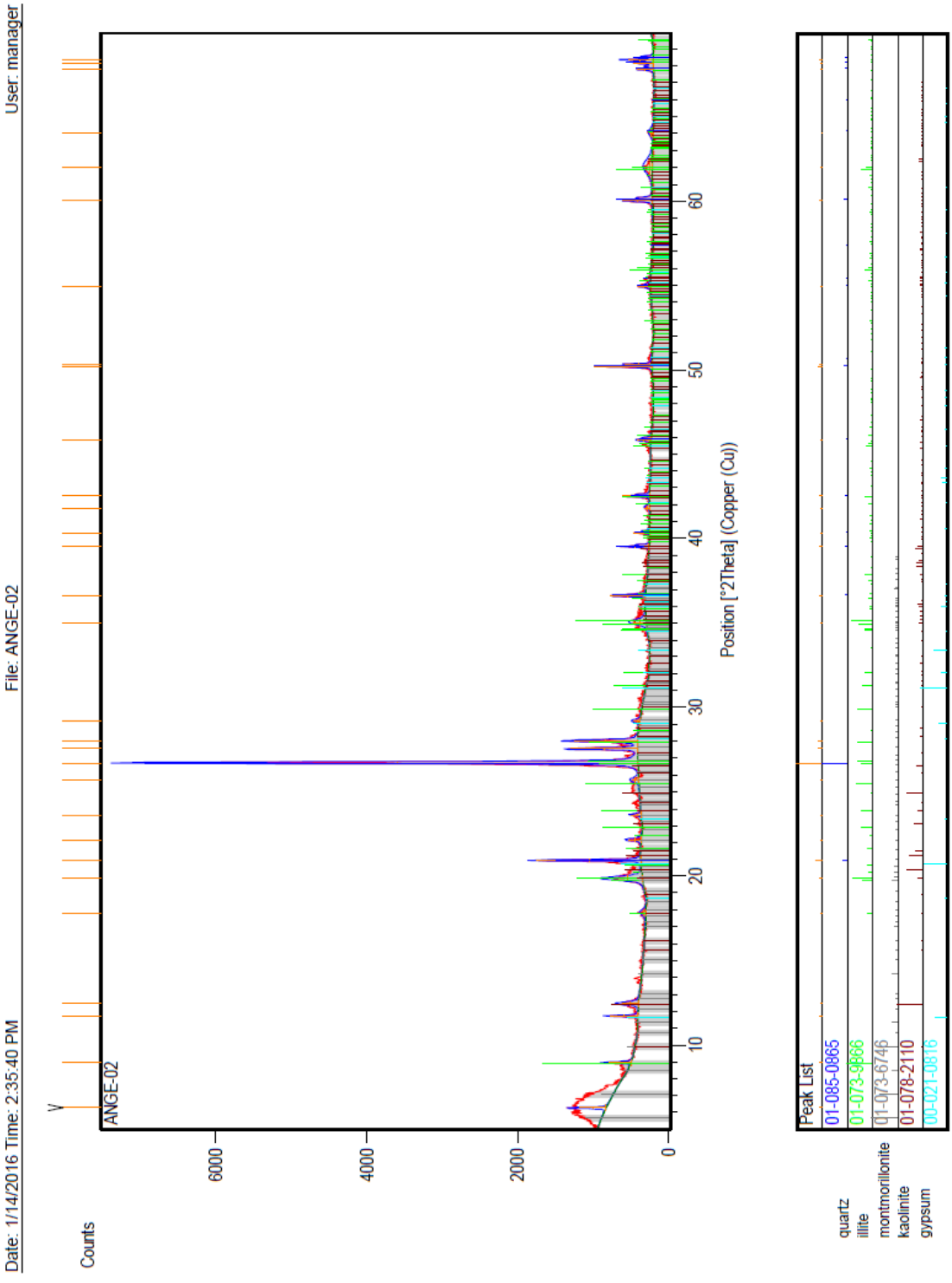
Date: 1/14/2016 Time: 2:35:40 PM
File: ANGE-02
User: manager
Counts
ANGE-02
6000
4000
2000
0
10
20
30
40
50
60
Position [°2Theta] (Copper (Cu))
Peak List
01-085-0865
01-073-9866
01-073-6746
01-078-2110
00-021-0816
quartz
illite
montmorillonite
kaolinite
gypsum

Date: 1/14/2016 Time: 2:42:48 PM File: ANGE-05 User: manager

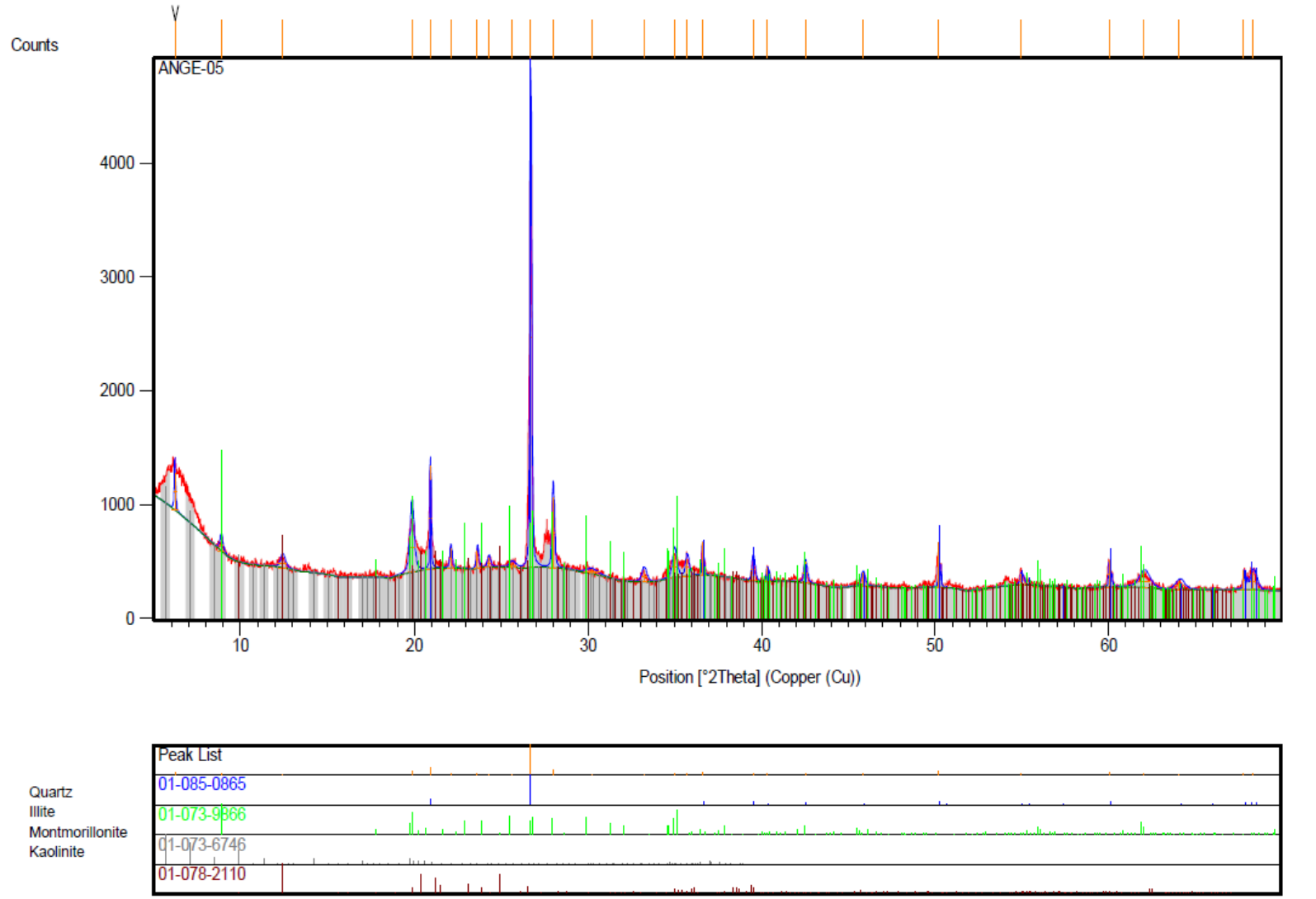

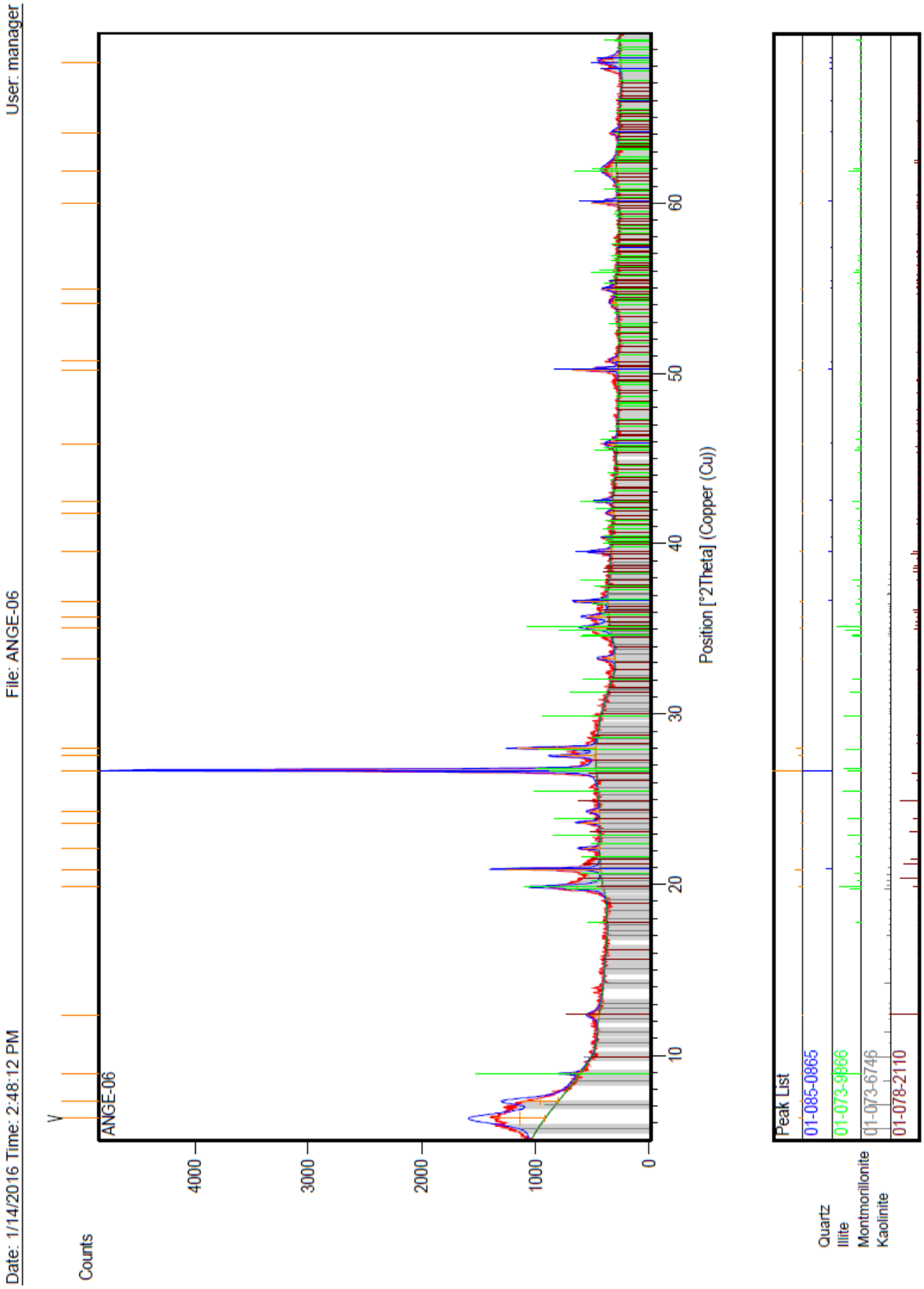
Date: 1/14/2016 Time: 2:48:12 PM
File: ANGE-06
User: manager
Counts
ANGE-06
4000
3000
2000
1000
0
10
20
30
40
50
60
Position [°2Theta] (Copper (Cu))
Peak List
01-085-0865
01-073-9866
01-073-6746
01-078-2110
Quartz
Illite
Montmorillonite
Kaolinite

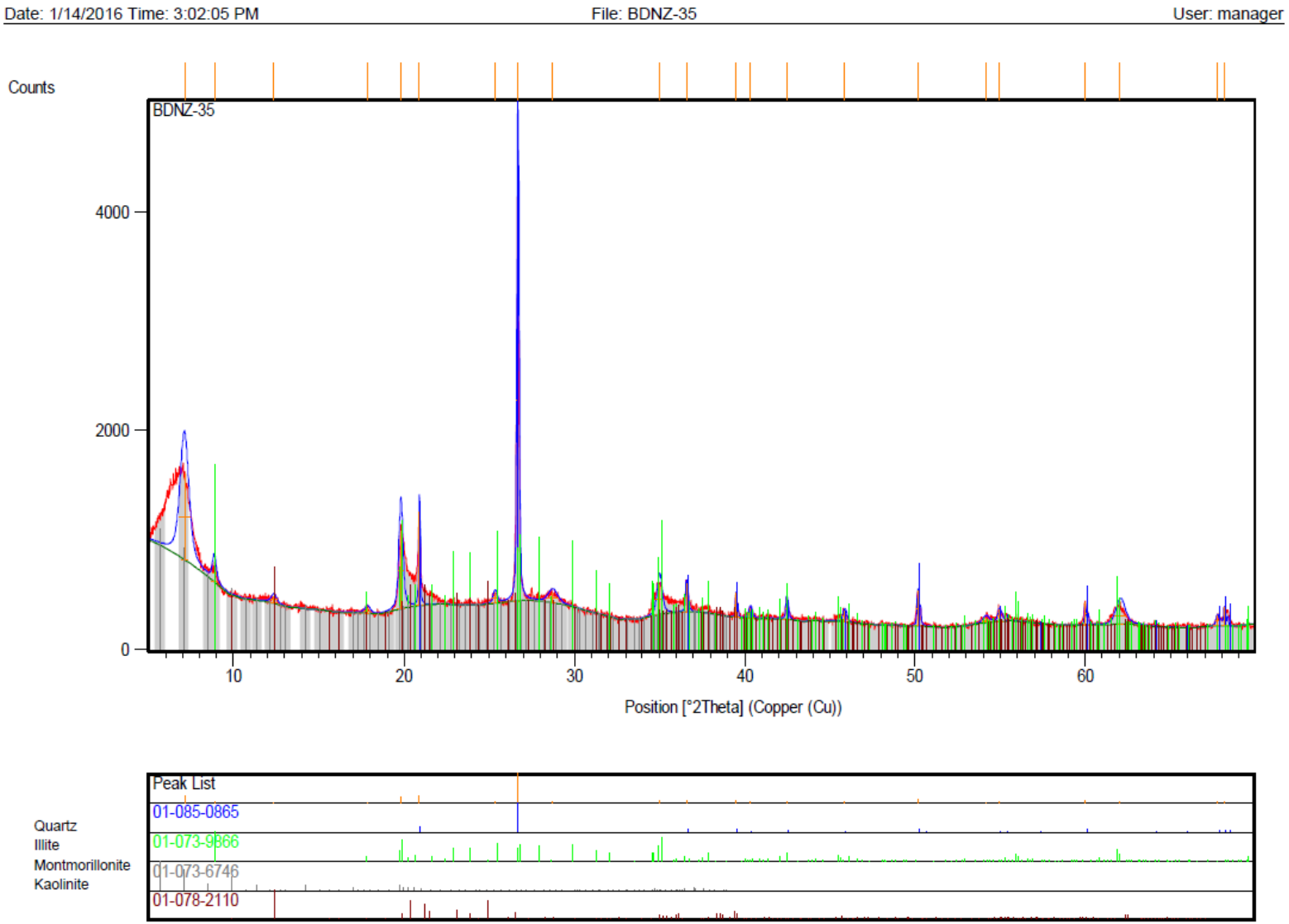
Date: 1/14/2016 Time: 3:02:05 PM
File: BDNZ-35
User: manager
Counts
BDNZ-35
4000
2000
0
10
20
30
40
50
60
Position [°2Theta] (Copper (Cu))
Peak List
01-085-0865
01-073-9866
01-073-6746
01-078-2110
Quartz
Illite
Montmorillonite
Kaolinite

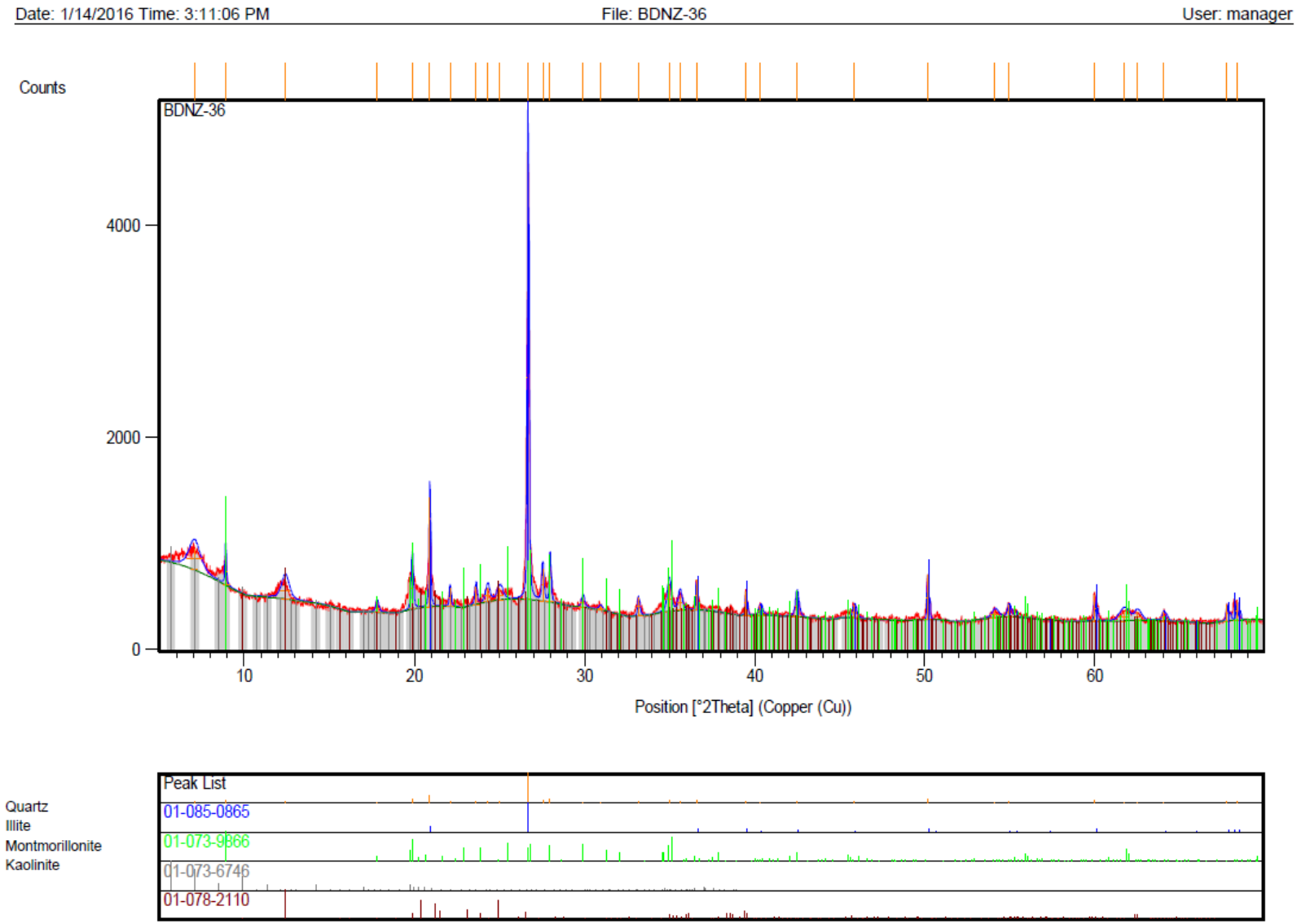
Date: 1/14/2016 Time: 3:11:06 PM
File: BDNZ-36
User: manager
Counts
BDNZ-36
4000
2000
0
10
20
30
40
50
60
Position [°2Theta] (Copper (Cu))
Peak List
Quartz
Illite
Montmorillonite
Kaolinite
01-085-0865
01-073-9866
01-073-6746
01-078-2110

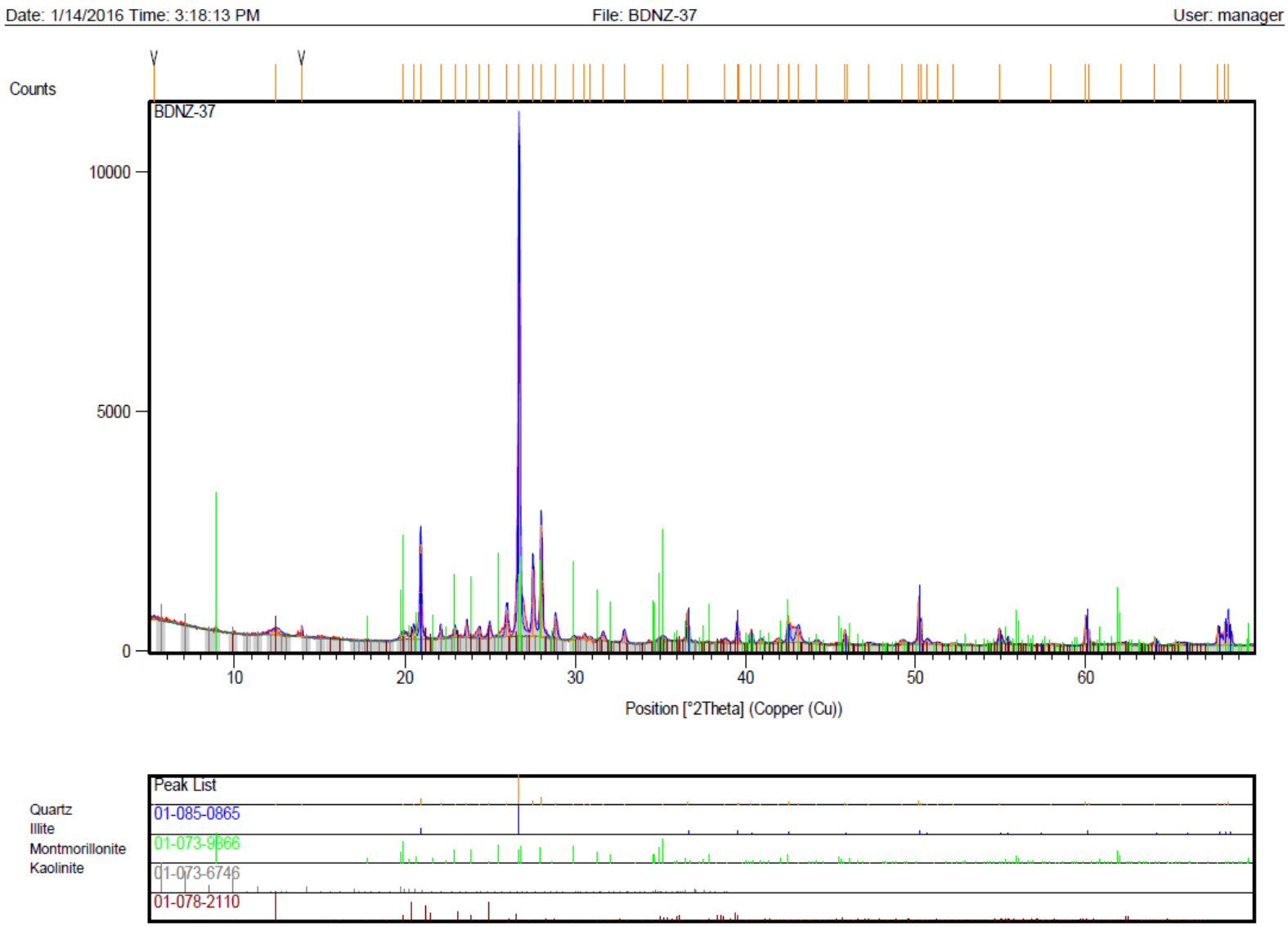
Date: 1/14/2016 Time: 3:18:13 PM
File: BDNZ-37
User: manager
Counts
BDNZ-37
10000
5000
0
10
20
30
40
50
60
Position [°2Theta] (Copper (Cu))
Peak List
Quartz
Illite
Montmorillonite
Kaolinite
01-085-0865
01-073-9866
01-073-6746
01-078-2110

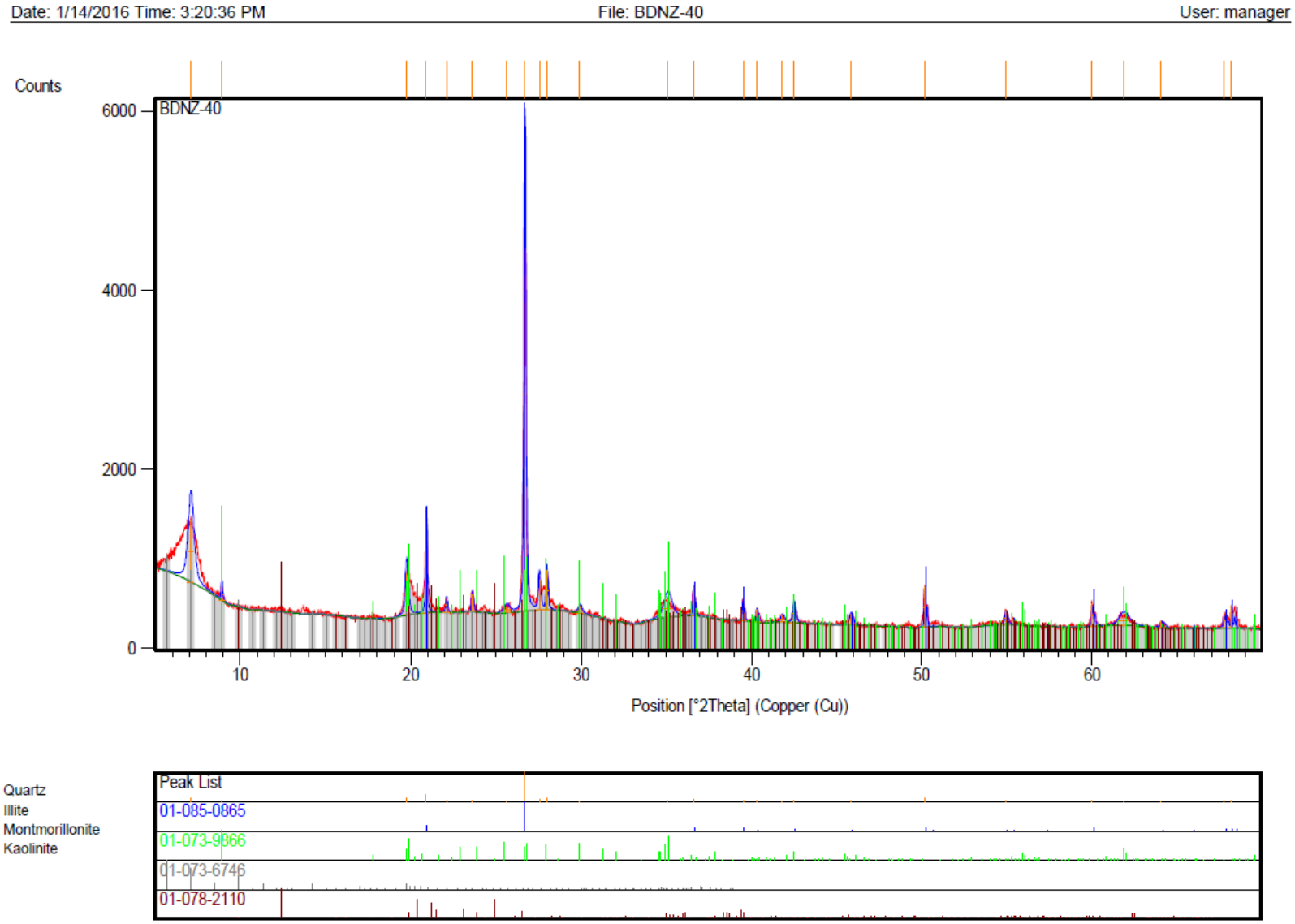
Date: 1/14/2016 Time: 3:20:36 PM
File: BDNZ-40
User: manager
Counts
BDNZ-40
6000
4000
2000
0
10
20
30
40
50
60
Position [°2Theta] (Copper (Cu))
Quartz
Illite
Montmorillonite
Kaolinite
Peak List
01-085-0865
01-073-9866
01-073-6746
01-078-2110

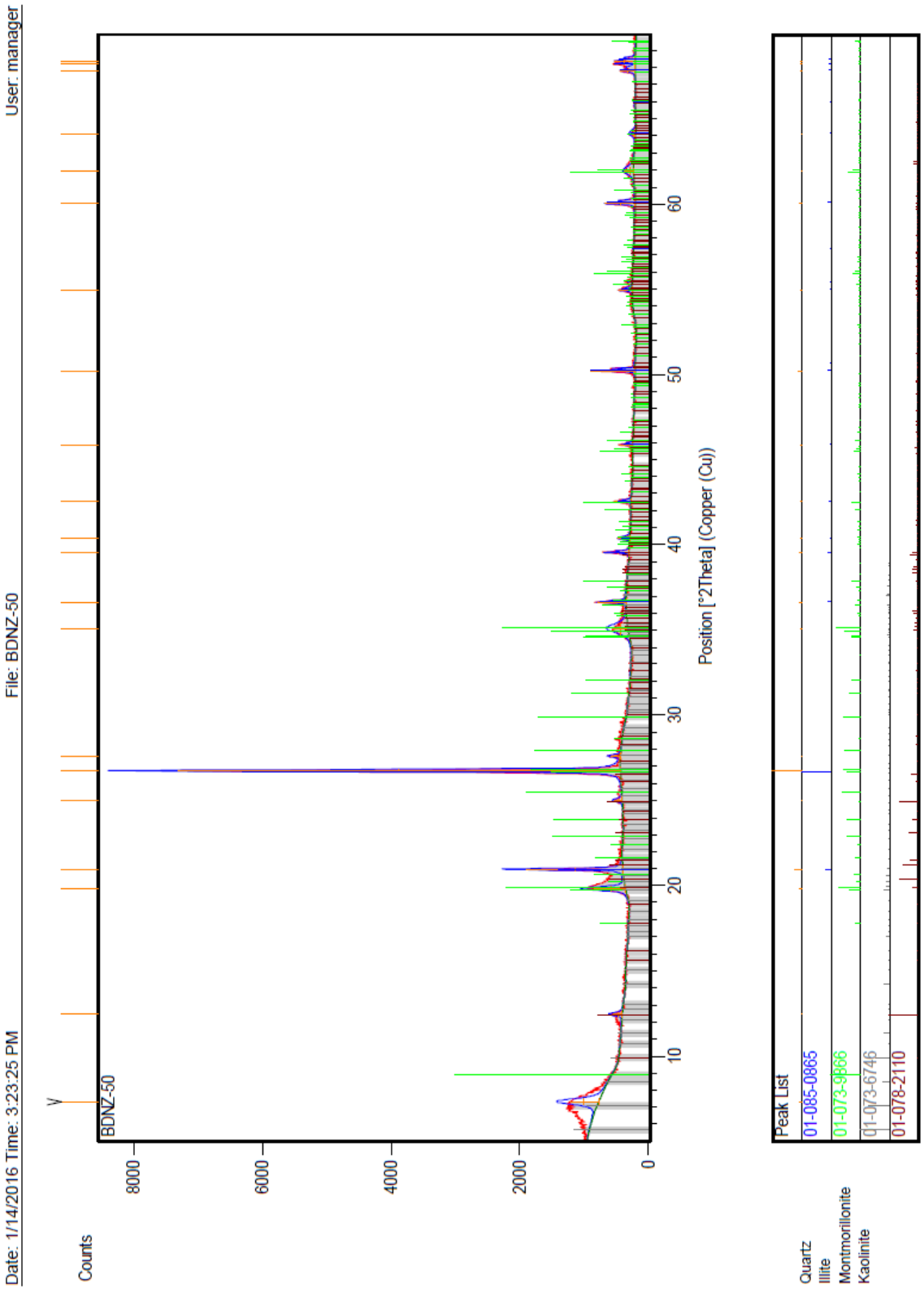
Date: 1/14/2016 Time: 3:23:25 PM
File: BDNZ-50
User: manager
Counts
y
BDNZ-50
8000
6000
4000
2000
0
10
20
30
40
50
60
Position [°2Theta] (Copper (Cu))
Peak List
01-085-0865
01-073-9866
01-073-6746
01-078-2110
Quartz
Illite
Montmorillonite
Kaolinite

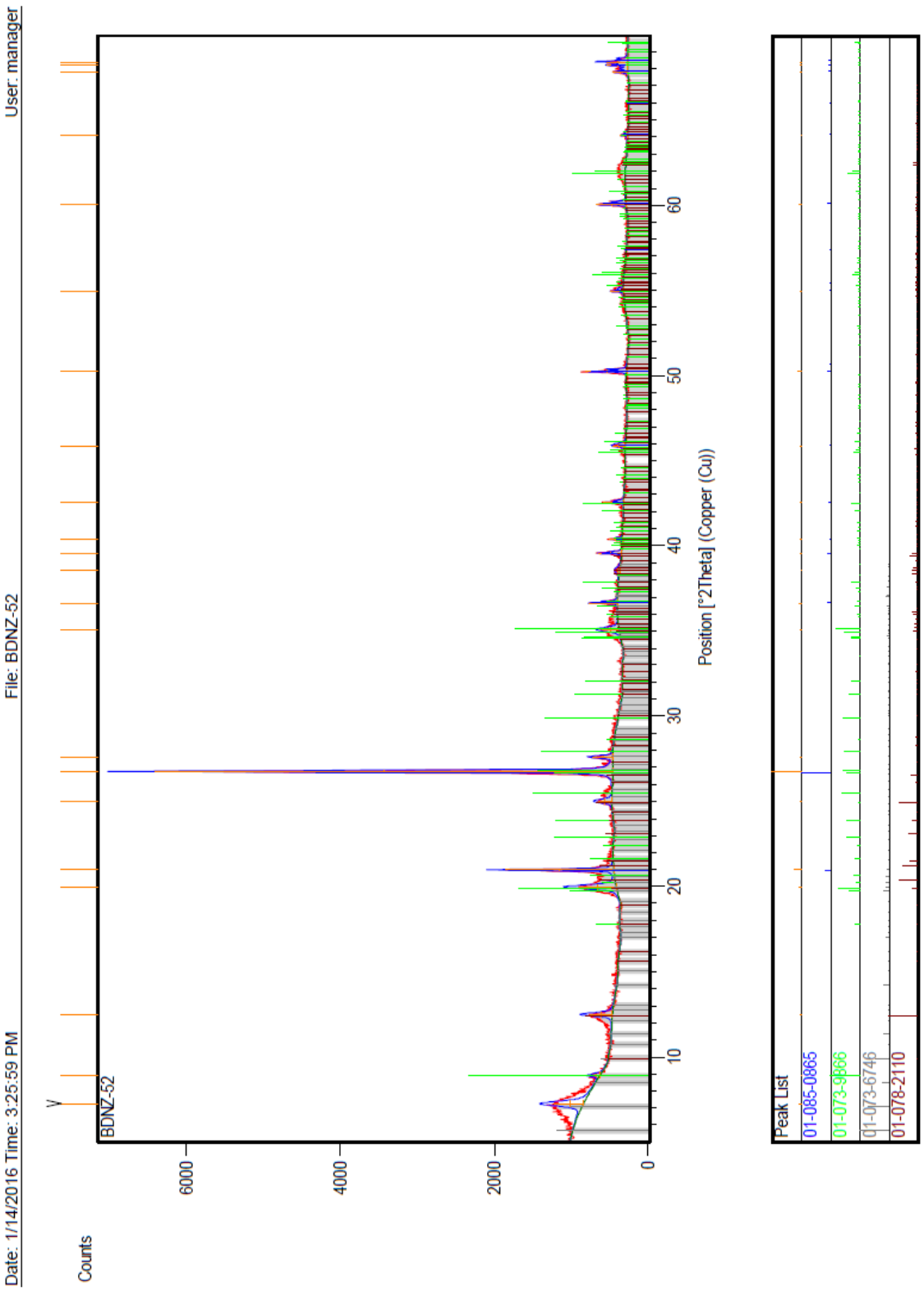
Date: 1/14/2016 Time: 3:25:59 PM
File: BDNZ-52
User: manager
Counts
BDNZ-52
6000
4000
2000
0
10
20
30
40
50
60
Position [°2Theta] (Copper (Cu))
Peak List
01-085-0865
01-073-9866
01-073-6746
01-078-2110

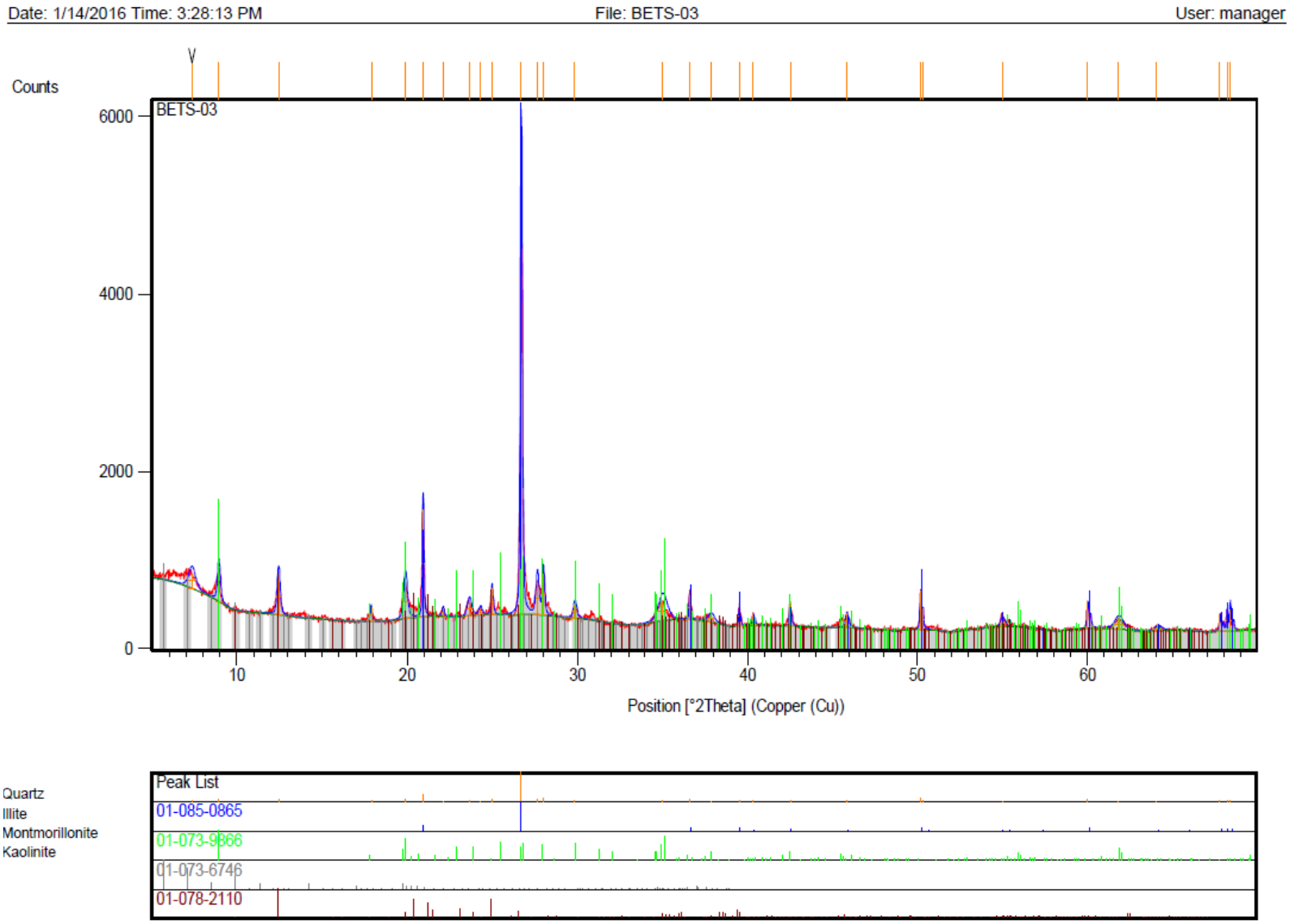
Date: 1/14/2016 Time: 3:28:13 PM
File: BETS-03
User: manager
Counts
BETS-03
6000
4000
2000
0
10
20
30
40
50
60
Position [°2Theta] (Copper (Cu))
Quartz
Illite
Montmorillonite
Kaolinite
Peak List
01-085-0865
01-073-9866
01-073-6746
01-078-2110

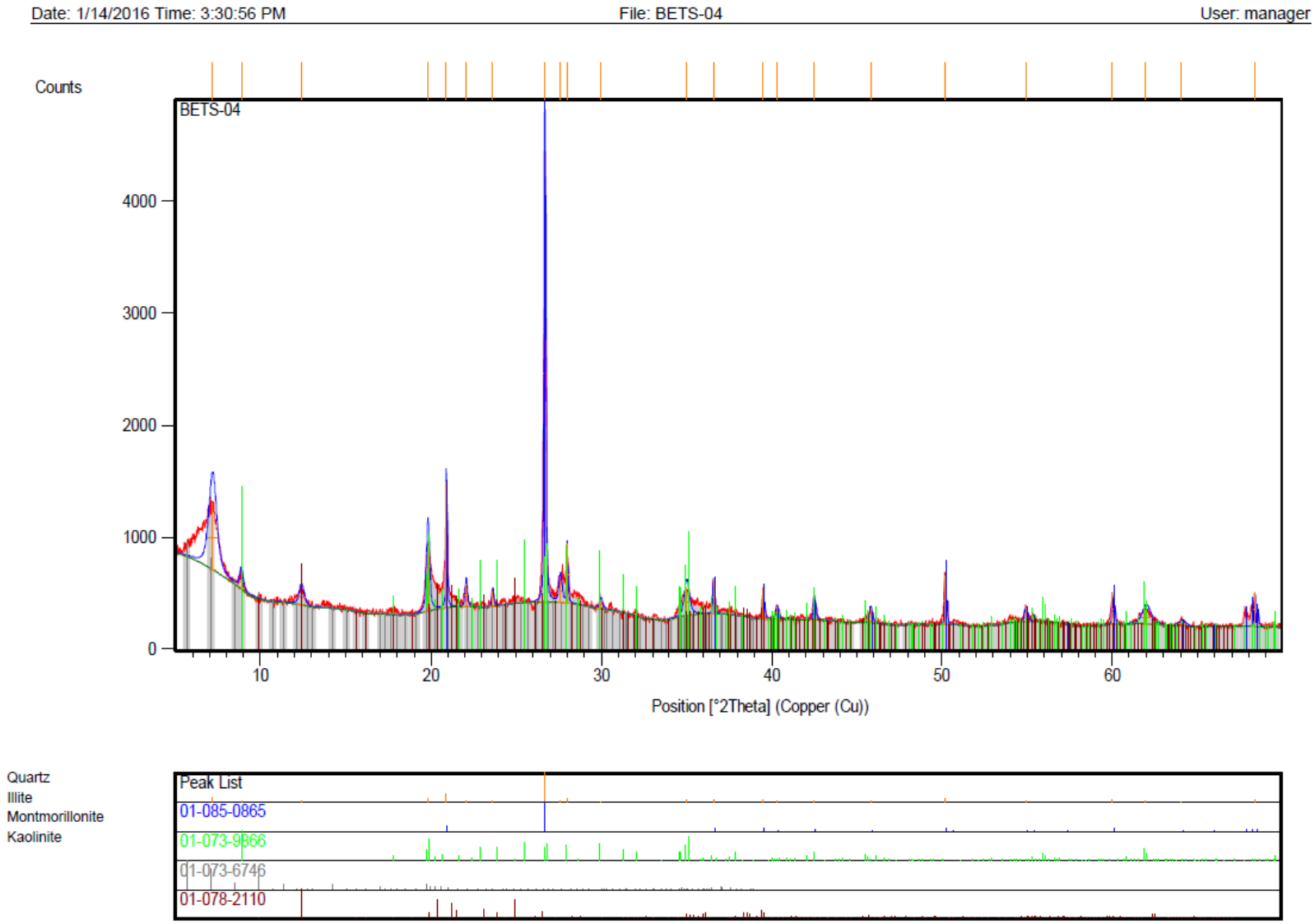
Date: 1/14/2016 Time: 3:30:56 PM
File: BETS-04
User: manager
Counts
BETS-04
4000
3000
2000
1000
0
10
20
30
40
50
60
Position [°2Theta] (Copper (Cu))
Quartz
Illite
Montmorillonite
Kaolinite
Peak List
01-085-0865
01-073-9866
01-073-6746
01-078-2110

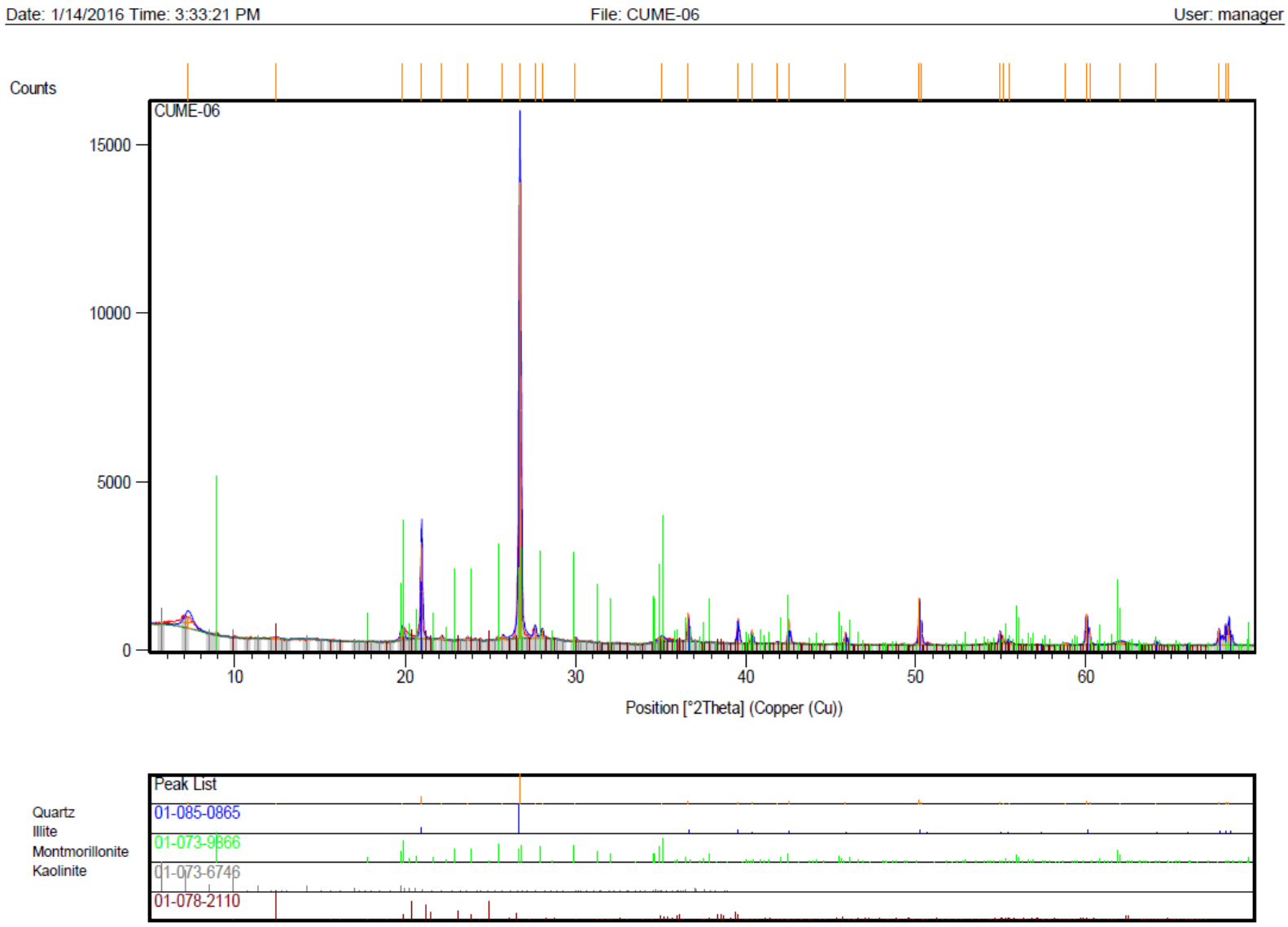
Date: 1/14/2016 Time: 3:33:21 PM
File: CUME-06
User: manager
Counts
CUME-06
15000
10000
5000
0
10
20
30
40
50
60
Position [°2Theta] (Copper (Cu))
Peak List
Quartz
Illite
Montmorillonite
Kaolinite
01-085-0865
01-073-9866
01-073-6746
01-078-2110

Date: 1/14/2016 Time: 3:35:32 PM File: CUME-14 User: manager

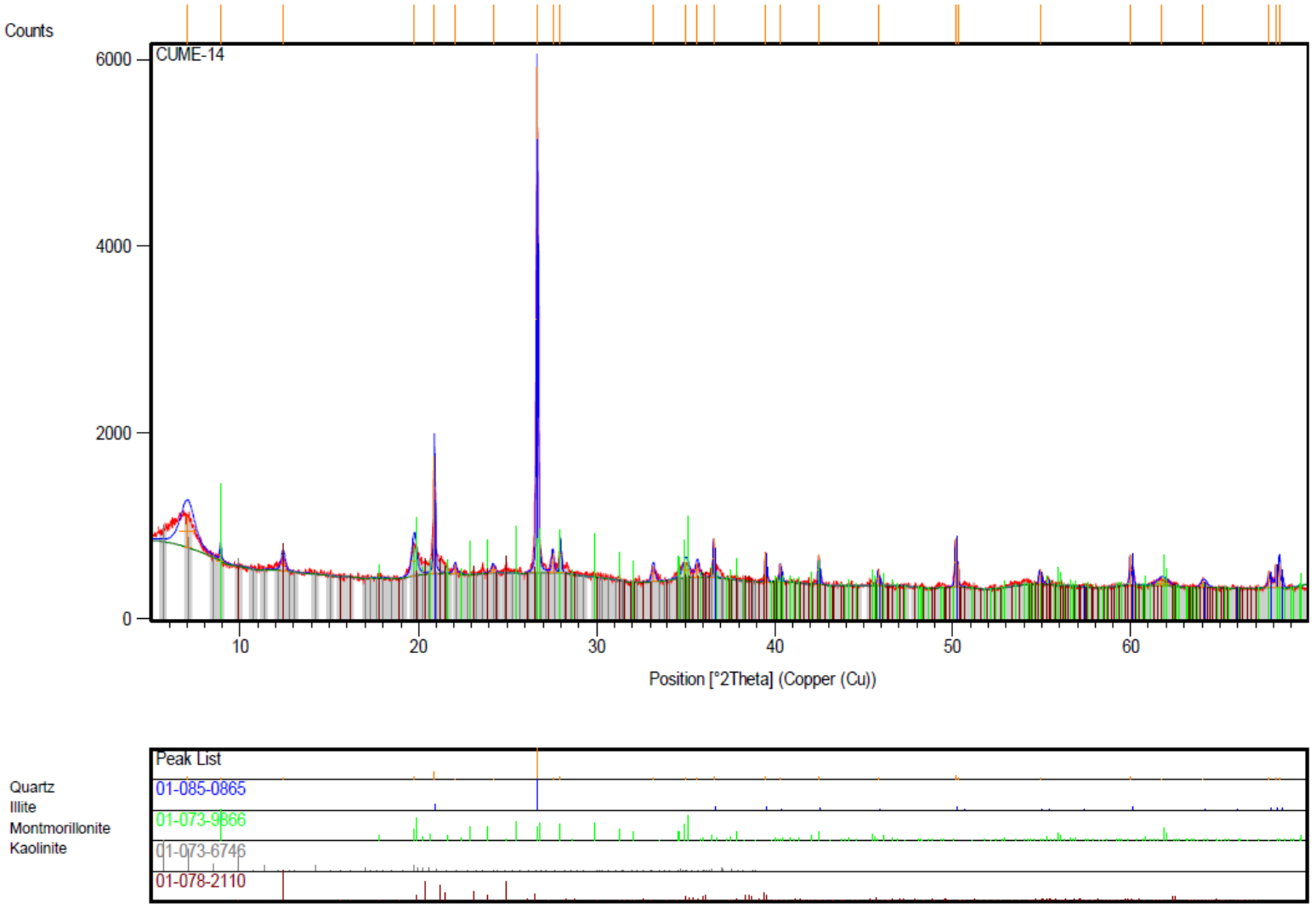

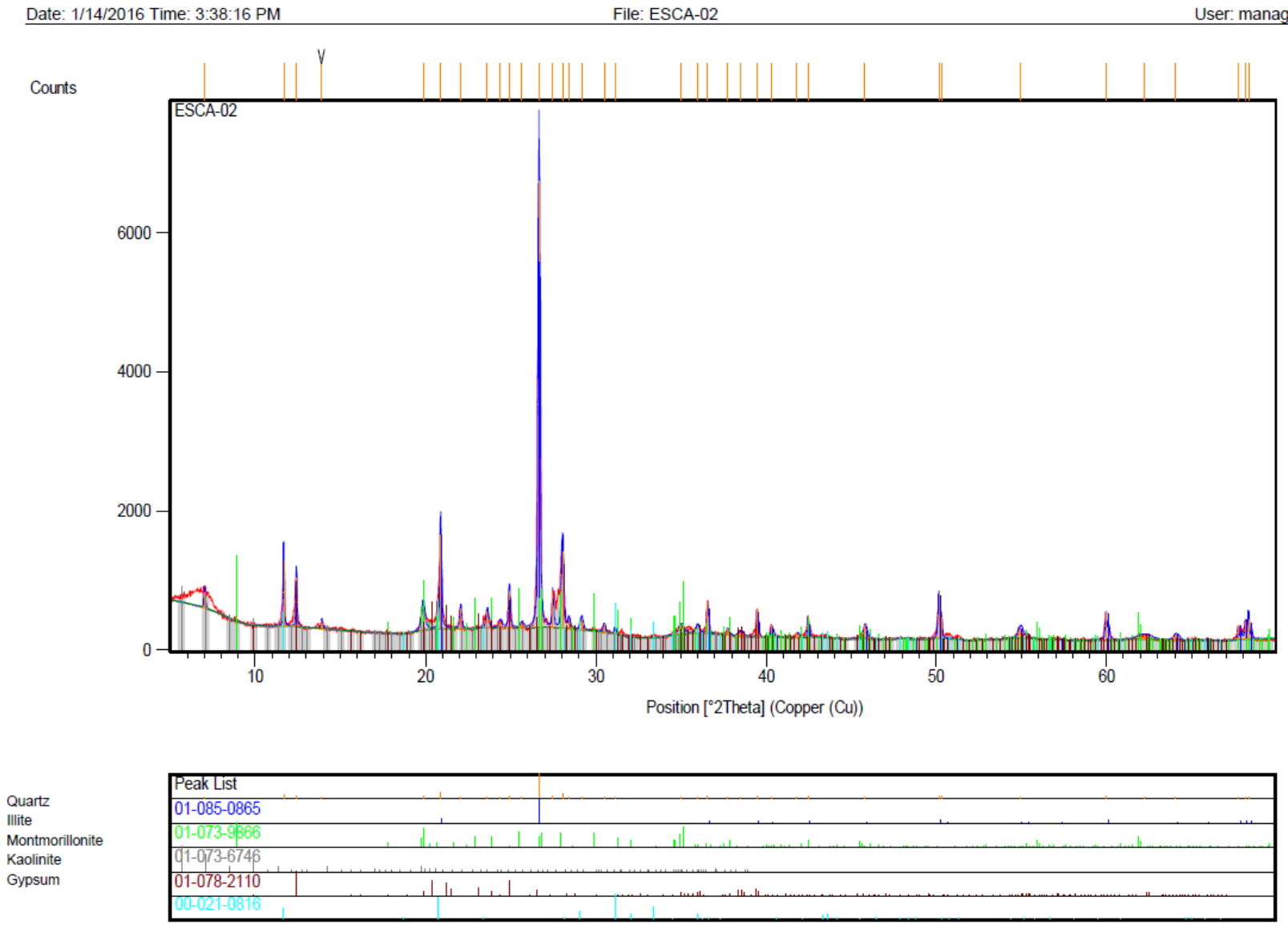
Date: 1/14/2016 Time: 3:38:16 PM
File: ESCA-02
User: manager
Counts
ESCA-02
6000
4000
2000
0
10
20
30
40
50
60
Position [°2Theta] (Copper (Cu))
Peak List
Quartz
Illite
Montmorillonite
Kaolinite
Gypsum
01-085-0865
01-073-9866
01-073-6746
01-078-2110
00-021-0816

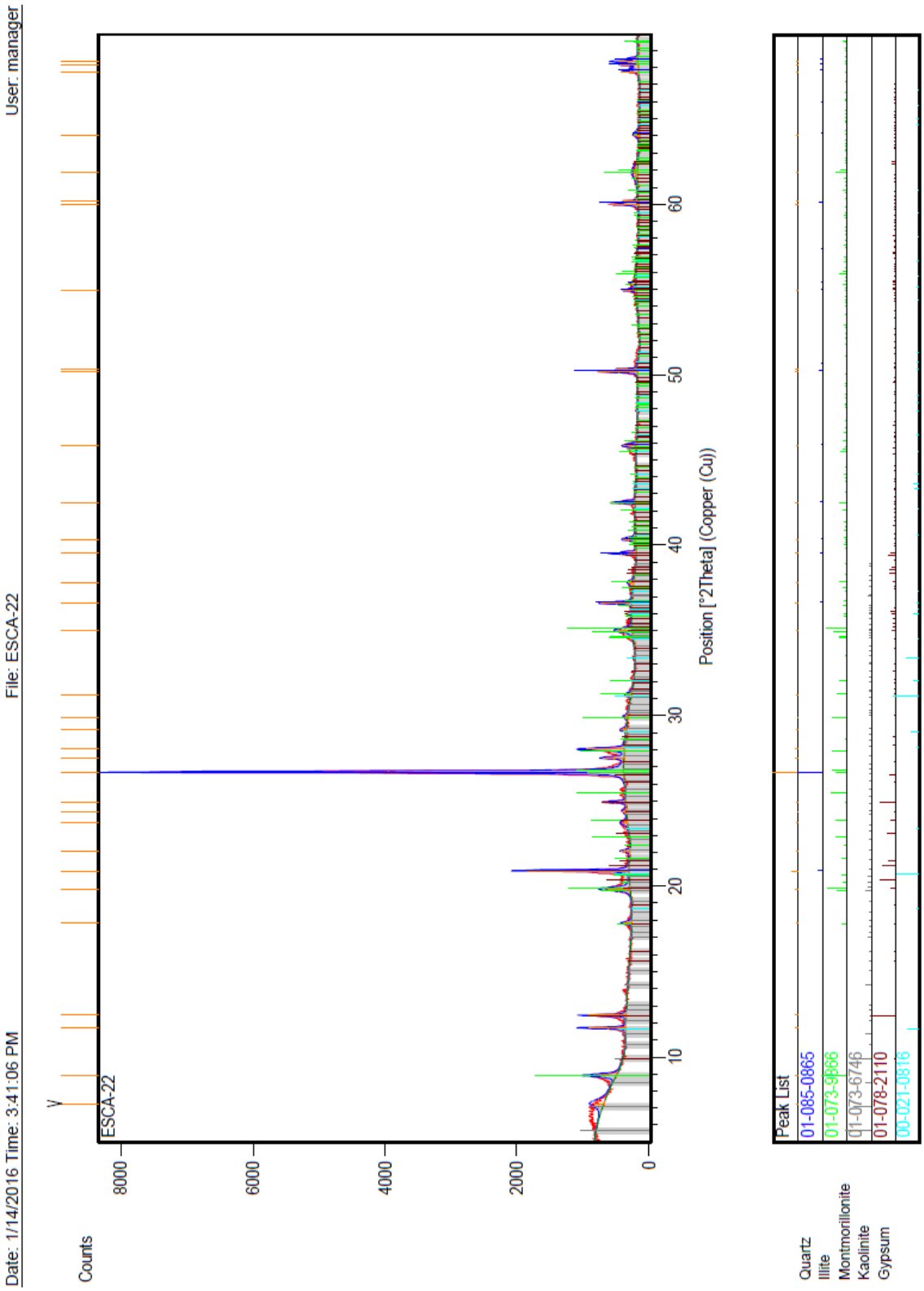
Date: 1/14/2016 Time: 3:41:06 PM
File: ESCA-22
User: manager
Counts
ESCA-22
8000
6000
4000
2000
0
10
20
30
40
50
60
Position [°2Theta] (Copper (Cu))
Peak List
01-085-0865
01-073-9866
01-073-6746
01-078-2110
00-021-0816
Quartz
Illite
Montmorillonite
Kaolinite
Gypsum

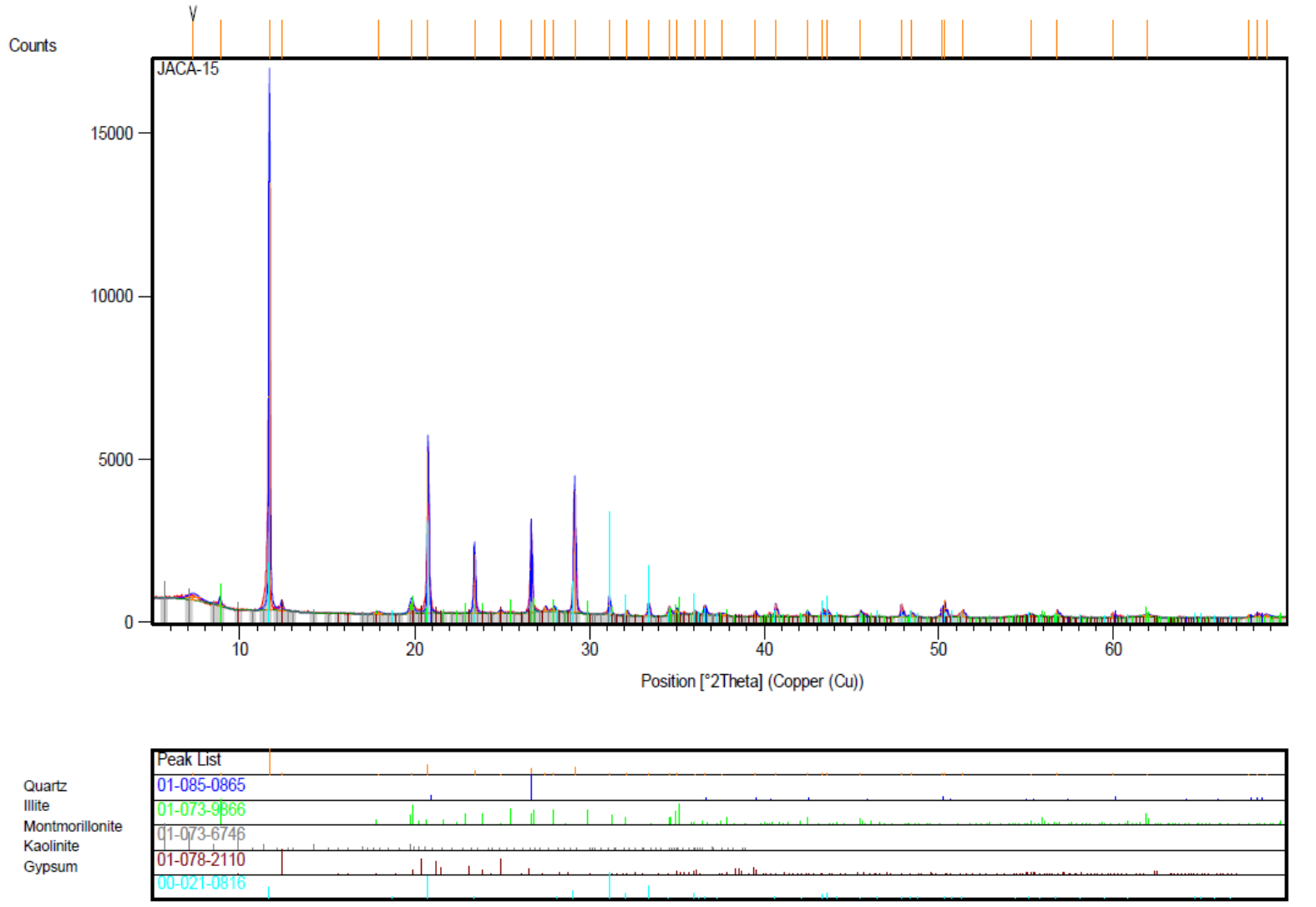
Date: 1/14/2016 Time: 3:43:58 PM
File: JACA-15
User: manager
Counts
JACA-15
15000
10000
5000
0
10
20
30
40
50
60
Position [°2Theta] (Copper (Cu))
Peak List
Quartz
Illite
Montmorillonite
Kaolinite
Gypsum
01-085-0865
01-073-9866
01-073-6746
01-078-2110
00-021-0816

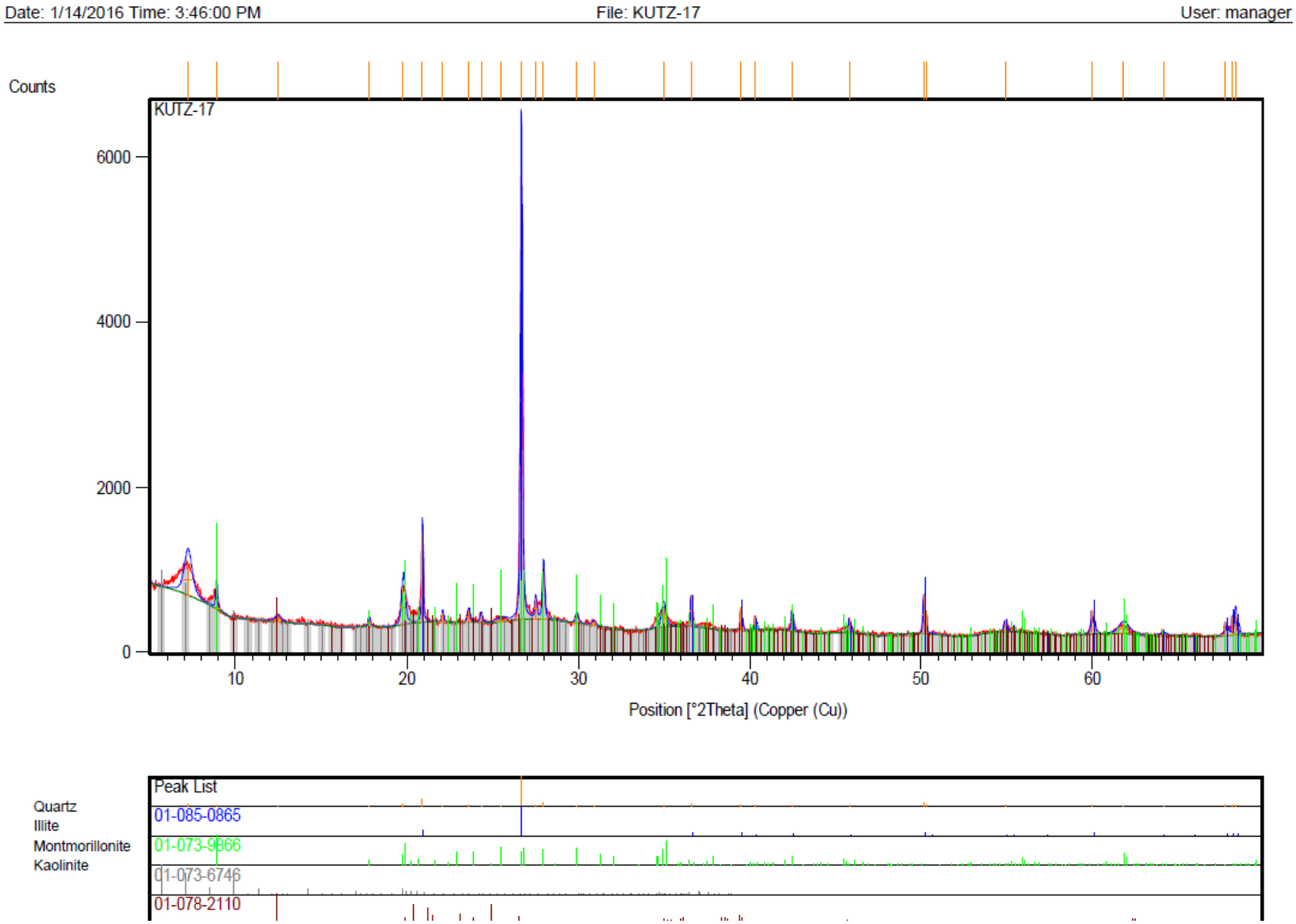
Date: 1/14/2016 Time: 3:46:00 PM
File: KUTZ-17
User: manager
Counts
KUTZ-17
6000
4000
2000
0
10
20
30
40
50
60
Position [°2Theta] (Copper (Cu))
Peak List
Quartz
Illite
Montmorillonite
Kaolinite
01-085-0865
01-073-9866
01-073-6746
01-078-2110

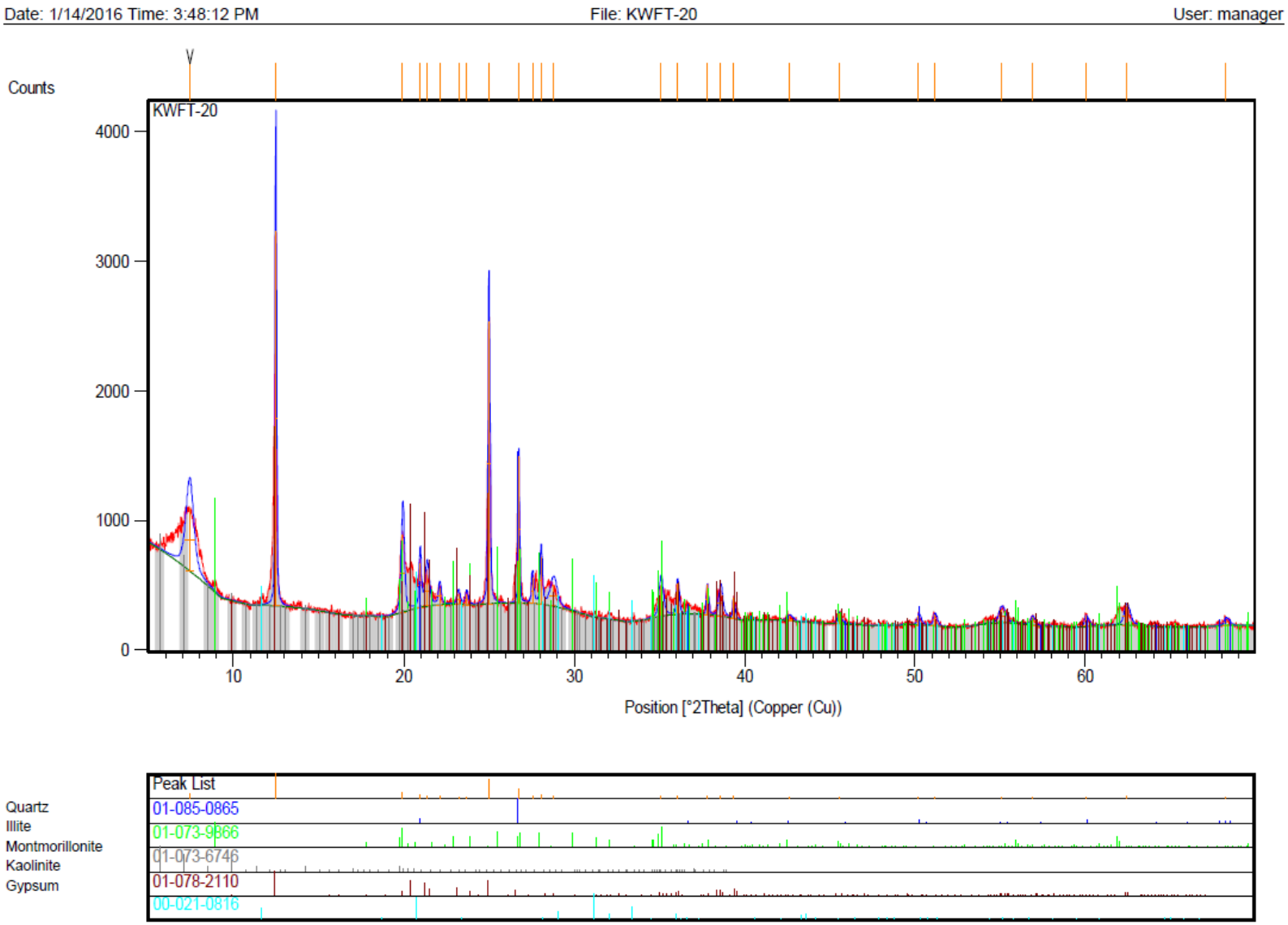
Date: 1/14/2016 Time: 3:48:12 PM
File: KWFT-20
User: manager
Counts
KWFT-20
4000
3000
2000
1000
0
10
20
30
40
50
60
Position [°2Theta] (Copper (Cu))
Peak List
Quartz
Illite
Montmorillonite
Kaolinite
Gypsum
01-085-0865
01-073-9866
01-073-6746
01-078-2110
00-021-0816

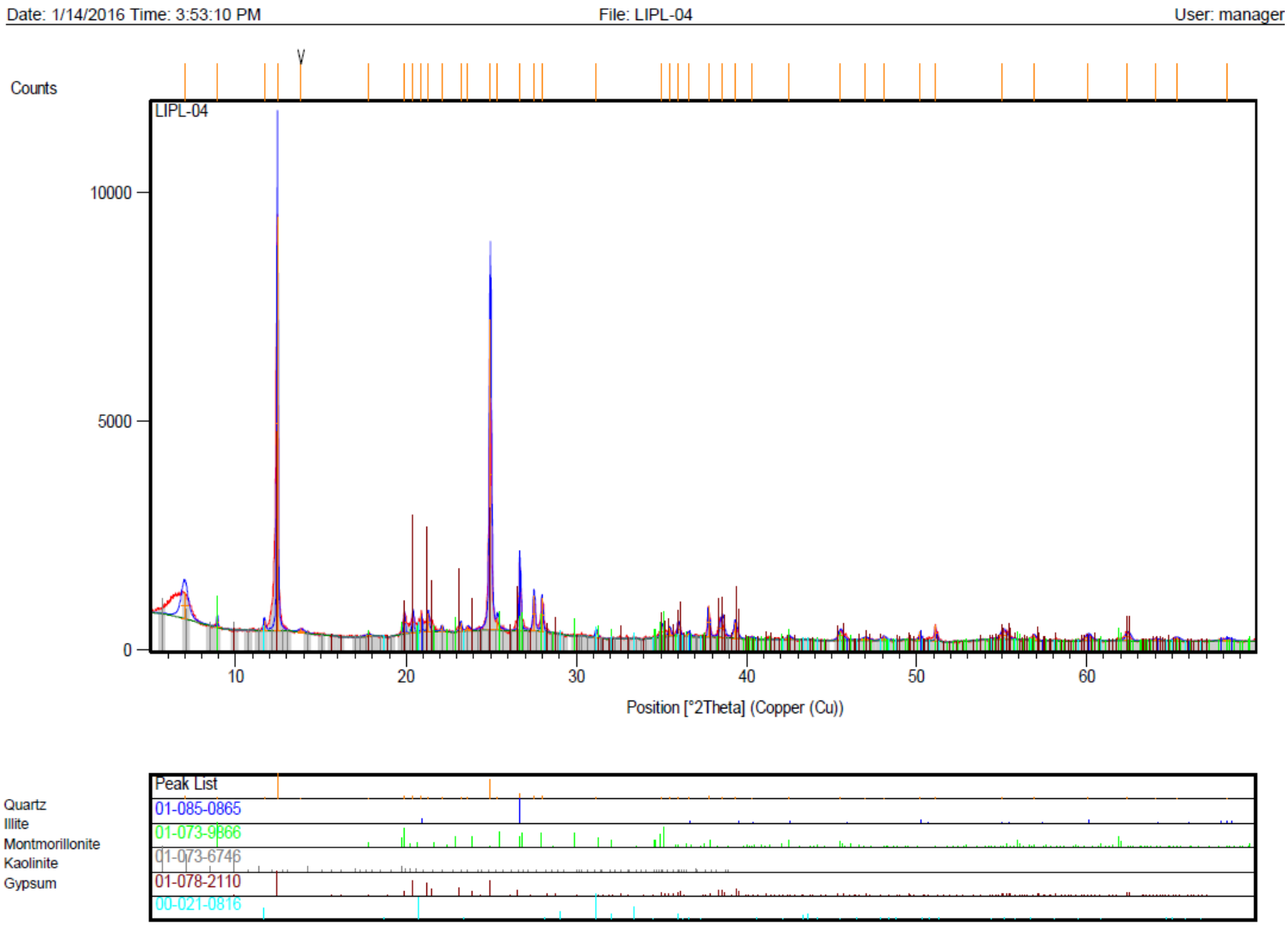
Date: 1/14/2016 Time: 3:53:10 PM
File: LIPL-04
User: manager
Counts
LIPL-04
10000
5000
0
10
20
30
40
50
60
Position [°2Theta] (Copper (Cu))
Peak List
Quartz
Illite
Montmorillonite
Kaolinite
Gypsum
01-085-0865
01-073-9866
01-073-6746
01-078-2110
00-021-0816

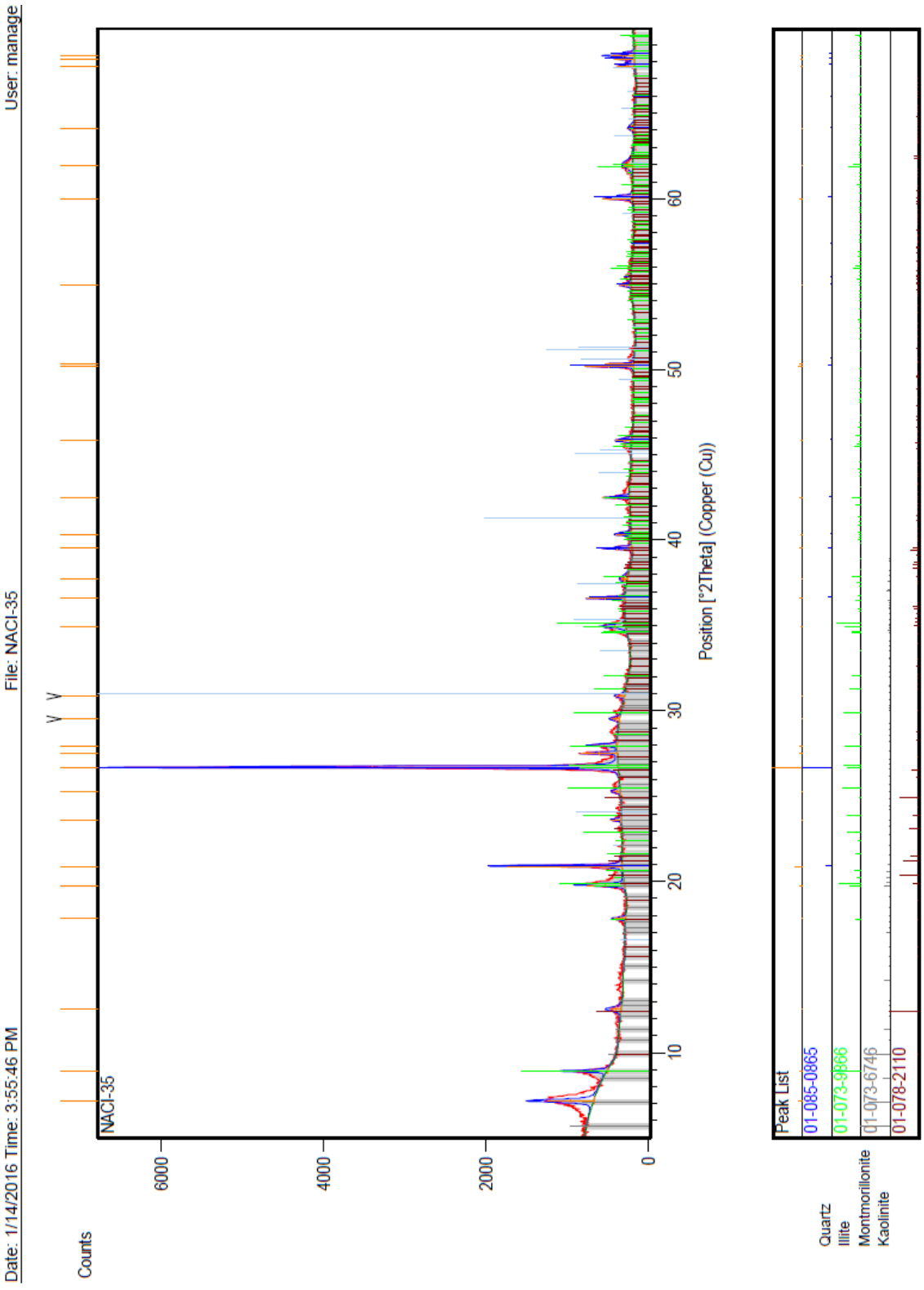
Date: 1/14/2016 Time: 3:55:46 PM
File: NACI-35
User: manage
NACI-35
Counts
6000
4000
2000
0
10
20
30
40
50
60
Position [°2Theta] (Copper (Cu))
Peak List
01-085-0865
01-073-9866
01-073-6746
01-078-2110
Quartz
Illite
Montmorillonite
Kaolinite

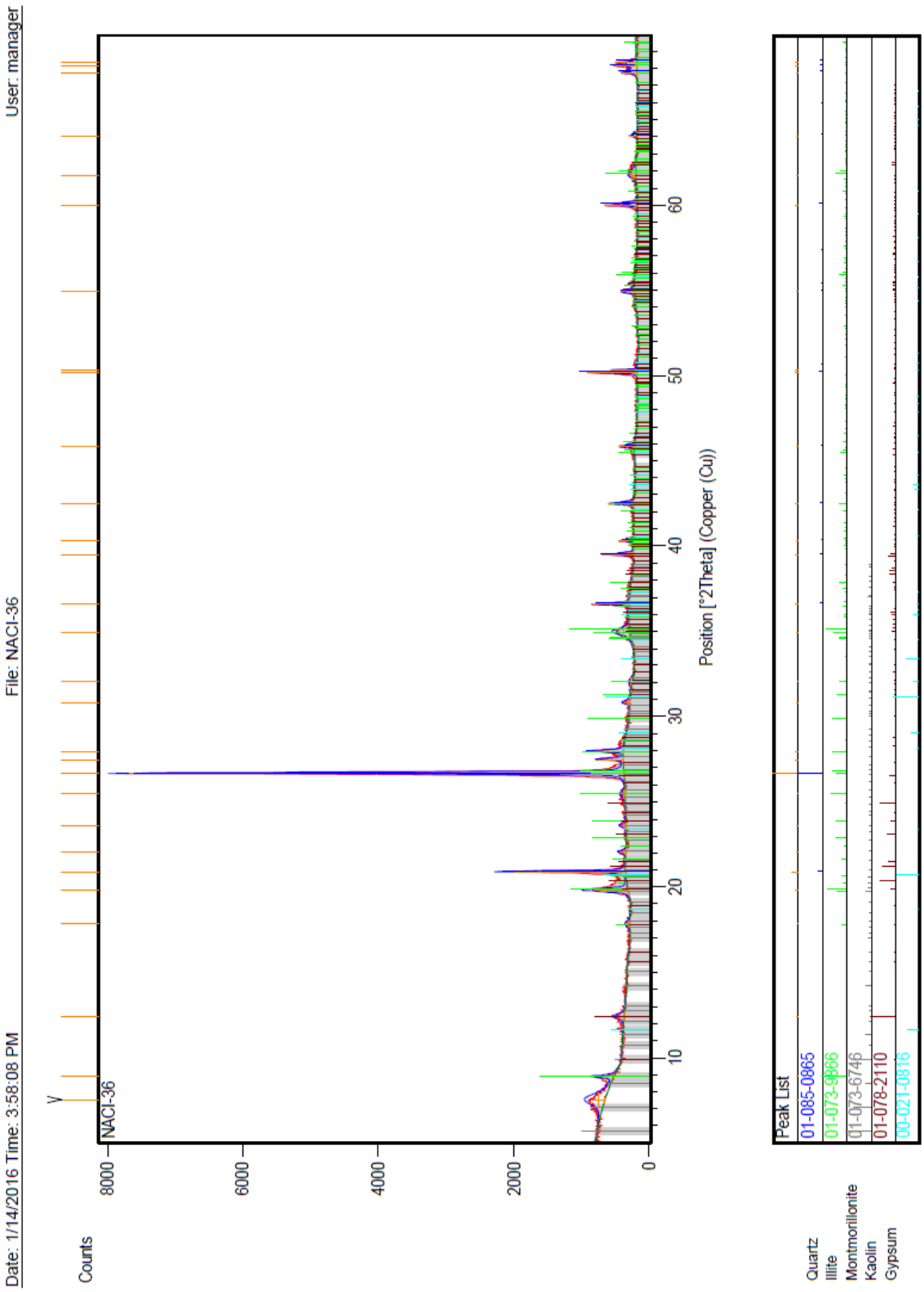
Date: 1/14/2016 Time: 3:58:08 PM
File: NACI-36
User: manager
Counts
NACI-36
8000
6000
4000
2000
0
10
20
30
40
50
60
Position [°2Theta] (Copper (Cu))
Peak List
01-085-0865
01-073-9866
01-073-6746
01-078-2110
00-021-0816
Quartz
Illite
Montmorillonite
Kaolin
Gypsum

Date: 1/14/2016 Time: 4:00:32 PM File: NACI-37 User: manager

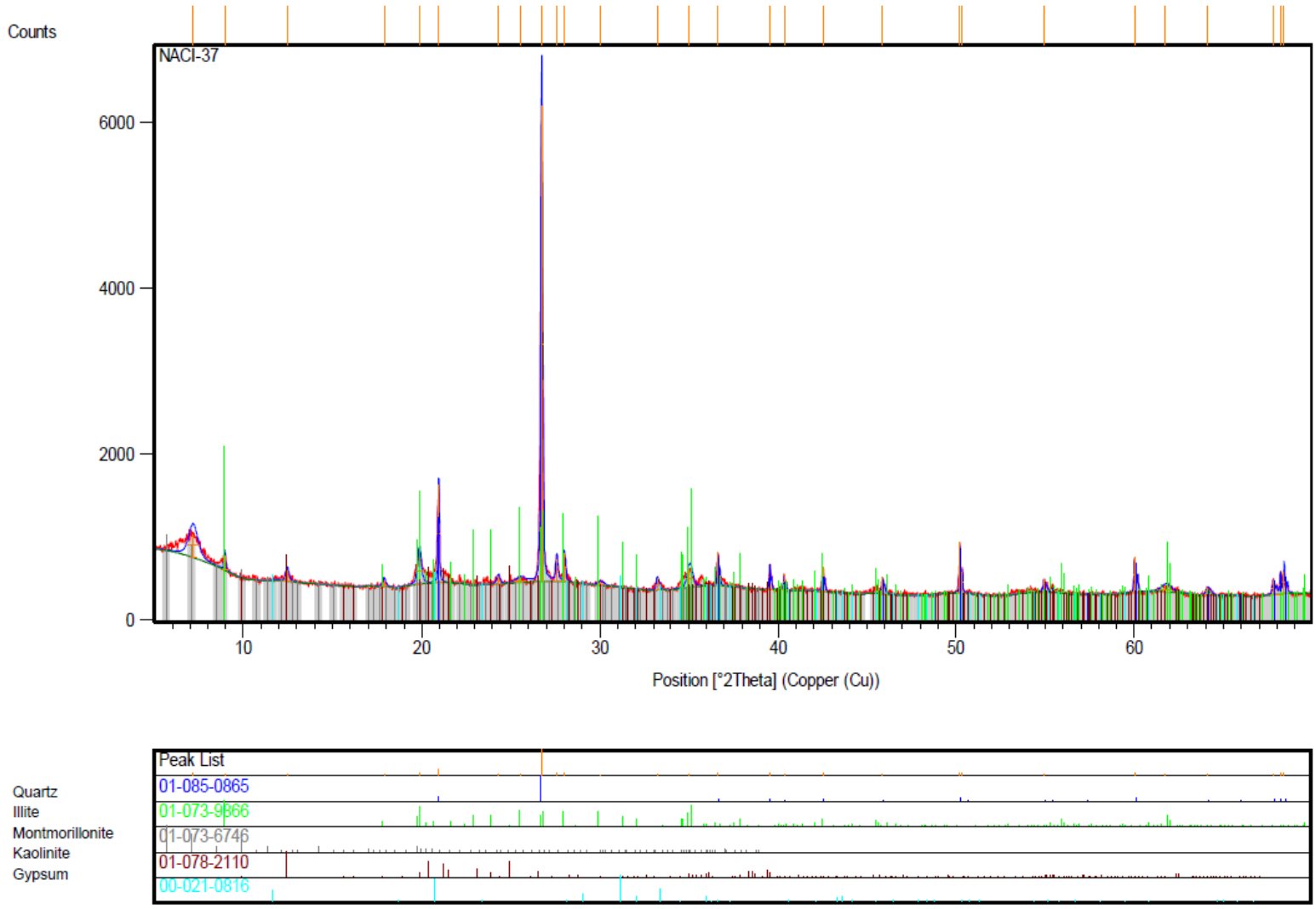

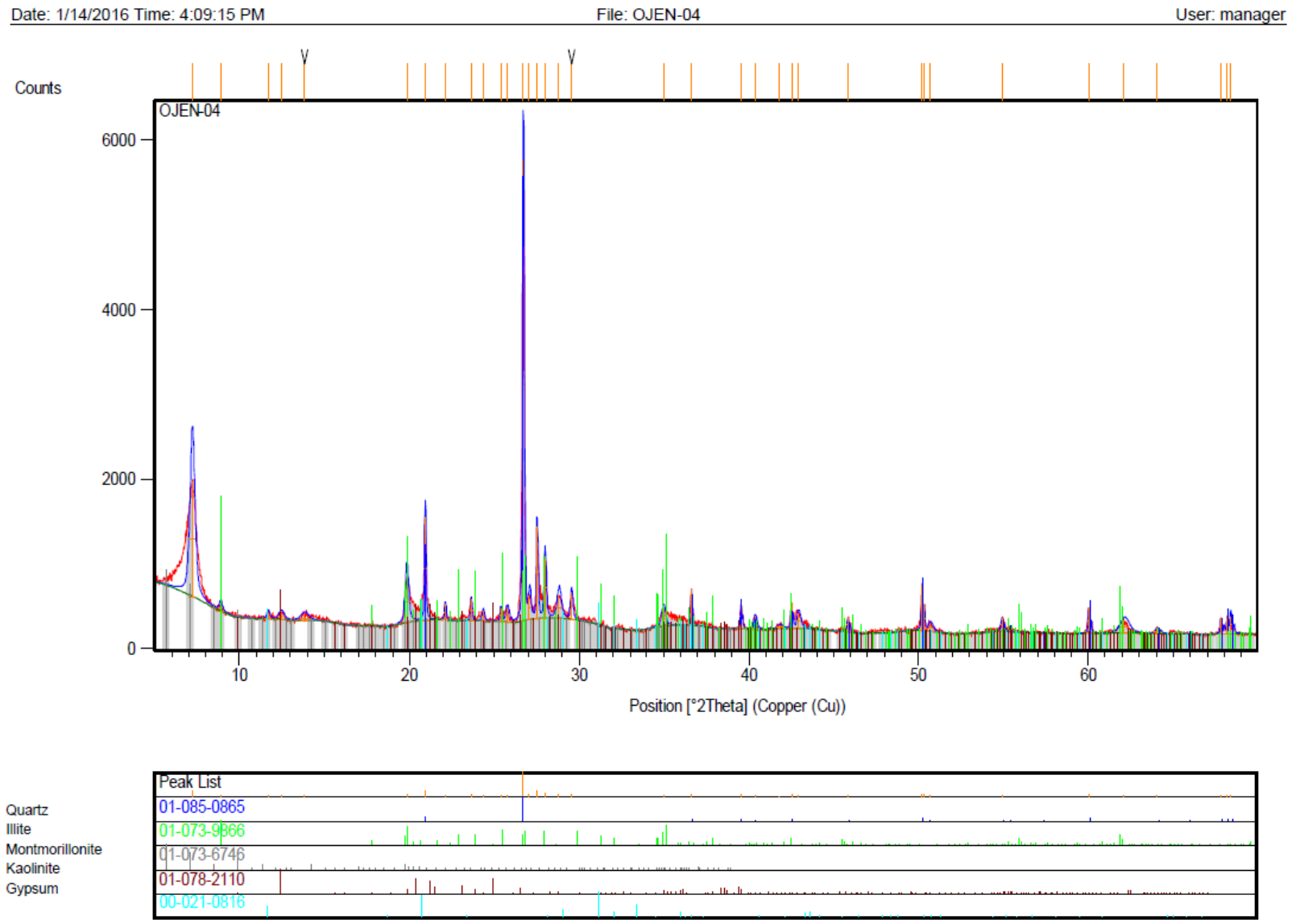
Date: 1/14/2016 Time: 4:09:15 PM
File: OJEN-04
User: manager
Counts
OJEN-04
6000
4000
2000
0
10
20
30
40
50
60
Position [°2Theta] (Copper (Cu))
Peak List
01-085-0865
01-073-9866
01-073-6746
01-078-2110
00-021-0816
Quartz
Illite
Montmorillonite
Kaolinite
Gypsum